Evaluation of International Satellite Cloud climatology Project (ISCCP) D2 Cloud Amount Changes and their Connections to Large-Scale Dynamics

By
Todd D. Ellis and Graeme L. Stephens

Department of Atmospheric Science
Colorado State University
Fort Collins, Colorado

Research was supported by NASA Research grant NNG04GB97G and in part by a one-year AMS Graduate Fellowship.

Colorado State University

Department of Atmospheric Science

Paper No. 759

EVALUATION OF INTERNATIONAL SATELLITE CLOUD CLIMATOLOGY PROJECT (ISCCP) D2 CLOUD AMOUNT CHANGES AND THEIR CONNECTIONS TO LARGE-SCALE DYNAMICS

Todd D. Ellis and Graeme L. Stephens

Research supported by NASA Research Grant NNG04GB97G
and in part by a one-year AMS Graduate Fellowship

Department of Atmospheric Science
Colorado State University
Fort Collins, Colorado 80523-1371

August 2005

Atmospheric Science Paper No. 759

ABSTRACT

EVALUATION OF INTERNATIONAL SATELLITE CLOUD CLIMATOLOGY PROJECT (ISCCP) D2 CLOUD AMOUNT CHANGES AND THEIR CONNECTIONS TO LARGE-SCALE DYNAMICS

The International Satellite Cloud Climatology Project (ISCCP) D2 dataset exhibits a 2.6% per decade decrease in the global all-cloud cloud amount from July 1983 through September 2001. This result is consistent with other recent findings that provide evidence that the cloud amount has decreased on a decadal-scale. Such changes in cloud amount should have an obvious impact on the climate system through changes in heating and the radiation budget of the atmosphere. However, the changes evident in the ISCCP data seem too large to be accepted without question. Because these data are used as a verification tool for the global climate modeling community, it is imperative that the nature of these changes are better understood and verified for similarities with other data sources. Otherwise, climate studies might be comparing their results with faulty information. This study represents an attempt to characterize and verify the ISCCP D2 cloud amount changes.

One possible reason why the ISCCP D2 trend might be too large is the presence of artifacts in the data related to changes in the number of geosynchronous satellites in orbit. This leads to changes in the viewing angle for each pixel in the dataset and explains roughly one-third of the trend in the global cloud amount. In order to account for this phenomenon, this study focuses on the region from 90°E to 180° and 30°N to 30°S where the satellite coverage has been relatively constant. It is shown that the slope

of the cloud amount change in this region is still very large. This leaves open the possibility that there is other contamination in the ISCCP data, and calls into question the validity of the large cloud amount trend.

Several steps are taken to examine the nature of the cloud amount changes in this region. First of all, the changes in the ISCCP cloud amount data are characterized by three criteria: where and when the changes are occurring and the types of clouds expressing them. These patterns are examined for features that appear physically reasonable. These patterns can then be checked against patterns obtained from the NOAA Interpolated OLR and PATMOS-A cloud amount datasets. These data, from sensors mounted on polar-orbiting satellites, do not experience the viewing-angle problem of ISCCP but should still corroborate evidence of real cloud amount changes.

The most unique aspect of this study is the use of reanalysis data to look for signals of climate change that are related to changes in the ISCCP cloud amount data. The average ISCCP all-cloud cloud amount for the region of interest is regressed onto wind fields, geopotential height fields, divergence fields, and other data that represent how the climate has changed over the span of the ISCCP dataset. Maps of regression coefficients represent how those fields change in response to a unit increase in cloud amount. These patterns help to identify atmospheric phenomena that are connected with variations in cloud amount in the region of interest. Furthermore, the true cloud amount trend in the region of interest can be diagnosed by making time series of how well the regression maps project onto reanalysis fields at each time step. These "proxy cloud time series" represent how the true cloud amount must be changing to effect the observable

changes in the reanalysis data. Both results provide a unique way to discover whether the ISCCP D2 cloud amount changes are also evident in other data sources.

It is shown that the cloud amount changes evident in the ISCCP D2 dataset are indicative of changes in the intensity and location of convection associated with the Inter-Tropical Convergence Zone (ITCZ). The spatial patterns of these changes are somewhat consistent with the NOAA Interpolated OLR and PATMOS-A cloud amount datasets. However the trends in the regionally averaged time series of these data are not significantly different from zero. This supports the conclusion that the ISCCP trend is too large. Using data from the NCEP/NCAR reanalysis and the ERA-40 reanalysis, it is shown that the changes in the ISCCP D2 cloud amount time series in the region of interest are highly correlated with changes in the Walker-Hadley circulation. The patterns of these changes are consistent with the redistribution of convection indicated by each of the satellite datasets, and appear to be associated with ENSO since they are also consistent with the results of Bjerknes (1969). The reanalysis data also provide independent confirmation that the actual cloud amount in the region of interest is likely not changing in a statistically significant way during the period spanned by the ISCCP D2 dataset. Therefore, while the variability of cloud amount due to ENSO is evidently captured by the ISCCP D2 dataset, the long-term trend in the ISCCP cloud amount is likely not physically realistic.

Todd D. Ellis
Department of Atmospheric Science
Colorado State University
Fort Collins, CO 80523
Fall 2005

ACKNOWLEDGEMENTS

This work was supported in part by NASA grant NNG04GB97G and in part by a one-year AMS Graduate Fellowship. The following sources also need to be acknowledged for their assistance in providing the data used in this study. The ISCCP data were obtained from the NASA Langley Research Center Atmospheric Sciences Data Center. The ECMWF ERA-40 data used in this study have been obtained from the ECMWF data server. Interpolated OLR data, NCEP-NCAR Reanalysis data, and CMAP data were provided by the NOAA-CIRES Climate Diagnostics Center, Boulder, Colorado, USA, from their web site at http://www.cdc.noaa.gov/. The PATMOS-A cloud amount data are available through the Comprehensive Large Array Stewardship Site of NOAA at http://www.saa.noaa.gov. The GPCP combined precipitation data were developed and computed by the NASA/Goddard Space Flight Center's Laboratory for Atmospheres as a contribution to the GEWEX Global Precipitation Climatology Project and were obtained from the World Data Center (WDC-A) for Meteorology, Asheville. The authors' thanks go out to each of these groups for making their data available for this study.

The authors would also like to acknowledge the following people and groups for their invaluable assistance: Dr. David Thompson, for his invaluable assistance in the planning and execution of this study, and for his extremely helpful reviews of this research; Drs. Wayne Schubert and Paul Mielke for their time, input, advice, support, and tolerance; Dr. G. Garrett Campbell, whose work on the source of errors in the ISCCP trend changed the face and focus of this research and whose advice helped us to make

this work a meaningful contribution to the satellite cloud community; Sue Lini and Heather Jensen, for always making sure everything runs smoothly; and the rest of the Stephens Research Group, for their advice, questions, and support along the way that helped us to prepare a scientifically sound argument.

TABLE OF CONTENTS

CHAPTER 1: INTRODUCTION

1.1 Motivation

Recent studies by Wielicki et al. (2002), Chen et al. (2002), and Pallé et al (2004) provide evidence of a decadal-scale decrease in the cloud amount (cloud fraction) in the tropics. Wielicki et al. use data from the Earth Radiation Budget Experiment (ERBE, Barkstrom 1984) to demonstrate a decadal-scale upward trend in the tropical mean longwave (LW) flux time series since 1985. They argue that this change must be reflected in changes in the tropical cloud amount because the anomalies are a factor of 4 to 8 larger than can be explained simply by surface and atmospheric warming. Chen et al. correlate ISCCP D2 data (Schiffer and Rossow 1983) to a principal component (PC) time series that shows decadal-scale changes in the tropical and sub-tropical top-of-atmosphere (TOA) LW flux. Their results show that the change in LW flux correlates with a decrease in the cloud amount in these regions. Pallé et al. correlate measurements of the Earth's reflectance, which are deduced from measurements of the earthshine on the lunar surface, with ISCCP D1 data. Their analysis concludes that the Earth's albedo decreased from 1999-2001, but that the reflectance was then beginning to increase afterwards. These observations are apparently consistent with the ISCCP D2 global all-cloud cloud amount time series shown in Figure 1.1.

The changes evident in these data have sparked debate in recent years, since a 4 to 5% decrease in the global all-cloud cloud fraction over a 19-year record seems unreasonably large. Recent work on ISCCP data has shown that this is indeed the case

(Campbell 2004). As the number of geosynchronous satellites in orbit has changed over the course of the 19 years spanned by ISCCP, the angles at which the satellites view certain regions of the world have declined in a nearly stepwise fashion. This decline is illustrated in Figure 1.2, which shows the ISCCP D2 all-cloud cloud amount anomaly, averaged over 50°N – 50°S, with the time series of the diurnal and regional average of 1/cosine(viewing angle) with the seasonal cycle removed for the same region. This quantity, called the air mass factor, approximates the depth of the atmosphere through which the satellites are observing. The step-like changes evident in the air-mass factor appear to be concurrent with low-frequency amplitude changes in the cloud amount. Furthermore, the air mass factor explains 54% of the variance in the cloud amount time series. It is evident that the changes in this quantity are a significant source of artificial cloud amount changes in the ISCCP D2 dataset.

This phenomenon is further demonstrated by comparing the map of the ISCCP D2 all-cloud cloud amount trends (Figure 1.3(a)) with a map showing the correlation of the time series of the air mass factor at each location to the collocated ISCCP all-cloud cloud amount time series (Figure 1.3(b)). The sharpest gradients in the cloud trends are coincident with regions where changes in the air mass factor account for most of the variance in the cloud amount time series. This indicates that there are artifacts in the cloud amount data; a situation referred to hereafter as the "viewing angle problem." However, this problem has only been shown to explain roughly one-third of the slope in the all-cloud global cloud amount time series (Campbell 2004). While this result calls into question the validity of the huge slope shown in Figure 1.1, two-thirds of the trend remains unaccounted for. Therefore, it is important to understand the nature of the cloud

amount changes and to look for patterns in those changes that suggest whether they are physically reasonable or not.

In order to do this, one must first find a way to reduce or eliminate the influence of the viewing angle problem. In this study, this requirement is addressed by examining the cloud amount in an area where the cloud amount and the air mass factor are not highly correlated. In Figure 1.3(b), the region spanning 30°N to 30°S and 90°E to 180° shows a relatively low correlation between these time series due to the relatively constant satellite coverage that existed in this area. This area will be hereafter referred to as the "region of interest". Figure 1.4 shows the average ISCCP D2 all-cloud cloud amount time series for this region. Despite this attempt to account for the large trend in cloud amount, the slope of this time series is still severe. This could either mean that there is another source of error in the ISCCP cloud amount data, or it could mean that the cloud amount in this region changes a great deal between 1983 and 2001. Either way, other data must be examined for signals of this kind of cloud change before there can be any confidence in the magnitude of the changes evident in Figure 1.4.

Satellite data provide a good place to start a search for signals of cloud amount changes. Datasets based on different sensors that either measure cloud amount or variables that can be related to cloud amount provide an independent estimate of how, when, and where the cloud amount in the region of interest is changing. This is especially true of data from polar-orbiting satellites since they do not suffer from the viewing angle problem and would provide results without the influence of changes in the air mass factor. Such data would not only help confirm the presence of a long-term trend, but would also help confirm some of the patterns of change evident in the ISCCP data.

Another means of observing signals of the cloud amount is through the use of reanalysis data. It has been shown that changes in cloud amount would almost certainly have important implications for the climate system. For example, Chen et al. (2002) show that the PCs for LW flux in the tropics correlate with changes in the 500 mb vertical velocity field of the NCEP/NCAR reanalysis dataset (Kalnay et al. 1996). This suggests that there are also decadal-scale changes in the general circulation of the atmosphere, although the use of reanalysis vertical velocity data in the tropics is suspect because large-scale dynamical forcings in that region are generally weak. There is also agreement that clouds are part of an important feedback mechanism affecting tropical SST, although there is broad disagreement as to whether this mechanism is a positive or negative feedback (see Miller 1997, Pierrehumbert 1995, Lindzen et al. 2001, Lin et al. 2002, and others). In light of this, reanalysis data provide a unique and perhaps more interesting opportunity for analysis. Changes in the general circulation that correlate with the cloud amount time series would not only provide a means to verify the cloud amount trend, they would also provide information on the patterns of coupling between cloud amount in the region of interest and the climate system as a whole. Such relationships would prove valuable in understanding processes that control long-term variations in cloud amount.

1.2 Thesis goals and outline

The overall goal of this project is to understand the nature of cloud amount changes in the region of interest and their connections with changes in the general circulation of the tropical atmosphere through the use of the ISCCP D2 cloud amount dataset. In order to achieve this goal, there are several tasks that must be accomplished.

First of all, the ISCCP D2 cloud amount data are characterized in terms of where and when the cloud amount is changing in the region of interest and the types of clouds that are expressing these changes. This not only sheds light on the nature of the cloud amount changes evident in the ISCCP data, but it also provides a basis for comparison with other data in the hopes of verifying that the cloud amount changes are evident in other datasets as well. The next task is to compare these results with the NOAA Interpolated OLR (Liebmann and Smith 1996) and the PATMOS-A cloud amount datasets (Stowe et al. 2002), both of which are based on sensors mounted on polar-orbiting satellites. After that, reanalysis data are then used to look for how changes in the climate system relate to changes in the ISCCP cloud amount. These steps will not only help to verify the changes evident in the ISCCP data, but the use of reanalysis data will also help to highlight how cloud amount changes are connected to changes in the climate system.

This thesis is divided into several distinct parts covering each of the tasks outlined above. Chapter 2 describes and characterizes each of the datasets used in this study as well as the methods used to process that data and the unique analyses used to study the nature of the ISCCP trend and its connections with the climate system. Chapter 3 shows the various aspects of the ISCCP D2 cloud amount changes, including where and when they are occurring and the types of clouds expressing them. This chapter also contains a discussion of preliminary evidence showing that the patterns of change may be related to variations in the general circulation of the atmosphere. Chapter 4 then characterizes any changes shown the NOAA Interpolated OLR and PATMOS-A cloud amount datasets. These results are shown to be significantly different from the ISCCP D2 cloud amount dataset and seem to indicate that some of the changes evident in ISCCP are anomalous.

Chapter 5 presents the most interesting results of this study. Using reanalysis data, this chapter demonstrates how the general circulation of the tropical atmosphere changes in connection with variations in the ISCCP D2 all-cloud cloud amount data. It is shown that much of the variation in the ISCCP cloud amount data can be explained by fluctuations in ENSO. The reanalysis data also demonstrate that the actual changes in the circulation of the tropical atmosphere are not consistent with a statistically significant change in the cloud amount of the region of interest. In conclusion, this study shows that, while the ISCCP D2 data captures variations in cloud amount that appear to be directly related to changes in ENSO, the long-term all-cloud cloud amount trend evident in the data is not reflected in any of the other datasets and does not appear to reflect the real cloud amount changes in the region of interest.

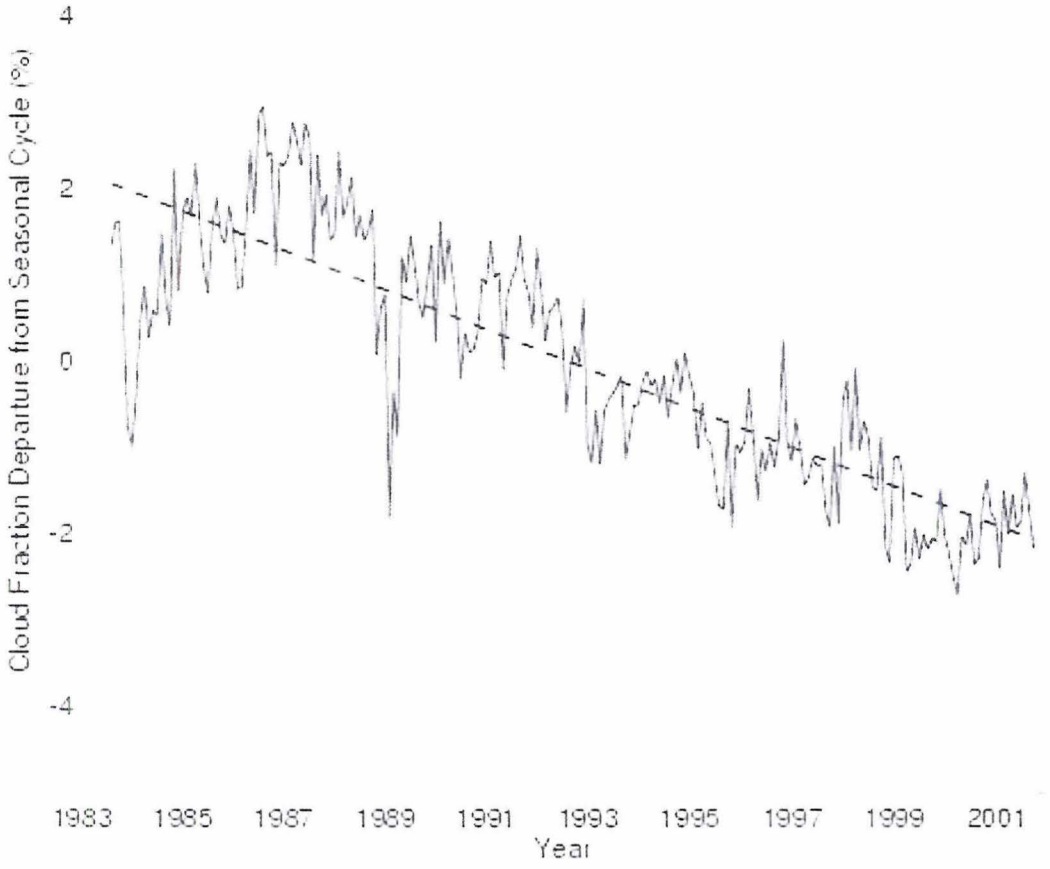

Figure 1.1: Time series of ISCCP D2 monthly mean all-cloud cloud amount with the seasonal cycle removed. The trend shown with the dotted line represents the slope of the changes in cloud amount over the entire period.

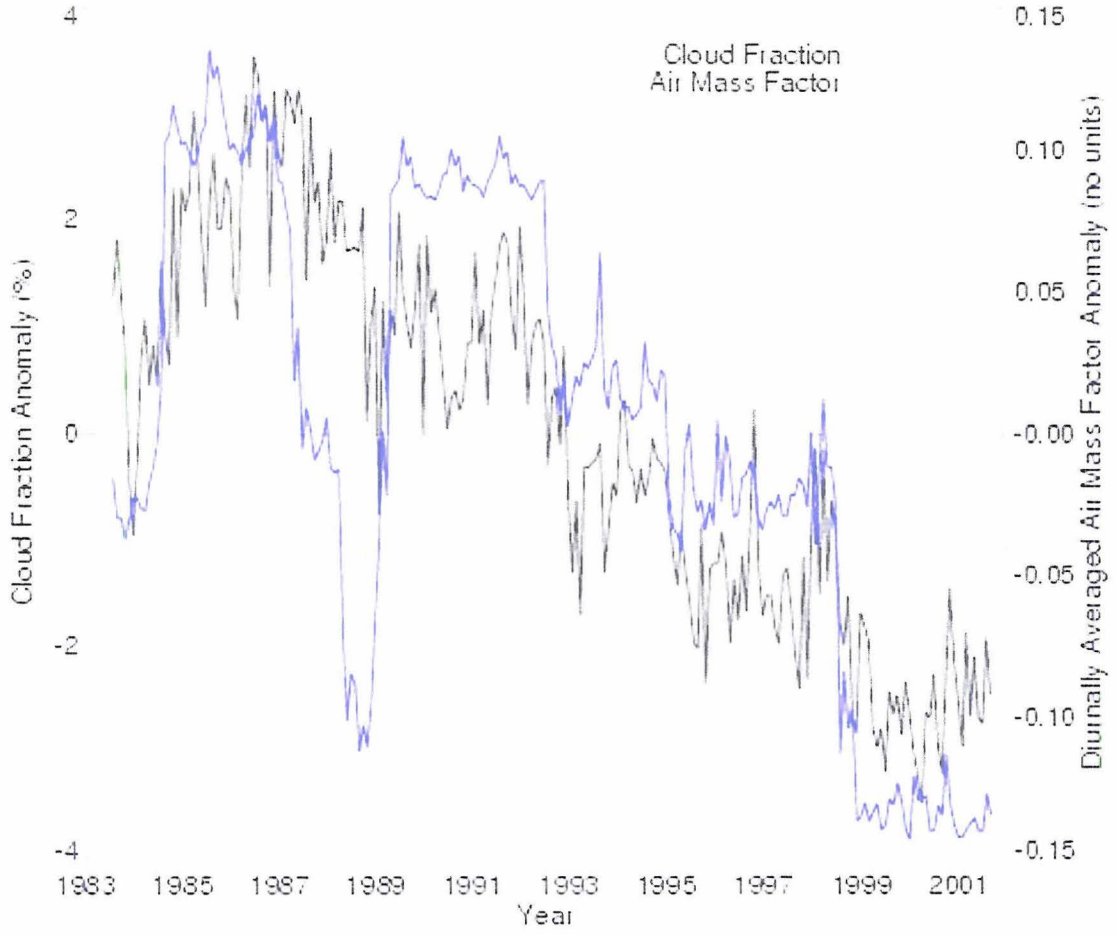

Figure 1.2: Time series of ISCCP D2 monthly mean all-cloud cloud amount anomaly from 50N to 50S (black) plotted over the anomaly time series of the diurnally averaged "air-mass factor" of the contributing satellites (blue). The air mass factor anomaly plotted above is calculated using the ISCCP D1 daily cloud data at each 3 hourly period to determine the average viewing angle for each grid point and then using:

$$amf(t) = \left\langle \sum_{\phi=50^\circ S}^{50^\circ N} \sum_{\lambda=0^\circ}^{360^\circ} \left(\frac{1}{\mu_i(\lambda,\phi,t)} \right) \right\rangle - \left\langle \sum_{\phi=50^\circ S}^{50^\circ N} \sum_{\lambda=0^\circ}^{360^\circ} \left(\frac{1}{\mu_i(\lambda,\phi,t)} \right) \right\rangle_{\text{climo}}$$

where μ is the cosine of the viewing angle each month and brackets denote the monthly average value. At the edges of the geosynchronous satellite views or when one satellite is missing for a certain time of day, some AVHRR data is used and the view angles from that satellite are mixed in. The air-mass factor thus defined accounts for 54% of the variability evident in the cloud amount time series.

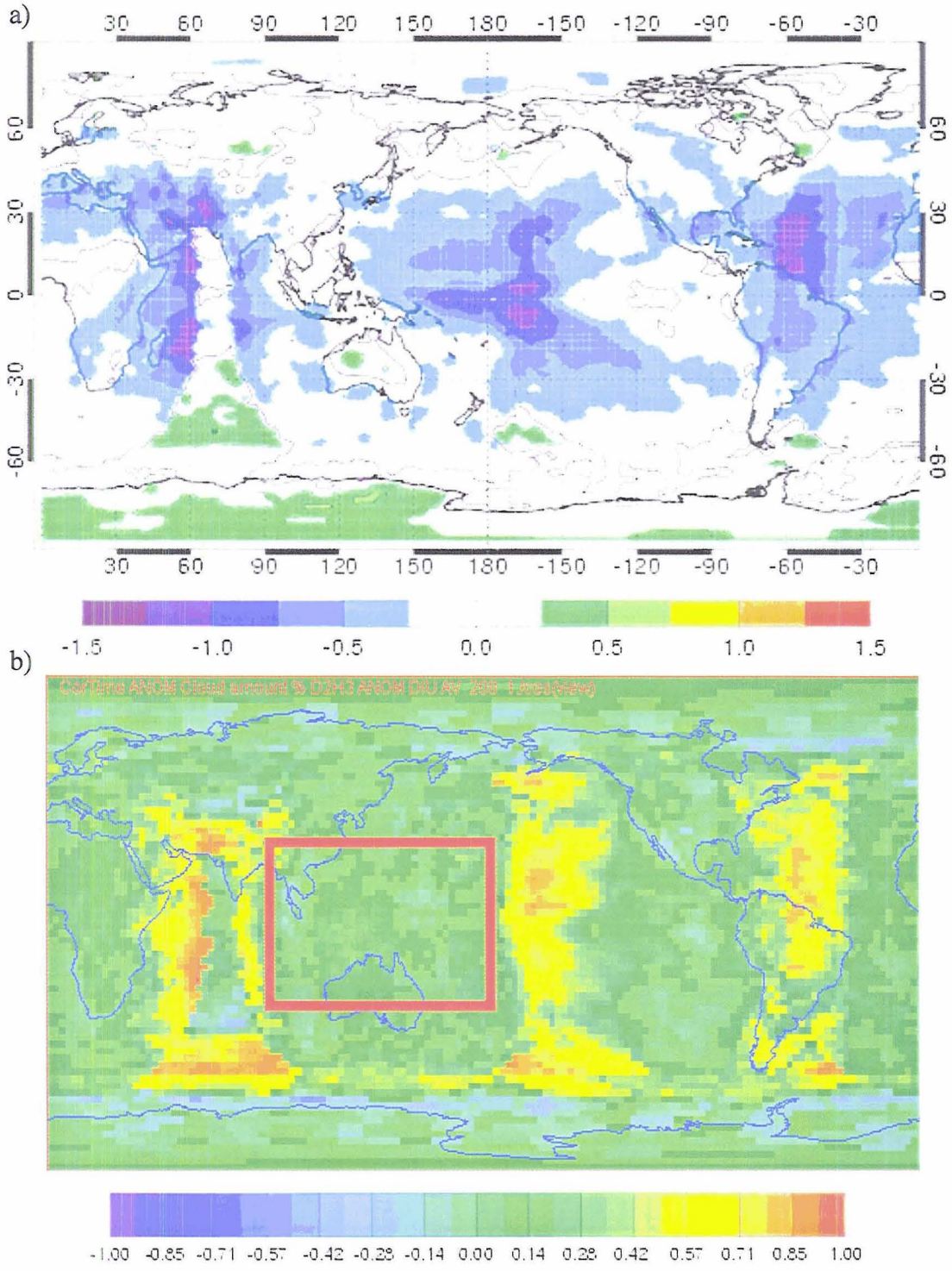

Figure 1.3: a) The ISCCP D2 all-cloud cloud amount trend from 1983-2001 (in % per year). Dotted contours indicate negative values and zero is indicated by the thickest contour; b) Map of correlation coefficients for the ISCCP D2 all-cloud cloud amount time series and 1/cosine(viewing angle) for each grid point. The box indicates the region of interest from 30°N to 30°S and 90°E to 180°.

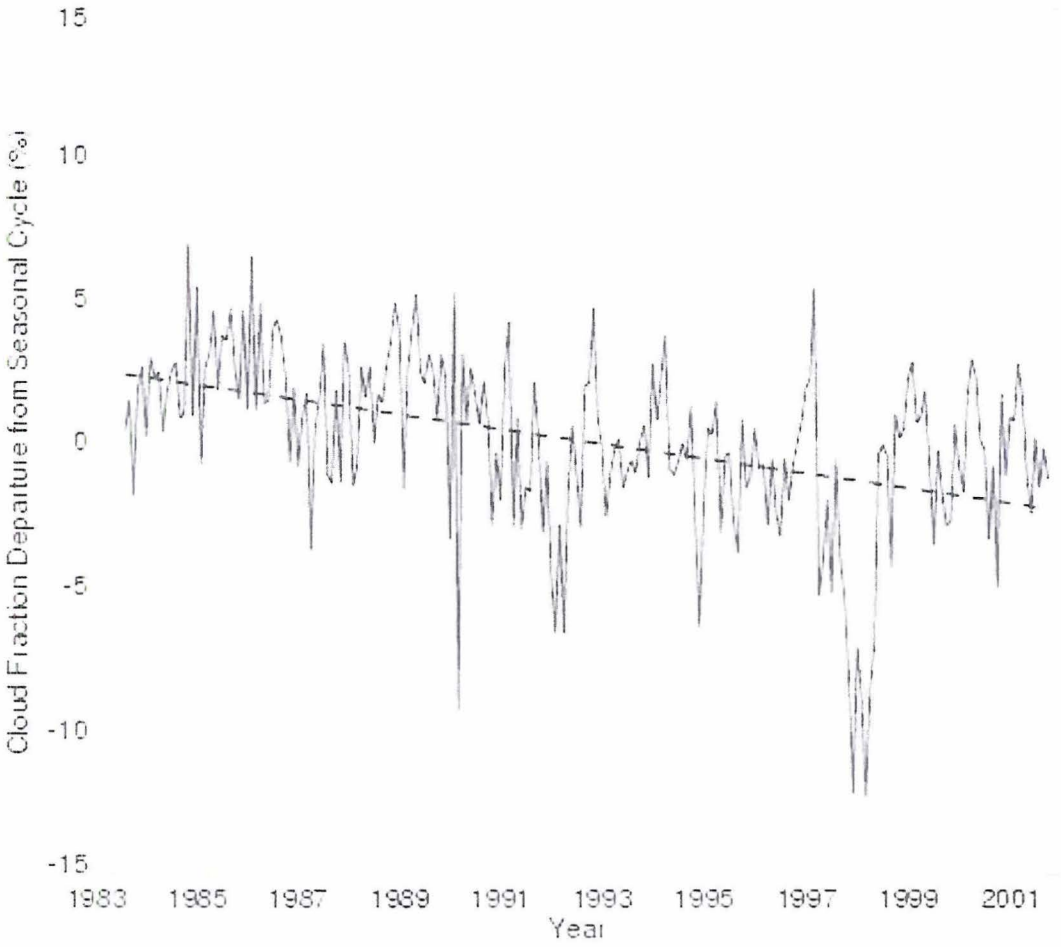

Figure 1.4: Time series showing the average ISCCP D2 all-cloud cloud amount anomaly for the region of interest (30°N - 30°S, 90°E - 180°). The slope of this time series is 0.26% yr^{-1}.

CHAPTER 2: DATA AND METHODOLOGY

2.1 Description of Data and Data Processing

This study relies on the use of both satellite observational data and atmospheric reanalysis data to validate and characterize the changes in the ISCCP D2 cloud amount and to evaluate how they are connected to changes in large-scale dynamics. Each of the datasets used in this study require different processing techniques in order to ensure that the analyses are logically consistent. In this section, each dataset is described in terms of its structure and characteristics, why it has been selected for this study, and the methods required for processing them.

2.1.1 The ISCCP D2 Cloud Climatology

The ISCCP D2 cloud dataset uses a combination of radiance measurements from up to five geostationary and two polar orbiting satellites along with NOAA TIROS Operational Vertical Sounder (TOVS) atmospheric temperature-humidity and ice/snow data to obtain information about clouds and the surface. The D2 data provides monthly averaged cloud and surface properties based on algorithms that use revised calibrations, improved cirrus detection, an improved radiative model, and improved product calculations over the C-series products produced through 1991 (Rossow et al 1996.) The resulting product is plotted on a 280 km^2 equal-area global grid that can be easily converted to a 2.5° latitude by 2.5° longitude equal-angle global grid using ancillary data

provided with the files. These data can be obtained in HDF format from the Langley Atmospheric Research Center (LARC).

The ISCCP D2 dataset includes 130 different variables at each point in the equal-area grid for each month from July 1983 through September 2001. These include mean cloud amount, cloud top pressure, cloud top temperature, cloud optical thickness, and cloud water path for all clouds at each grid point. It also provides this same information for each of 15 different cloud types, defined by cloud top pressure, optical thickness, and water phase, along with average values of these variables for all cloud types that fall into broad categories of low, middle, and high clouds. The cloud types found in the D2 dataset are defined in Table 2.1. In order to characterize the nature of the changes in the cloud amount in the region of interest, the all-cloud cloud amount and a subset of these cloud categories and types are analyzed. These categories are low cloud, middle cloud, cirrus cloud, cirrostratus cloud, and deep convective cloud (Rossow et al. 1996). While it was deemed unimportant to separate the low and middle cloud categories into more specific cloud types, high clouds are separated into distinct cloud types because deep convective clouds have a much different impact on their dynamic and thermodynamic environments than cirrus or stratocirrus clouds have. Therefore, it is important to note how each cloud type is changing when conducting a study involving cloud impacts on the climate system.

The equal-area grid on which the ISCCP D2 data are provided simplifies the process of creating a time series of the spatial-average of a given variable. This is because there is no need for weighting the data at each grid point by the cosine of the latitude at that point before calculating the average like there is for an equal-angle grid.

Therefore, creating a time series of a variable averaged over a regional or global domain only involves taking the arithmetic mean of that variable for each grid box in the region of interest. Linear regressions are then performed to quantify the slope of any changes detected in these cloud amount time series over the length of their time domain.

In order to verify the downward changes in the ISCCP D2 cloud amount time series, those changes are tested for statistical significance using the Student's t-test. In order to conduct this test, however, one first needs to know how many degrees of freedom there are in the data. Many atmospheric datasets exhibit some redness, which means that the value of a given measurement is not wholly independent of prior measurements. Wilks (1995) provides a mechanism to estimate the degrees of freedom for such a dataset, assuming that it follows a first-order autoregressive process. Using the autocorrelation at a lag of one month, Wilks uses the following relation to determine an effective sample size that reflects the number of truly independent data points:

$$N^* = N\left(\frac{1 - r(\Delta t)}{1 + r(\Delta t)}\right) \tag{1}$$

where N^* is the effective sample size, N is the original sample size, r is the lag-1 autocorrelation coefficient, and Δt is the time interval between samples. According to Figure 2.1, which shows the autocorrelation of the average ISCCP D2 all-cloud cloud amount in the region of interest as a function of lag, the lag-1 autocorrelation is 0.37. According to Equation 1, this means that there are 99 degrees of freedom in the ISCCP cloud amount time series. This estimate is applied to all of the significance tests conducted in this study since it is assumed that, because the other satellite data are related to cloud amount, they will have similar lag-1 autocorrelations and degrees of freedom.

2.1.2 NOAA Interpolated OLR

The NOAA Interpolated OLR dataset is based on estimates of the outgoing long-wave radiation from twice daily AVHRR OLR soundings on NOAA Polar Orbiting Environmental Satellites. The interpolated nature of this dataset comes from the fact that missing values are interpolated both linearly in time and spatially with neighboring grid points (Liebmann and Smith 1996). This algorithm is applied as an improvement to the original NOAA OLR dataset described by Gruber and Krueger (1984). OLR data can be used as an analog for cloud amount since OLR is related to the cloud top temperature of optically thick clouds. Therefore, an increase in OLR from a given area would be a signal of a decrease in the amount of optically thick high clouds. It will be shown in the next chapter that high clouds are responsible for most of the downward changes in the ISCCP cloud amount data, and therefore, if these changes are actually occurring they should be reflected by changes in OLR. Since these data are derived from polar-orbiting satellites, it should be free of the viewing angle problem described in the introduction, and therefore, will serve as an independent verification of the changes in cloud amount exhibited by the ISCCP D2 cloud amount dataset.

The NOAA Interpolated OLR dataset is plotted on a 2.5° x 2.5° equal-angle grid, and is available from June 1974 through the present in NetCDF format from the Climate Diagnostics Center (CDC) of NOAA. For this study, the monthly mean OLR data from July 1983 to September 2001 are selected in order to coincide with the temporal coverage of the ISCCP D2 dataset. Because the OLR dataset is plotted on an equal-angle grid, spatial averages require weighting the data by the cosine of the latitude at the center of each grid box to account for the fact that the area of the globe covered by an equal-angle

grid box decreases with distance from the equator. Otherwise, the procedures for analyzing the OLR data are the same as for the ISCCP D2 data.

2.1.3 AVHRR Pathfinder Atmosphere (PATMOS-A) Project Cloud Amount

The AVHRR Pathfinder Atmosphere Project (PATMOS-A) is part of the NOAA-NASA Pathfinder project. It uses five-channel AVHRR data from NOAA Polar Orbiting Environmental Satellites to produce a long-term record of atmospheric products covering the period from September 1981 through December 1999. This dataset includes channel reflectances, infrared reflectances, components of the earth's radiation budget at the top of the atmosphere, OLR, absorbed solar radiation, and total cloud amount (Stowe et al. 2002). The PATMOS processing system is based on the Clouds from AVHRR Phase-1 (CLAVR-1) algorithm (Stowe et al. 1999). The cloud amount from PATMOS-A tends to be about 10-15% less than that given by the ISCCP D2 data, which is believed to be caused by differences in the way the two algorithms classify partially cloud-filled or overcast pixels with variable cloud heights and thicknesses (Stowe et al. 2002). This offset should not affect this study since it focuses on long-term changes in the cloud amount and not absolute measurements of the cloud amount.

The PATMOS-A data used in this study was obtained by request from the Comprehensive Large-Array Stewardship Site of NOAA NESDIS in NetCDF format for the period from July 1983 through December 1999. The monthly mean cloud amount data are plotted on a 1° x 1° equal-angle grid, which means that spatial averages must employ cosine weighting as described in the previous section. The data for each month comes in two files, one each for the ascending (mostly daytime) and descending (mostly nighttime) nodes. The ascending node is affected by the gradual shifting of the

equatorial-crossing times of the satellite platforms since gradual changes in the solar zenith angle may introduce a trend in any algorithms using visible channels to deduce cloud amount (G.G. Campbell, personal communication). Therefore, in order to avoid introducing an anomalous trend to the analysis, only the descending node data are used in calculating the time series of cloud amount. Finally, because this dataset is derived solely from polar-orbiting satellites, it also should not be affected by the viewing angle problem the way the ISCCP D2 data are, and can therefore be to evaluate the presence of a long-term change in the cloud amount in the region of interest.

2.1.4 NCEP/NCAR 40-Year Reanalysis

The NCEP/NCAR 40-Year Reanalysis provides a global analysis of atmospheric data fields that spans more than four decades designed to support the climate modeling and research communities. It assimilates quality-controlled land surface, rawinsonde, pibal, ship, aircraft, and satellite observational data into an operational model designed to calculate several variables at 17 different pressure levels, plus the surface and tropopause (Kalnay et al. 1996). These data are available in NetCDF format from the Climate Diagnostics Center (CDC) and covers the period from January 1948 through the recent past and is plotted on a 2.5° x 2.5° equal-angle grid.

For this study, reanalysis fields from July 1983 through September 2001 were selected to examine correlations in the changes of the general circulation of the atmosphere with changes in the ISCCP D2 cloud amount. These include 200 mb zonal wind, 200 mb meridional wind, 850 mb zonal wind, 850 mb meridional wind, and sea level pressure. Vertical velocity reanalysis data are often problematic because of the lack of large-scale dynamical forcings in the tropics. Therefore, divergence is used to identify

large-scale vertical motions that are correlated with changes in cloud amount. The divergence at each grid point is calculated on both the 200 mb and 850 mb levels by applying a finite-differencing scheme to the zonal and meridional wind fields at each level. Where regions of divergence aloft are collocated with regions of convergence at low levels, one can assume by continuity that there is upward vertical motion occurring. Conversely, downward motion is implied where convergence aloft is collocated with divergence at low levels. Finally, it will be shown that there is a connection between changes in the ISCCP time series and changes in the El Niño – Southern Oscillation (ENSO). As this connection became apparent, the 200 mb and 850 mb geopotential height fields were examined in order to identify regions where the redistribution of convective heating associated with ENSO has led to greater 850-200 mb thicknesses in accordance with the results found by Horel and Wallace (1981).

2.1.5 ECMWF 40-Year Reanalysis (ERA-40)

The European Centre for Medium-range Weather Forecasting (ECMWF) developed the ERA-40 40-year Reanalysis to assimilate observational data into their global forecasting model to create a record describing the state of the atmosphere and land and ocean-wave conditions from mid 1957 through 2001 (Simmons and Gibson 2000). Similar to the NCEP/NCAR Reanalysis described in the previous section, the ERA-40 project ingests surface, upper-air, and satellite data into their model to produce consistent pictures of how the atmosphere is behaving. These reanalyses are also available on 2.5° x 2.5° equal-angle grids and are available in both GRIB and NetCDF format from the ECMWF Data Center online.

This dataset was used to provide an independent verification of the results found using the NCEP/NCAR reanalysis data, since ERA-40 uses different forecast and data assimilation procedures. For this reason, the same meteorological fields as those selected from the NCEP/NCAR reanalysis were also selected from the ERA-40 dataset: 200 mb zonal winds, 200 mb meridional winds, 200 mb geopotential heights, 850 mb zonal winds, 850 mb meridional winds, 850 mb geopotential heights, and sea level pressure. The ERA-40 dataset does not actually report geopotential heights, but rather geopotentials, which are converted to geopotential height by dividing by **g**, the gravitational acceleration constant at sea level. The ERA-40 dataset also provides divergence fields that have already been calculated, so that the 200 mb and 850 mb divergence fields can be downloaded "as is" without the need for any additional preprocessing.

It should be noted, however, that difficulties arise when ERA-40 data are used to calculate long-term trends. Bengtsson et al. (2004) demonstrate that changes in the data assimilation system for ERA-40, specifically in the amount and type of satellite information ingested, may have introduced anomalous trends in the temperature, integrated water vapor, and kinetic energy fields. They point specifically to two changes: the significant upgrade to the satellite observing system that began in 1979 and the addition of more extensive Special Satellite Microwave Imager (SSM/I) data around 2000. Obviously, the first change is not relevant to this study since the temporal coverage of ISCCP begins in 1983. The second was documented to have had an effect on temperature, which means that there is a possibility that this may have cascaded into other fields, including ones selected for this study. While this should have no effect on

most of the analyses in this study since in many cases the data were detrended first, it could have an impact on calculating trends using only ERA-40 data. No study has yet explored whether this effect is evident in the NCEP/NCAR dataset. While the NCEP/NCAR reanalysis also ingests SSM/I surface wind speed data, there has been no report of similar problems. In fact, Kistler et al. (2001) show that there are noted differences between temperature trends of the NCEP/NCAR and ERA-15 reanalyses. Therefore, when trends in reanalysis fields are calculated, only the NCEP/NCAR data are used.

2.1.6 Precipitation Datasets

Two different reanalysis datasets were used to examine connections between the ISCCP D2 cloud amount time series and precipitation: the Global Precipitation Climatology Project (GPCP) version 2 combined precipitation dataset (Huffman et al. 1997) and the Climate Prediction Center (CPC) Merged Analysis of Precipitation (CMAP; Xie and Arkin 1997). Both datasets merge rain gauge observations with satellite observations to create global climatologies of precipitation. The CMAP dataset, however, uses more observational data sources (6 versus 3 for the GPCP data) and also ingests NCEP/NCAR reanalysis precipitation forecasts in its merging algorithm. Thus, these data are different enough that both provide independent analyses of rainfall. The GPCP dataset is provided as yearly unformatted binary files containing 12 monthly 2.5° x 2.5° equal-angle grids. These can be obtained from the World Data Center (WDC-A) for Meteorology, Asheville. The CMAP data are provided as NetCDF files on 2.5° x 2.5° equal-angle grids as well, and can be obtained from the CDC.

2.1.7 Other Datasets

There were two other datasets used in this study. The first is the NOAA Optimal Interpolation version 2 SST (OI v.2 SST) dataset (Reynolds et al. 2002). These data were used to explore connections between the ISCCP D2 cloud amount and the variability of SST in the tropics. It is available in a 1° x 1° equal-angle grid from 1981 through present and is available in ASCII format from the CDC. The other dataset used in this study is the Niño-3.4 Index for the El Niño – Southern Oscillation (Trenberth and Stepaniak 2001). This index is based on SST anomalies in the Niño-3.4 region (defined as 5°N – 5°S, 170°-120°W), and generally indicates the presence of El Niño events when the value of this index exceed 0.4°C. Data covering the period from July 1983 through September 2001 are used to evaluate the connection between the ISCCP D2 cloud amount and ENSO.

2.2 Overview of Analysis Methodology

This project can be divided into two distinct types of analysis because each involves a completely different methodology. The first involves characterizing the ISCCP D2 cloud amount changes in the region of interest and then verifying these changes by comparing them with characterizations based on the OLR and PATMOS-A data. Meanwhile, the second half of this study uses the various reanalysis data for two purposes: to confirm or deny the presence of an ISCCP all-cloud cloud amount trend and to explore the relationships between the changes in the ISCCP all-cloud cloud amount and each of the reanalysis fields. In this section, the methodologies for each part of the analysis are described in detail.

2.2.1 Characterization and Evaluation of ISCCP Changes

The process of characterizing the changes in the ISCCP D2 cloud amount in the region of interest involves examining how, when, and where the cloud amount is changing. The first step of this process requires calculating time series of how the regionally averaged total cloud amount is changing and a map of the linear regression coefficients that shows where those changes are largest for the all-cloud cloud amount and each of the 5 categories listed in section 2.1.1. These time series are tested to see of their slopes are significantly different from zero using a two-tailed Student's t-test at the 95% confidence level with 99 degrees of freedom using the coefficient of correlation between the time series in question and the linear best-fit line. In order to determine when the changes are largest, the regionally averaged all-cloud cloud amount time series is subdivided into 12 time series representing how the cloud amount changes from year to year for each month. Linear regressions are performed on each of these time series to determine the slope of those changes.

Once the ISCCP changes have been characterized, these procedures are then applied to both the NOAA OLR and PATMOS-A data by calculating the regional average time series, calculating maps of where each dataset is changing, and then calculating when those changes are strongest. These results are then used to independently verify the characteristics of the ISCCP changes. The regionally averaged time series of OLR and PATMOS-A are also correlated to the ISCCP cloud amount time series to see how much of the variance in ISCCP is also captured by the other datasets. However, when examining the correlations of two independent time series, it must be noted that the presence of trends in both will lead to anomalously high correlations even when the time series are not physically related. Therefore, before calculating

correlations, the linear trends in the time series were removed, leaving time series that describe variations about those trends. Furthermore, because the presence of seasonal cycles in two otherwise independent time series might also cause anomalously high correlations, the monthly climatologies of each of these three datasets were calculated and removed from the data. After performing both of these operations, the resulting time series describe departures from their respective seasonal cycles as well as variations about their trends. These time series, hereafter called "anomaly time series," can then be correlated to examine how they are related.

2.2.2 Utilization of Reanalysis Data to Evaluate ISCCP Changes and Their Connections to Large-Scale Dynamics

As mentioned previously, the second part of this study uses reanalysis data to both independently verify how the cloud amount is changing in the region of interest and study how changes in the ISCCP cloud amount are associated with changes in the general circulation of the tropics. In order to accomplish this, three important questions must be answered. First of all, what are the patterns of change in the reanalysis fields associated with changes in the ISCCP cloud amount? Then, which of those patterns are significantly correlated with the cloud amount changes? And finally, have the patterns of change in the reanalysis field indicated that the cloud amount must be changing in a significant way? The methodology that follows allows each of these questions to be explored simultaneously.

Initially, the reanalysis data listed in sections 2.1.4–2.1.7 are used to generate anomaly maps for each field and for each month by removing the monthly climatology from each of the monthly maps for a given field. This also creates time series of changes

in the anomaly field at each grid point if one looks at variations along the time domain. The anomaly time series of the ISCCP D2 cloud amount for the region of interest is then regressed onto and correlated with the anomaly time series at each location, generating maps of both regression and correlation coefficients. The map of the regression coefficients shows where and by how much a given field changes with a one-percent increase in cloud amount while the map of correlation coefficients shows how the time series of the reanalysis data at each point correlate with the anomaly time series of cloud amount. By applying a one-tailed Student's t-test at the 95% confidence level and 99 degrees of freedom to the map of correlation coefficients, one can also determine which regression coefficients are statistically significant. A one-tailed test is used because there is an *a priori* expectation for what sign the regression coefficients will take based on the overall spatial patterns shown by the regression map. These maps can then help to answer the questions of what the patterns of change look like as well as which changes are correlated with the ISCCP D2 cloud amount in the region of interest.

The regression coefficient map is also used to answer the question of whether the reanalysis data indicate that the cloud amount in the region of interest has actually changed. First of all, if maps of the trends in the NCEP/NCAR reanalysis fields show similar spatial patterns to the regression coefficient maps, this can be used to draw conclusions about the sign and magnitude of the actual cloud amount changes in the region of interest and reinforce any conclusions drawn from looking at the satellite data from the first part of this study. Therefore, trend maps were calculated for each of the NCEP/NCAR reanalysis fields for comparison with the respective regression maps. Taking the inner product of the regression coefficient map, weighted by the cosine of the

latitude of the center of each grid box, with the corresponding anomaly map for each month of the time series results in an expansion coefficient time series that shows how strongly the anomaly field reflects the pattern of the regression map over time. As the regression map shows how a field changes in response to increasing cloud amount, this time series then reflects how the cloud amount in the region of interest is actually changing. For example, an increase in the expansion coefficient time series would indicate that the regression map pattern is expressed more strongly by the anomaly reanalysis field with time. By proxy, the true cloud amount in the region of interest must then be increasing with time. Therefore, this time series will hereafter be referred to as a "proxy cloud time series" corresponding to that field. Finally, since we are using the anomaly time series of ISCCP cloud amount, there is no trend in the cloud amount data. Therefore, any statistically significant trend in the proxy cloud time series will only reflect actual changes in the average cloud amount of the region of interest.

Finally, it is acknowledged that reanalysis data ingest selected satellite information to calculate various fields, especially over the oceans where there is a dearth of surface-based data. If unaccounted for, this could lead to the presence of artificially high correlations between the reanalysis and satellite data. However, the use of a combination of different reanalysis products likely minimizes any impact this may have on our ability to verify the presence of a trend in the ISCCP cloud amount. Thus, the analyses included in this methodology should produce robust conclusions about how the ISCCP D2 cloud amount dataset is changing in the region of interest, whether those changes reflect how the cloud amount is truly changing in that same region, and how those changes are connected with changes in the general circulation of the atmosphere.

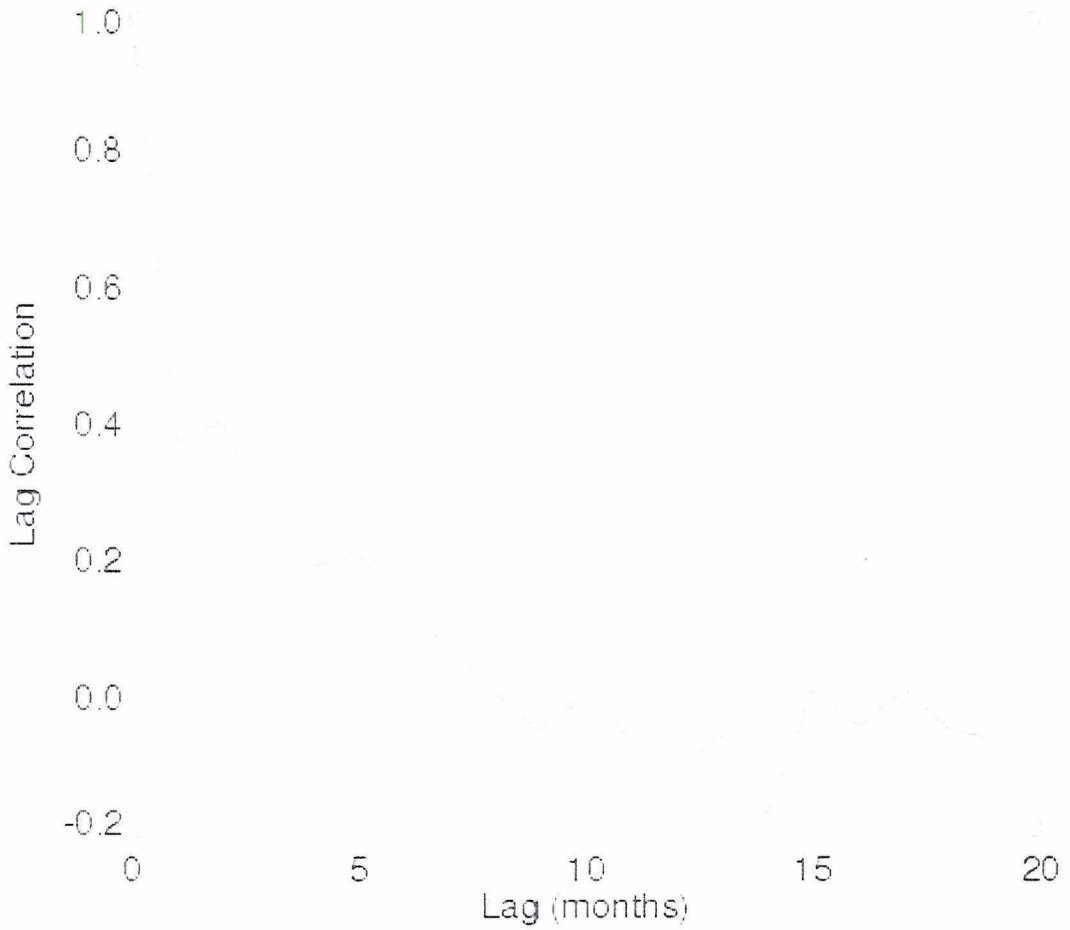

Figure 2.1: Autocorrelation of the ISCCP D2 total cloud amount anomaly time series as a function of lag. The dotted line represents the e-folding time scale, which indicates the value below which lag correlations demonstrate a sufficient lack of memory to be considered independent.

Table 2.1: Definitions of the ISCCP D2 cloud amount types as specified in Rossow and Schiffer (1991)

Cloud Type	Optical Depth	Cloud Top Pressure (mb)	Liquid Phase
Cumulus	$0.02 \leq \tau \leq 3.55$	$p > 680$	Liquid
Cumulus	$0.02 \leq \tau \leq 3.55$	$p > 680$	Ice
Stratocumulus	$3.55 < \tau \leq 22.64$	$p > 680$	Liquid
Stratocumulus	$3.55 < \tau \leq 22.64$	$p > 680$	Ice
Stratus	$\tau > 22.64$	$p > 680$	Liquid
Stratus	$\tau > 22.64$	$p > 680$	Ice
Low Cloud	**$0.02 \leq \tau \leq 378.65$**	**$p > 680$**	**Liquid and Ice**
Altocumulus	$0.02 \leq \tau \leq 3.55$	$440 < p \leq 680$	Liquid
Altocumulus	$0.02 \leq \tau \leq 3.55$	$440 < p \leq 680$	Ice
Altostratus	$3.55 < \tau \leq 22.64$	$440 < p \leq 680$	Liquid
Altostratus	$3.55 < \tau \leq 22.64$	$440 < p \leq 680$	Ice
Nimbostratus	$\tau > 22.64$	$440 < p \leq 680$	Liquid
Nimbostratus	$\tau > 22.64$	$440 < p \leq 680$	Ice
Middle Cloud	**$0.02 \leq \tau \leq 378.65$**	**$440 < p \leq 680$**	**Liquid and Ice**
Cirrus	**$\tau \leq 3.55$** **$\tau \leq 9.38$**	**$310 < p \leq 440$** **$p \leq 310$**	**Ice**
Stratocirrus	**$3.55 < \tau \leq 22.64$** **$9.38 < \tau \leq 22.64$**	**$310 < p \leq 440$** **$p \leq 310$**	**Ice**
Deep Convection	**$\tau > 22.64$**	**$p \leq 440$**	**Ice**
High	$0.02 \leq \tau \leq 378.65$	$p \leq 440$	Ice

Boldface indicates that this cloud type was included in this study

CHAPTER 3: CHARACTERIZATION OF THE ISCCP D2 CLOUD AMOUNT TREND

3.1 Introduction

This chapter describes the characteristics of the ISCCP D2 cloud amount changes in the region of interest obtained using the data and methods described in the previous chapter. This includes showing where the all-cloud cloud amount is changing, how much it is changing, and whether those changes have a seasonal dependence. It also demonstrates how those attributes vary by cloud type so that it is possible to determine if certain kinds of clouds are dominating the overall cloud amount trends. Using these results, it is possible to draw some preliminary conclusions about the kinds of mechanisms that might be associated with the evident changes and develop expectations about what the remainder of the analysis should show if these changes are in fact real.

3.2 Changes in the total cloud amount

Following the procedure outlined in Section 2.2, the average all-cloud cloud amount change for the region of interest (90°E – 180°, 30°N – 30°S) is calculated as a function of time. This time series, which is first displayed as Figure 1.4, is reproduced as Figure 3.1. The slope of the linear fit to this time series is -0.26% yr^{-1}, which translates to a 2.6% decrease per decade. The t-score for this trend is -5.77, which exceeds the critical t-score of -2.00. Therefore, the downward trend in these data is statistically significant at the 95% confidence level. While there is a lot of small amplitude, high-frequency variability, there are also some large excursions from the linear trend evident in the time

series. Most notable is the downward excursion in 1997-8, which coincides with the large El Niño event that occurred around the same time. This could be an indication that there is a connection between the cloud amount in the region of interest and ENSO. As we proceed through the various analyses in this study, we will come back to this point several times and hope to build a case that demonstrates that ENSO is indeed related to each of the large excursions evident in the all-cloud cloud amount time series.

Figure 3.2(a) shows the spatial distribution of the all-cloud cloud amount trend in the region of interest. The most significant downward trends are located over open ocean eastward of 150°E longitude, with the primary center of action located just south of the Equator and a secondary center of action located around 15°N latitude. Over land, the all-cloud cloud amount is shown to be slightly increasing with time, but over the water and much of the maritime continent the cloud amount is decreasing with time. The pattern of downward trends in the eastern portion of Figure 3.2(a) is consistent with the location of the Inter-Tropical Convergence Zone (ITCZ) as determined by the satellite climatology of Waliser and Gautier (1993). This suggests that the amount of convection in the ITCZ over the West Pacific Ocean could be decreasing, or that the distribution of convection in the ITCZ is changing in such a way as to cause an apparent decrease in the all-cloud cloud amount associated with the ITCZ. Figure 3.2(b) shows that these featured changes are significantly different from zero at the 95% confidence level.

Figure 3.3(a) shows how the zonal mean all-cloud cloud amount trend varies as a function of month of year. From this figure, it appears that the strongest negative trends occur from August through December for the cloud amount at and just south of the Equator. Meanwhile, the trends in the all-cloud cloud amount near 15 – 20°N are

strongest from March through June. Beginning in May and running through October, there is an oscillatory behavior to the trends in the region around 20°N that seems suspect. This feature, along with all of the others noted in this chapter, will be readdressed when the ISCCP data are compared with other satellite data in Chapter 4. Figure 3.3(b) indicates that these features are statistically significant.

The pattern of the strongest trends appears to be out of phase with the undulation of the ITCZ. In April, the ITCZ is often found near the Equator and is just beginning to move northward in the Western Pacific, but it doesn't often get to 15°N until late summer and early fall and is back down near the Equator by January (Waliser and Gautier 1993). Thus, the trends in the ISCCP D2 cloud amount seem to be strongest when the ITCZ is elsewhere. This would seem to contradict the previous conclusion that the strength of the ITCZ convection is changing. However, by examining how the amounts of different cloud types are changing, a resolution to this contradiction can be found.

3.3 Changes in cloud amount for individual cloud types

In order to further investigate the ISCCP D2 cloud amount trend, it is broken down into the five cloud type categories described in Chapter 2: low cloud, middle cloud, cirrus cloud, cirrostratus cloud, and deep convective cloud. Figure 3.4 shows the time series of the average cloud amount in the region of interest for each of these categories. Table 3.1 lists characteristics of these changes, including the slopes of the linear fits to each time series and the t-scores for those slopes. From these data, it is apparent that low cloud and cirrus cloud changes are dominating the all-cloud cloud amount changes evident in Figure 3.1, though all of the cloud types listed are changing in a statistically significant manner at the 95% confidence level.

Figure 3.5 shows the spatial distributions of the trends for each cloud type, similar to Figure 3.2(a) and Figure 3.7 shows the zonal mean cloud amount changes as functions of latitude and month, similar to Figure 3.3(a). Figures 3.6 and 3.8 present evidence of the statistical significance of Figures 3.5 and 3.7 respectively. From these figures, it is apparent that the cloud amount changes occurring around 15°N in the spring and early summer are primarily low cloud changes, while the cloud amount changes occurring near the equator in the fall and early winter are primarily cirrus cloud changes. However, there is also a signal of decreasing cirrus cloud amount at 15°N latitude from January through July shown in Figure 3.7. It is impossible to say whether there is or is not a low cloud amount change near the equator in the northern hemisphere winter because, due to the preponderance of cirrus cloud near the Equator, the satellites will not be able to detect emissions from low clouds since that radiation would be masked by the optically thick high level clouds.

If one focuses on the cirrus clouds and assumes that the cirrus cloud in this region is a signal of the cirrus anvils of convective clouds, then one could argue that the decrease in cirrus cloud away from the location of the ITCZ is an indication of decreased anvil coverage in the tropics. This could indicate a decrease in the amount of convection in the ITCZ. The portion of Figure 3.7 that corresponds to deep convective cloud does indicate a small decrease in deep convection near the Equator from November to April, which may be consistent with this conclusion. However, there is no corresponding decrease in deep convective cloud near 15°N from May through October. Instead, the deep convective cloud shows more of the strange oscillatory trend pattern mentioned previously in regard to Figure 3.3(a). Therefore, it would be difficult to say for certain

that there is a decrease in ITCZ related convection using ISCCP cloud amount alone. This is another point that will be revisited in the subsequent chapters.

3.4 Conclusions

It has been shown that the character of the ISCCP D2 cloud amount changes in the region of interest indicates a possible change in the strength and/or spatial distribution of ITCZ convection in the Western Pacific Ocean. Overall, the cloud amount is changing by 2.6% per decade and is predominately driven by changes in low and cirrus clouds. The spatial distribution of these trends seem to indicate that the trends are strongest when the ITCZ is located elsewhere and may reflect changes in the spatial coverage of the cirrus anvils associated with ITCZ convection. However, there are inconsistencies with this conclusion because the deep convection data do not wholly corroborate the cirrus cloud data and because this conclusion does not explain the low cloud changes located at 15°N. Therefore, the characterization of the ISCCP D2 cloud amount changes is incomplete without looking toward independent data sources for additional information.

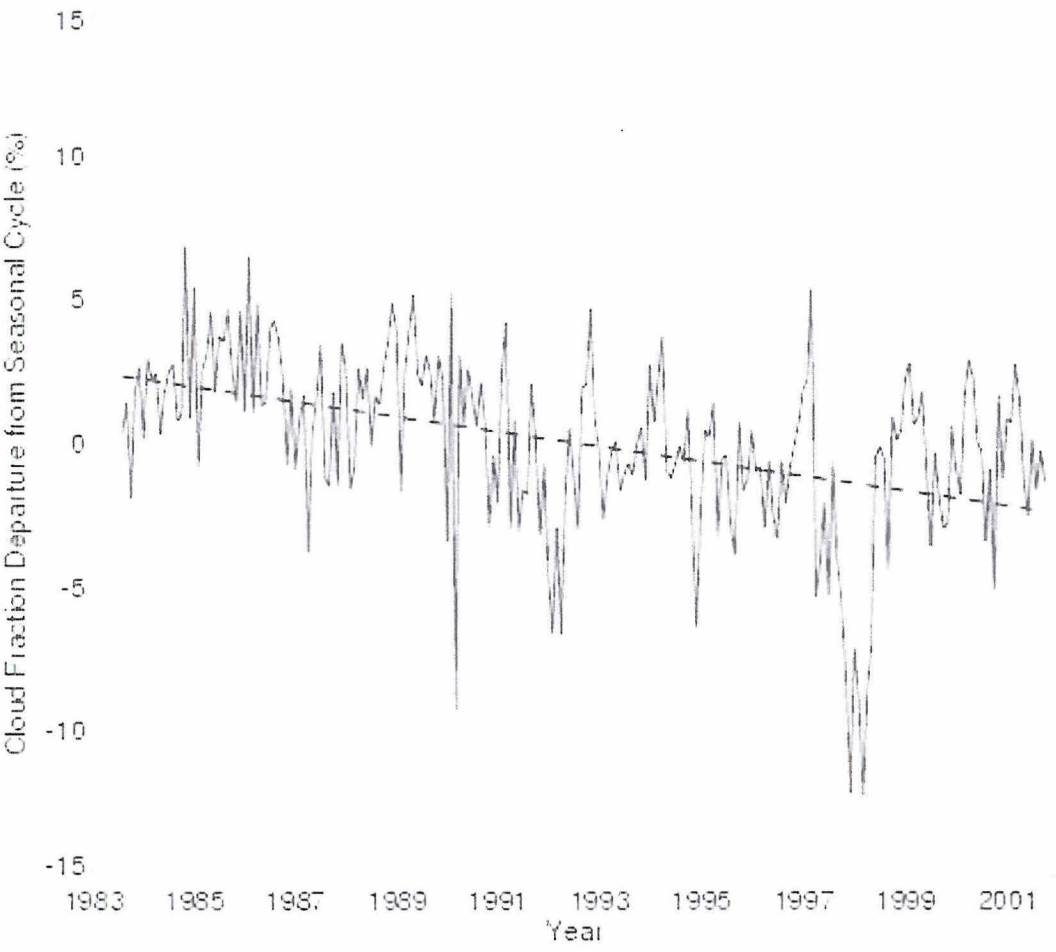

Figure 3.1: Time series showing the average ISCCP D2 all-cloud cloud amount anomaly for the region of interest (30°N - 30°S, 90°E - 180°). The slope is 0.26% yr^{-1}. This is the same as Figure 1.4, reprinted for convenience.

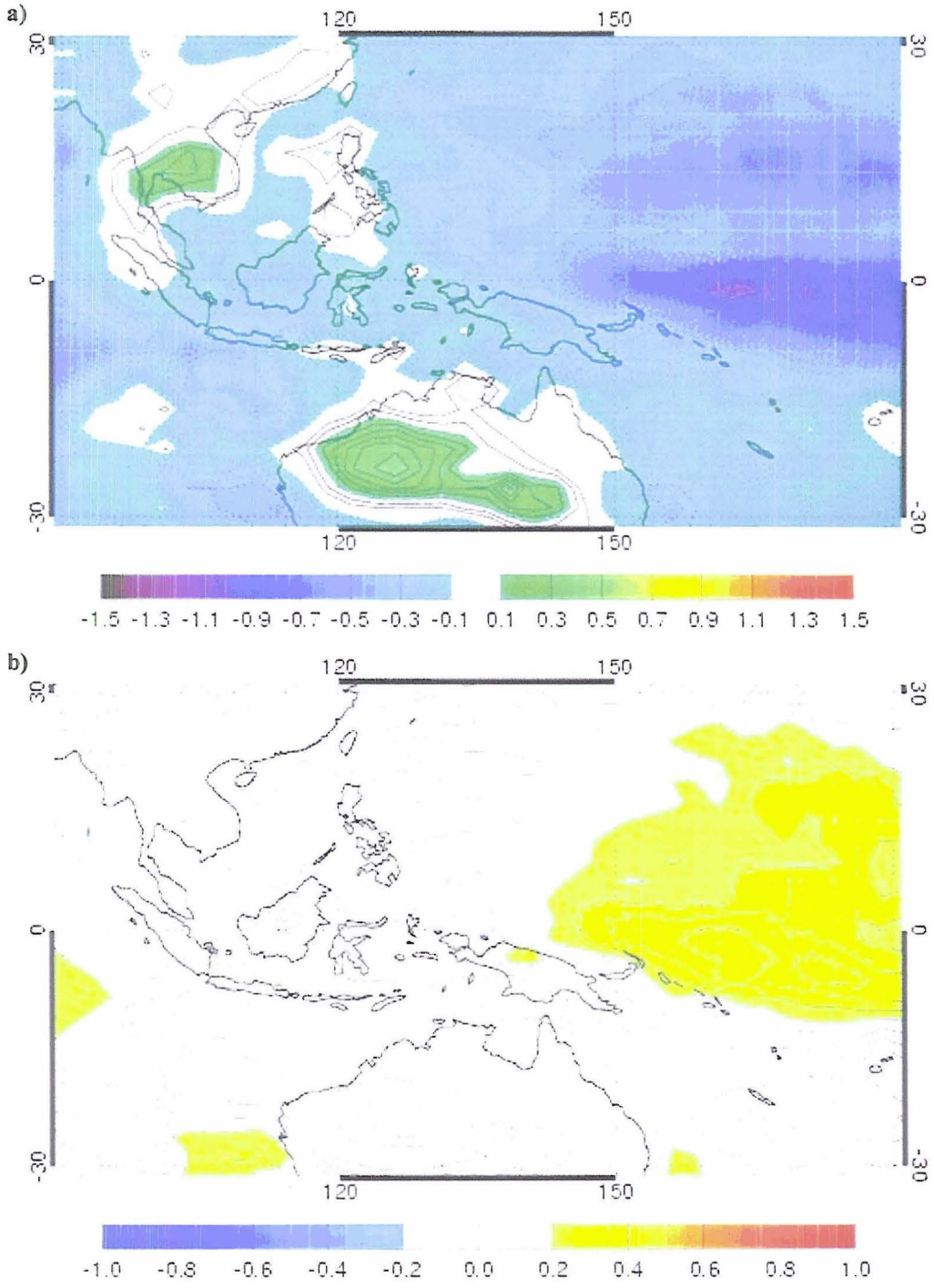

Figure 3.2: (a) Map of ISCCP D2 all-cloud cloud amount trends (in % yr^{-1}) for the region of interest (30°N – 30°S, 90°E – 180°). The contour interval is 0.05% yr^{-1}. Negative values are contoured with dotted lines and zero is represented by the thickest contour. (b) Map of coefficients of correlation between the ISCCP D2 all-cloud cloud amount time series and the corresponding linear best-fit trend at each point. Colored regions indicate where the trends from (a) are significantly different from zero (the absolute value of the t-score exceeds 2.00).

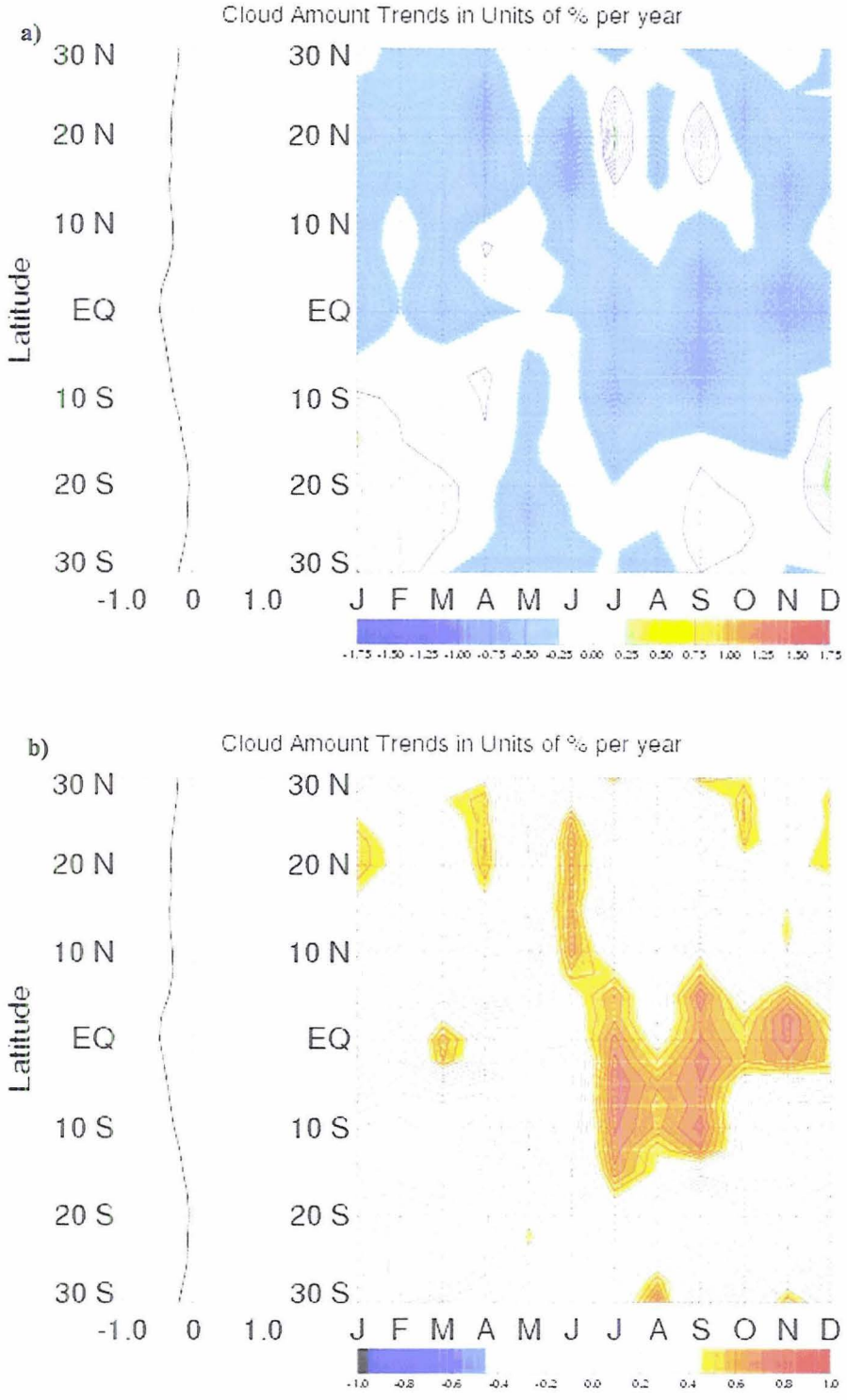

Figure 3.3: (a) Zonal mean ISCCP D2 all-cloud cloud amount trends as functions of latitude (left) and latitude and month of year (right) for the region of interest. Contour interval is 0.05% yr^{-1}. Negative values are shown with dotted contours and zero is represented by the thickest contour; (b) Map of coefficients of correlation between the ISCCP D2 all-cloud cloud amount monthly time series and the corresponding linear best-fit trend at each latitude. Colored regions indicate where the trends from (a) are significantly different from zero (the absolute value of the t-score exceeds 2.11).

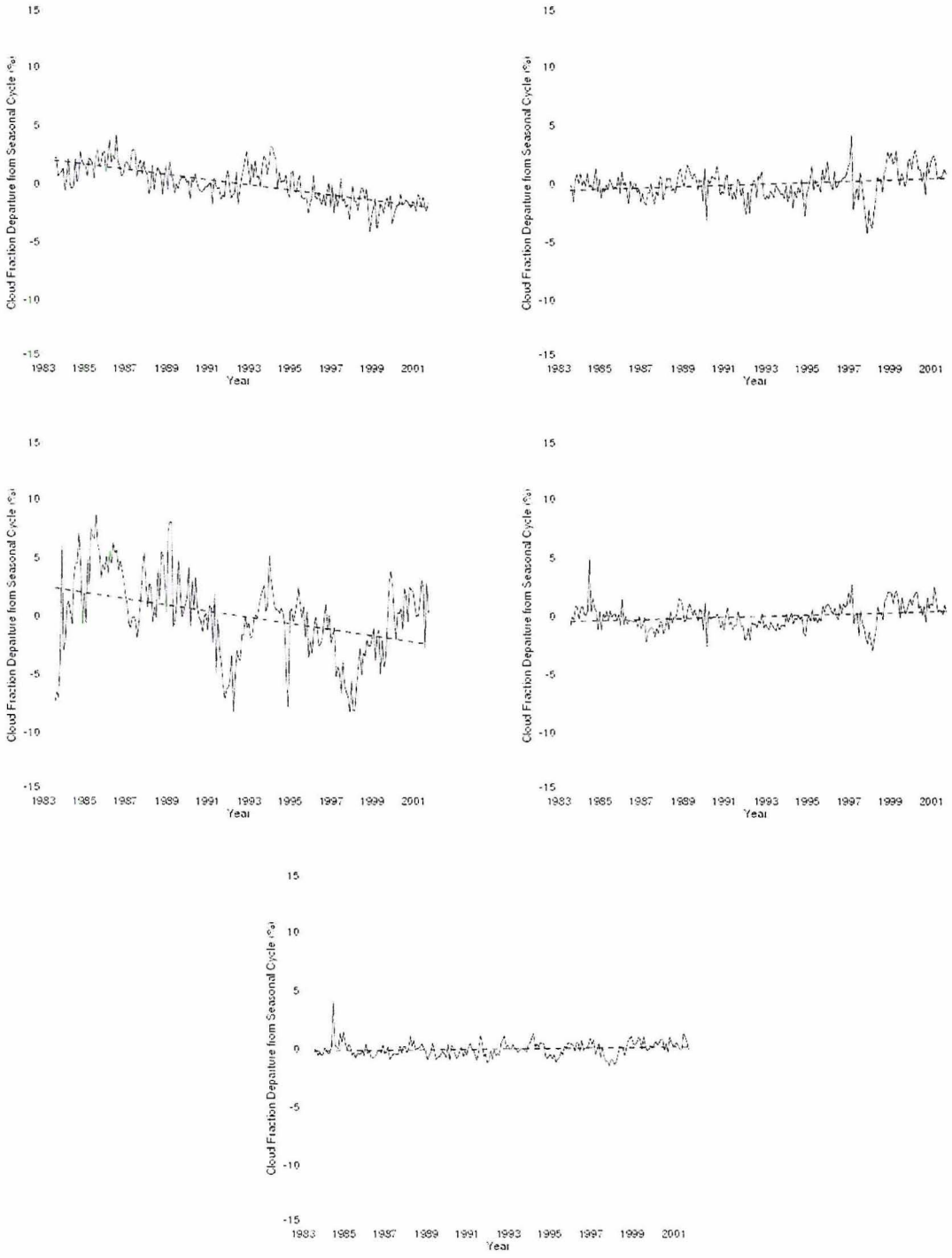

Figure 3.4: ISCCP D2 cloud amount anomaly time series with trends for the region of interest broken down by cloud type: low cloud (top left), middle cloud (top right), cirrus cloud (middle left), cirrostratus (middle right), and deep convection (bottom). The slopes of these time series are listed in Table 3.1.

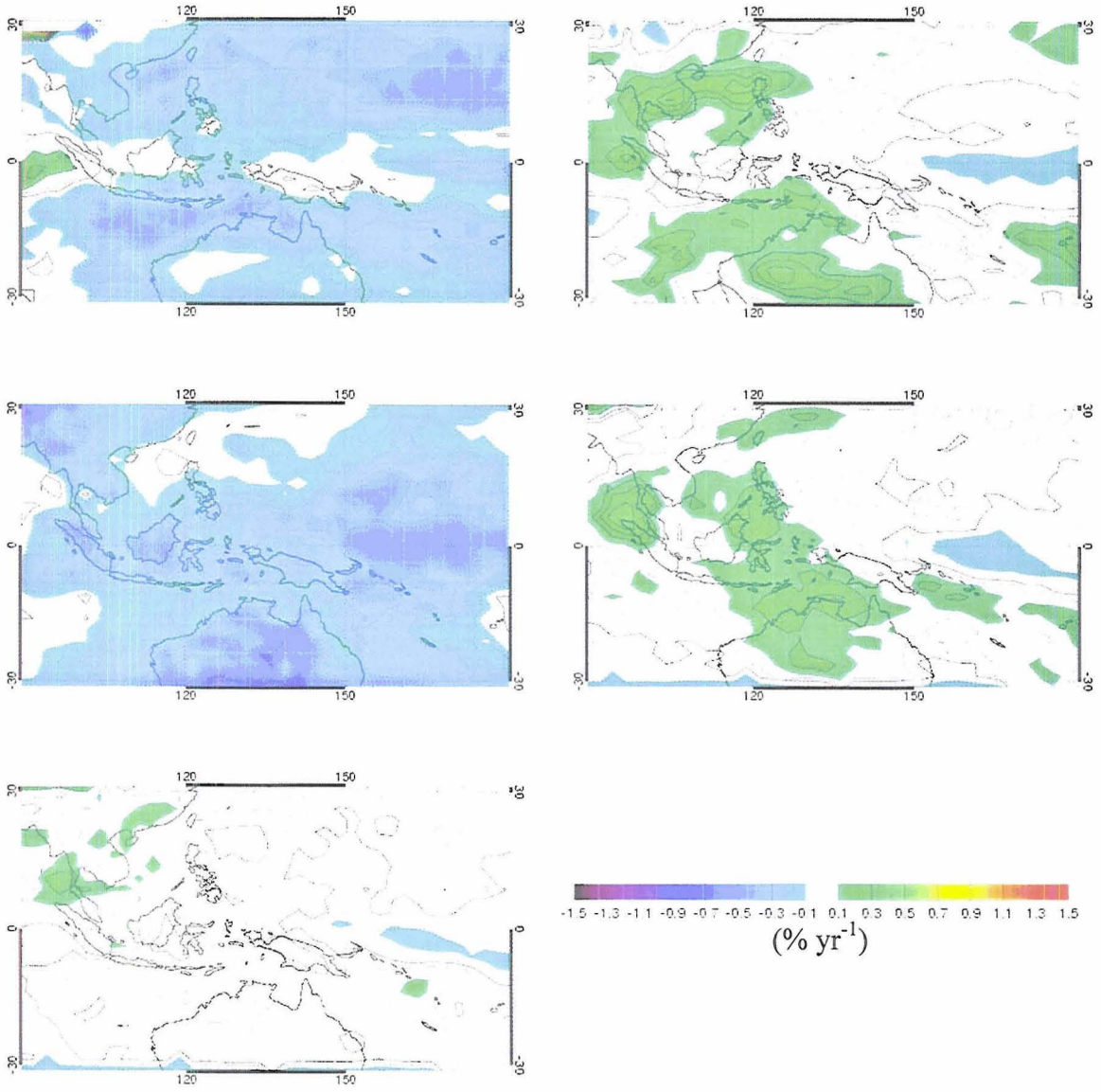

Figure 3.5: ISCCP D2 cloud amount trends for the region of interest (in % yr^{-1}) for low cloud (top left), middle cloud (top right), cirrus (middle left), cirrostratus (middle right), and deep convection (bottom left). Dotted contours indicate negative values and zero is indicated by the thickest contour.

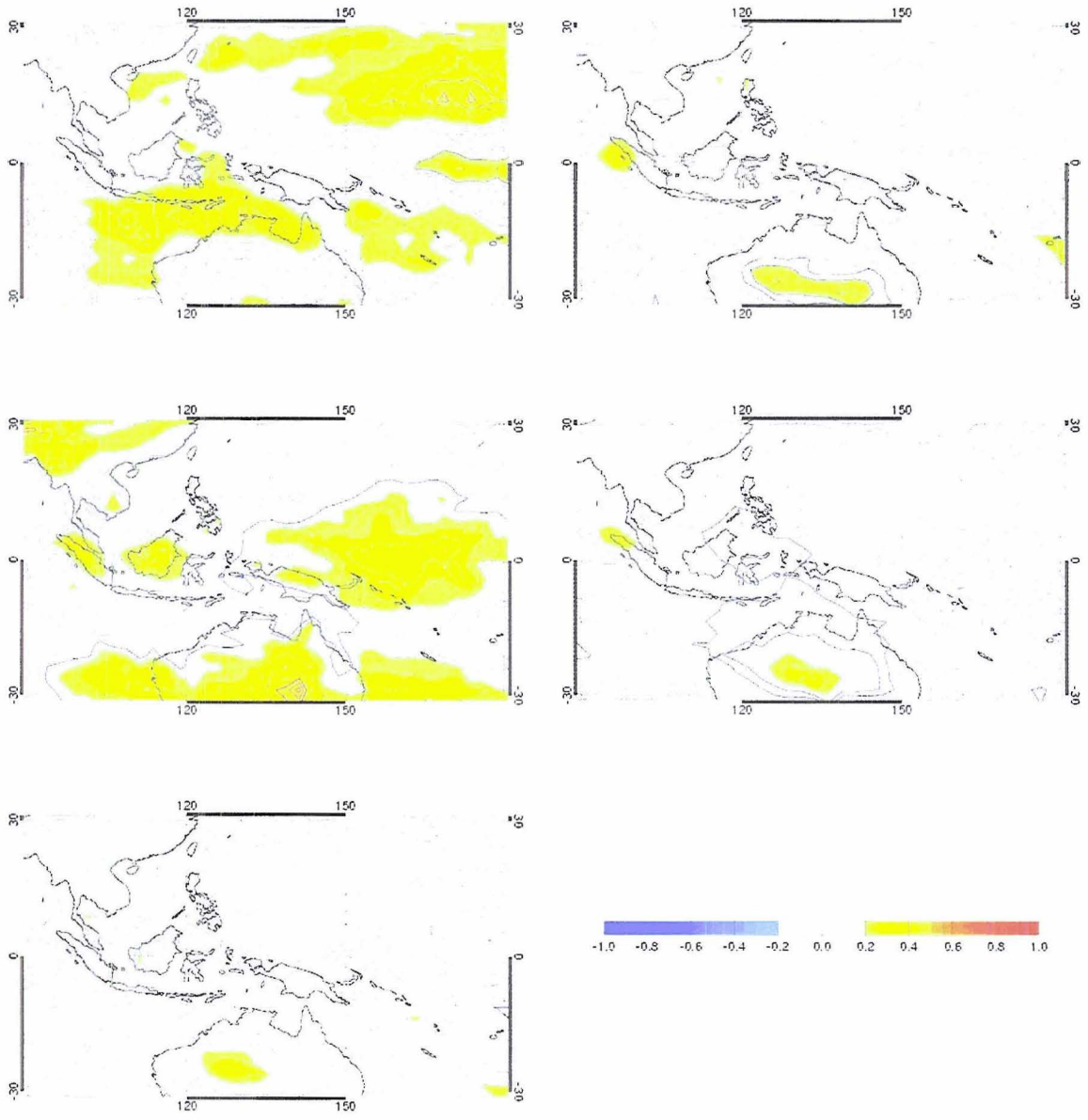

Figure 3.6: Maps of coefficients of correlation for the linear best fit trends for the 5 cloud types of the ISCCP D2 cloud amount in the region of interest and their corresponding time series: low cloud (top left), middle cloud (top right), cirrus (middle left), cirrostratus (middle right), and deep convection (bottom left). Colored regions indicate where the trends from Figure 3.5 are significantly different from zero (the absolute value of the t-score exceeds 2.00).

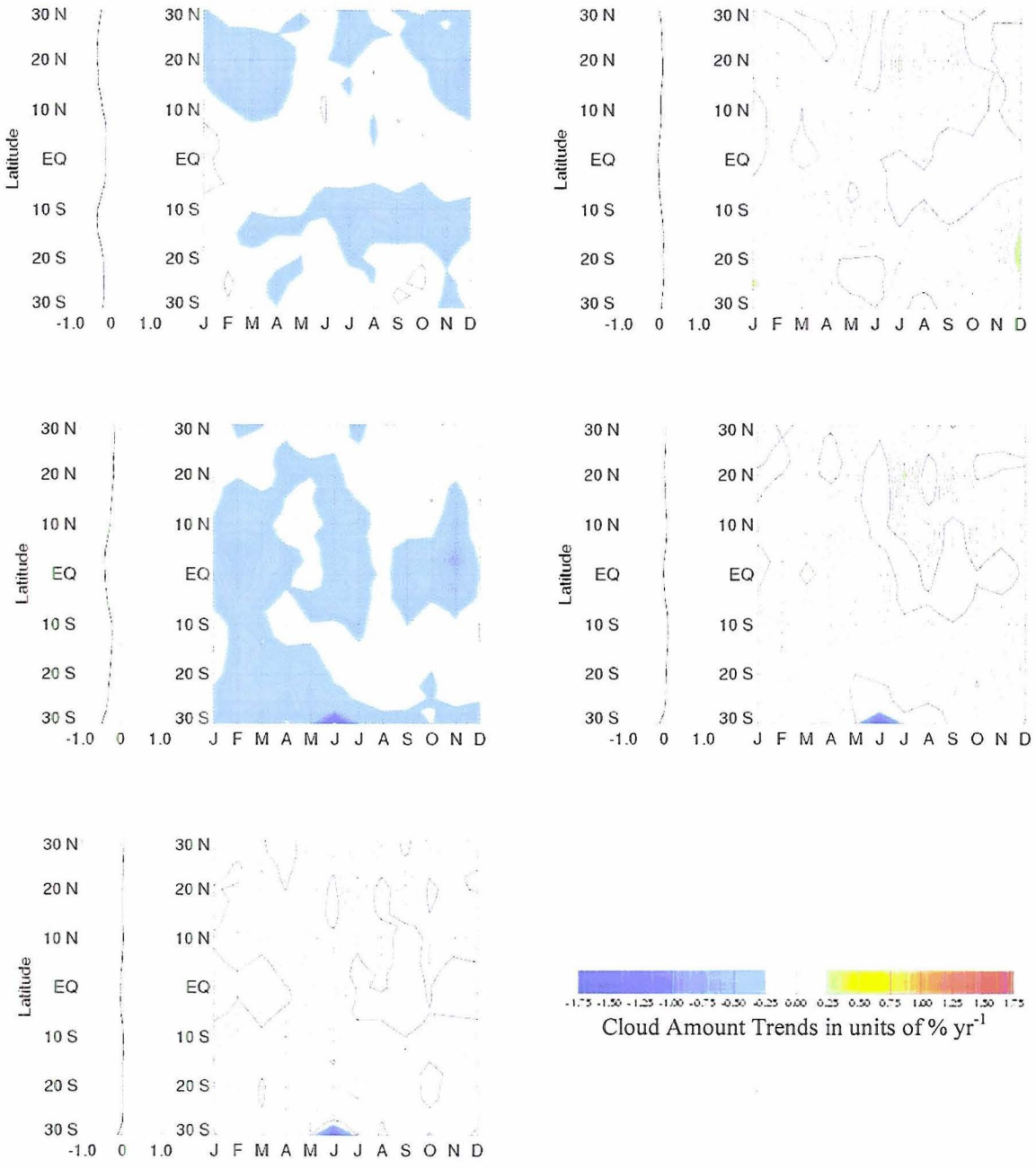

Figure 3.7: Zonal mean ISCCP D2 cloud amount trends (in % yr^{-1}) in the region of interest as functions of latitude (left) and latitude and month of year (right) for each cloud type: low cloud (top left), middle cloud (top right), cirrus cloud (middle left), cirrostratus (middle right), deep convection (bottom left).

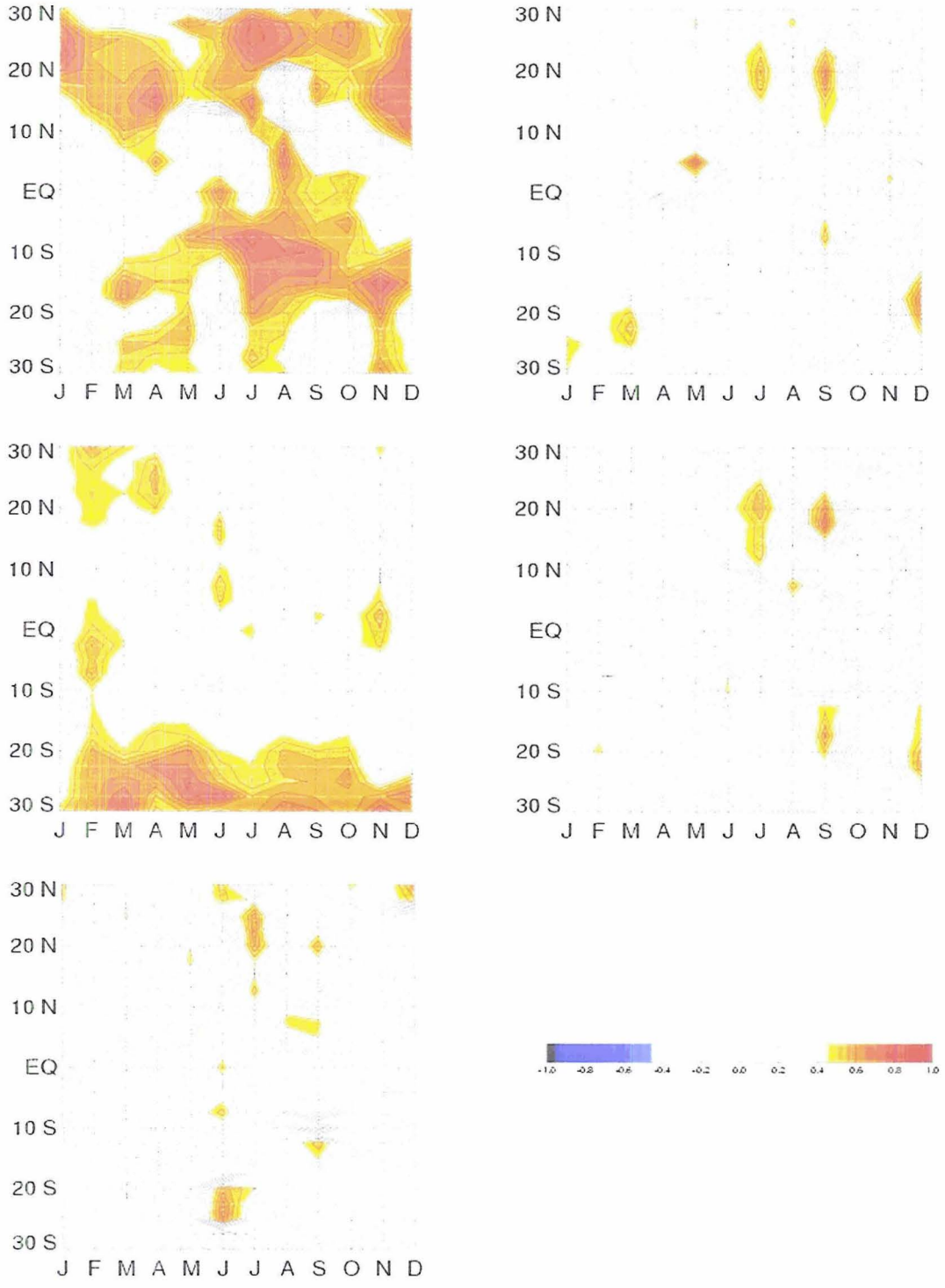

Figure 3.8: Monthly and latitudinal distributions of coefficients of correlation between the linear best fit trends for each of the 5 cloud types of the ISCCP D2 cloud amount in the region of interest and their corresponding time series: low cloud (top left), middle cloud (top right), cirrus (middle left), cirrostratus (middle right), and deep convection (bottom left). Colored regions indicate where the trends from Figure 3.5 are significantly different from zero (the absolute value of the t-score exceeds 2.11).

Table 3.1: Regionally averaged characteristics of selected ISCCP D2 cloud types for the region of interest

Cloud Types	Low	Middle	Cirrus	Cirrostratus	Deep Convective
Change (% yr^{-1})	-0.22	0.06	-0.26	0.05	0.02
t-score*	**-9.77**	**3.37**	**-6.06**	**3.40**	**2.21**

*To reject null hypothesis that slope is zero at 95% confidence level, t-score must exceed ±2.00

Bold values represent those that pass the significance test.

CHAPTER 4: COMPARISON OF ISCCP D2 CLOUD AMOUNT DATA TO OBSERVATIONS FROM POLAR-ORBITING SATELLITES

4.1 Introduction

There are two main reasons why conclusions drawn from the ISCCP D2 dataset about the behavior of cloud amount in the region of interest should be verified by polar-orbiting satellite data. First of all, there is the matter of the viewing angle problem as described in Chapter 1. While the selection of the region of interest is meant to mitigate problems that arise due to this phenomenon, the use of polar-orbiting satellite data will enable an analysis that is truly independent of viewing angle difficulties. The other reason is the problem of the apparent inconsistencies in the conclusions drawn from the behavior of the changes in the ISCCP data. As demonstrated in the previous chapter, if we believe that the distribution of convection is indeed changing in such a way that the regional all-cloud cloud amount is decreasing, then the deep convective cloud amount data are not wholly consistent with the cirrus cloud data. Furthermore, changes in the intensity or distribution of convection do not explain the low cloud changes. Therefore, in order to obtain more robust conclusions, characteristics evident in the ISCCP data should also be looked for in polar-orbiting satellite data.

In Chapter 2, the two polar-orbiting satellite datasets used for this verification process, the NOAA Interpolated OLR and the PATMOS-A datasets, are described in detail. In order to look for characteristics similar to those of the ISCCP D2 cloud amount data, they are subjected to the same analysis. This chapter describes the sign and

magnitude of the changes in these polar-orbiting data, where those changes are occurring, and when they are strongest.

4.2 Characteristics of the NOAA Interpolated OLR dataset

Figure 4.1 presents the attributes of the changes evident in the NOAA Interpolated OLR dataset. It includes a time series of how the average OLR over the region of interest (90°E – 180°, 30°N – 30°S) changes with time, a figure showing how the zonal-mean OLR trend changes as a function of latitude and month, and a map showing where the OLR changes are occurring. This figure also shows coefficients of correlation for the latitude/month and map plots so that it is possible to evaluate the significance of those trends. Colored regions on these plots signify statistical significance.

Keeping in mind that OLR and cloud amount are inversely related, the two datasets should show similar patterns in terms of where and when their changes are occurring. Indeed, both do show some interesting similarities. The OLR data exhibit a strong positive trend centered on the Equator and east of 150°W longitude – a center of action that is collocated with the strongest trends in ISCCP all-cloud cloud amount and cirrus cloud amount. The OLR data show strong positive trends both north and south of the Equator from November through April. This may be similar to the trends shown in Figure 3.3 since the strongest negative cloud amount trends tend to occur to the north of the Equator. It must be conceded, however, that it is difficult to conclude that there is a strong relationship between ISCCP and the OLR in this region.

The differences in these data, however, are more remarkable. First of all, there is no indication of a secondary trend located at 15°N latitude in either the trend map or the

plot of zonal mean trends as a function of month. Given that the ISCCP data showed the trend in this region to be dominated by low cloud, the presence of any higher clouds that are not changing might be responsible for masking this trend in the OLR data. Secondly, there are negative OLR trends located to the west of the 150° meridian and poleward of the Equator and over water. These should correspond to positive cloud amount trends, but there is no evidence of this from ISCCP data. There is also no indication that OLR trends oscillate in time around 15° - 20°N like the trends evident in Figure 3.3 (all-cloud) and Figure 3.7 (deep convection). This supports the conclusion that there is likely something suspect occurring in the ISCCP data. Finally, an examination of the time series of the regionally averaged OLR indicates that there is a small, but statistically insignificant negative trend in OLR, which would correspond to an equally small positive cloud amount trend. This discrepancy occurs even though the OLR and ISCCP cloud amount time series are significantly correlated at the 95% confidence level as shown in Table 4.1. This indicates that, while the shorter-term variability in cloud amount is captured by both datasets, there is also a serious disagreement in the nature of long-term trends between them. By examining the PATMOS-A cloud amount data, one can determine which of these datasets is likely providing the more accurate picture of what is going on with the cloud amount in the region of interest.

4.3 Characteristics of the PATMOS-A cloud amount dataset

Figure 4.2 presents the characteristics of the PATMOS-A cloud amount data in a manner similar to that of Figure 4.1. Immediately, one can see that the patterns exhibited by the PATMOS-A data are more consistent with the OLR data than the ISCCP cloud amount data. This is to be expected since the data come from the same AVHRR sensor.

There are, however, a couple of limited similarities between the PATMOS-A and the ISCCP D2 data. An examination of Table 4.1 shows that the variations in the PATMOS-A and ISCCP data are significantly correlated, which likely means that both datasets are capturing the same sorts of short-term variability. There are also negative trends in the PATMOS-A cloud amount east of 150°W longitude, though they are not centered on the Equator but are poleward to the north and south. Thus, they are roughly collocated with the strongest negative ISCCP cloud amount trends. This is, however, the apparent extent of their similarities.

The differences between the PATMOS-A and ISCCP cloud amount data are much more obvious and remarkable. First of all, the trend in the PATMOS-A cloud amount is both statistically insignificant and positive, again in spite of the fact that both datasets are significantly correlated and apparently capturing similar short-term variations. The map showing where PATMOS-A trends are strongest demonstrates that there are only small regions of decreasing cloud amount in the region of interest. The regions of increasing cloud amount west of 150°E longitude in the PATMOS-A data are consistent with those in the OLR dataset, but not ISCCP, which is dominated by negative trends. Finally, the PATMOS-A data indicate that the cloud amount is increasing poleward of the Equator towards both the north and the south during the months of February through May. This result seems inconsistent with both the ISCCP and OLR datasets, though it seems to have a little more in common with the OLR results since, among other reasons, it does not show evidence of oscillatory trends near 15-20°N. Overall, though, the PATMOS-A data and the ISCCP D2 data appear to lead to completely different trend results.

4.4 Conclusions

The OLR and PATMOS-A data present some features that appear consistently in both datasets, though the overall spatial correlation in the region of interest is -0.174, which is statistically insignificant if we assume that there are no more than 20 spatial degrees of freedom. This assumption is likely valid since a back of the envelope spatial autocorrelation calculation indicates that there are likely less than 10 spatial degrees of freedom; a result that is consistent with the fact that atmospheric phenomena in the tropics tend to be large in the absence of a strong coriolis force. Therefore, the most valid conclusion that can be made with these data is that their common result, that the cloud amount in the region of interest is not changing in a statistically significant way, is more likely to represent what is really happening with cloud amount in the region of interest. This casts doubt on the results obtained from the ISCCP analysis of the previous chapter. In fact, only two of the conclusions from that analysis remain intact. The first is that the trends all seem to gradually become more negative from west to east over the region of interest. All three datasets demonstrate that their most negative or least positive cloud amount trends occur to the east of 150°W while the most positive or weakest negative trends occur to the west of that line. More importantly though, all data point toward changes in the amount or distribution of convection in the tropics over the time period studied. These datasets appear to exhibit trends that are symmetrical about the Equator during the time of year when the ITCZ is closest to the Equator. While neither the OLR or PATMOS-A data have specific information about the types of clouds that are exhibiting these changes, the pattern does seem to suggest that these may be changes in the distribution of cirrus anvils as a result of ITCZ convection. If this is true,

then there should be signatures of these changes evident in the general circulation of the atmosphere. In the following chapter, reanalysis data will be used to determine if there are changes in the general circulation that correlate with changes in the ISCCP all-cloud cloud amount and to provide more insight into the true nature of the cloud amount changes in the region of interest.

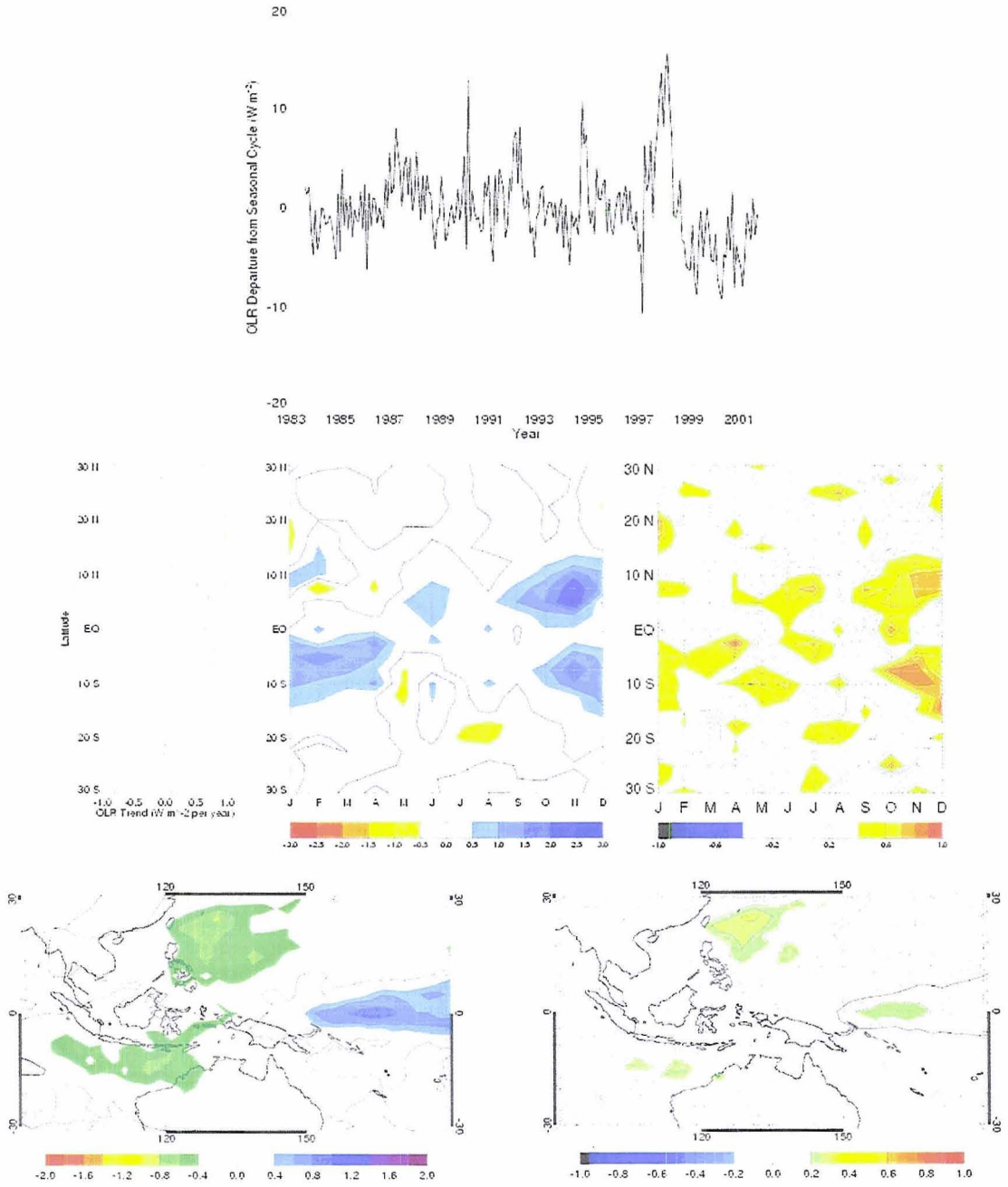

Figure 4.1: (top) The NOAA Interpolated OLR anomaly time series for the region of interest with trend plotted in green. (middle) The slope of zonal mean OLR plotted as functions of latitude (left) and latitude and month (middle) in W m^{-2} yr^{-1}. The coefficients of correlation between the linear best fit trends and their corresponding time series are shown on the right. (bottom) OLR trends in the region of interest in W m^{-2} yr^{-1} (left) and the coefficients of correlation between the OLR time series and the corresponding linear best-fit trend at each point. Colored regions on the correlation maps indicate where the trends are significantly different from zero. Note that the color bars are reversed to indicate that positive OLR changes are equivalent to decreasing cloud amount changes.

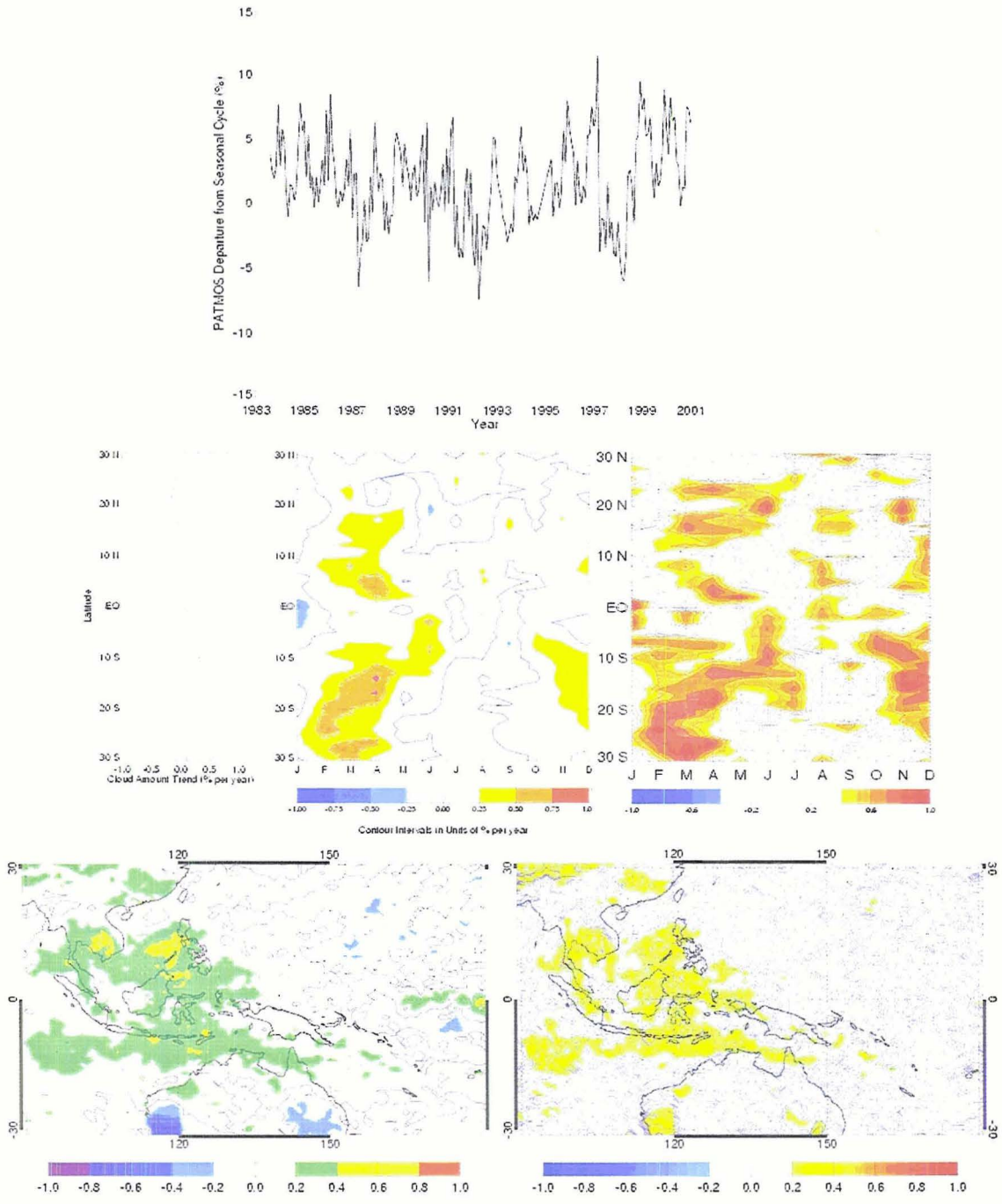

Figure 4.2: (top) The PATMOS-A cloud amount anomaly time series for the region of interest with trend plotted in green. (middle) The slope of the zonal mean PATMOS-A cloud amount plotted as functions of latitude (left) and latitude and month (middle) in % yr^{-1}. The coefficients of correlation between the linear best fit trends and their corresponding time series are shown on the right. ((bottom) PATMOS-A cloud amount trends in the region of interest in % yr^{-1} (left) and the coefficients of correlation between the PATMOS-A time series and the corresponding linear best-fit trend at each point. Colored regions on the correlation maps indicate where the trends are significantly different from zero.

Table 4.1: Regionally averaged characteristics of OLR and PATMOS-A cloud amount time series and correlations to the ISCCP D2 cloud amount time series

Data Set	NOAA Interpolated OLR	PATMOS-A Cloud Amount
Slope of Change	-0.10 W m^{-2} yr^{-1}	0.05 % yr^{-1}
T-score for trend*	-1.72	1.01
Correlation to ISCCP D2	-0.86	0.35
T-score for correlation**	**-16.78**	**3.56**

*To reject null hypothesis that slope is zero at 95% confidence level, t-score must exceed ±2.00
**To reject null hypothesis that there is no correlation at the 95% confidence level, t-score must exceed ±2.00

CHAPTER 5: CORRELATION OF ISCCP D2 CLOUD AMOUNT CHANGES TO CHANGES IN THE GENERAL CIRCULATION OF THE TROPICS

5.1 Introduction

The previous chapter highlights inconsistencies between the cloud amount changes evident in the ISCCP D2 cloud amount data and the corresponding results obtained from using OLR and cloud amount data from polar-orbiting satellites. In particular, while ISCCP indicates a large decrease in cloud amount in the region of interest, the other data suggest that the cloud amount is not changing significantly over the same period. While the consistency of the polar-orbiting satellite data might encourage the conclusion that those data are more likely to be representative of reality, it is still important to draw in yet another source of information to finally make that determination.

As mentioned in the introduction, clouds and the heating associated with them have a perceptible influence on the general circulation of the atmosphere. While the true nature of the feedback loop between clouds and climate is still a matter of investigation and discussion, the fact that such interactions occur is not disputed. Therefore, changes in the cloud amount, if real, should also manifest themselves in the way the climate changes. By following the methodology laid out in Section 2.2, one can use reanalysis data both to determine how the general circulation of the atmosphere changes in association with cloud amount changes and also obtain more information about how the actual cloud amount in the region of interest might be changing.

Figures 5.1 through 5.21 show the results of this analysis. From top to bottom, each figure presents the map of regression coefficients, the map of correlation coefficients, and the proxy cloud time series corresponding to each reanalysis field. Colored portions of the correlation coefficient maps show regions where regression coefficients are statistically significant. Table 5.1 shows how well each of the proxy cloud time series correlates to the ISCCP D2 cloud amount time series for the region of interest. It also shows the linear regression coefficients for each proxy cloud time series and the t-score for the significance of each slope. These results not only identify the physical mechanism that explains much of the low-frequency variability in the ISCCP cloud amount, but they also provide a strong argument for why the polar-orbiting satellite data, which did not indicate a significant trend in the cloud amount, are more likely to be indicative of the true nature of cloud amount changes in the region of interest.

5.2 Changes in the general circulation that are correlated with ISCCP cloud amount changes

A complete examination of the regression coefficient maps reveals a consistent pattern of how the reanalysis data change in connection with a 1% increase in the ISCCP all-cloud cloud amount for the region of interest. In the wind field analyses, an increase in cloud amount is correlated with increased NCEP/NCAR 200 mb westerlies to the east of 150°W and 200 mb easterlies to the west of that meridian, shown in the regression map of Figure 5.1. According to the regression map in Figure 5.2, this feature is collocated with a modest increase of the NCEP/NCAR 200 mb equatorward flow to the north and south of the Equator in the region from 130°W to 150°E. The patterns in the regression maps of the NCEP/NCAR 850 mb wind fields, shown in Figures 5.3 and 5.4,

are similar though with opposite sign. Not surprisingly, the regression map for the NCEP/NCAR 200 mb divergence field in Figure 5.5 shows a region of increased divergence aloft centered on this region while the regression map of Figure 5.6 shows that there is increased low level convergence in response to an increase in cloud amount in the region of interest. The regression maps from ERA-40 data, shown in Figures 5.7 – 5.12, corroborate these results. By fluid continuity arguments, the patterns of divergence indicate that a decrease in cloud amount in this region should correlate with a collocated decrease in upward motion. Comparing these patterns to the maps of satellite trends, all of these patterns appear to be consistently centered over the main region of decreasing cloud amount. Furthermore, because convection has been demonstrated to be primarily responsible for upward motion in the tropics (Riehl and Malkus 1958), this result appears to support the conclusion that the cloud amount changes in this region are primarily due to changes in convection. This conclusion is also supported by the regression patterns from both the GPCP (Figure 5.13) and CMAP (Figure 5.14) precipitation reanalyses, which indicate that a change in the ISCCP cloud amount is correlated with a change in precipitation of the same sign.

This conclusion, that the reanalysis data suggest a systematic change in the location or intensity of convection in the region of interest is also consistent with previous results. In Chapter 3, it was noted that the patterns of ISCCP D2 cirrus cloud amount changes are consistent with changes in the intensity and/or location of convection associated with the ITCZ. This result was then corroborated in Chapter 4 using the NOAA Interpolated OLR and PATMOS-A datasets. No explanation has thus far been offered for the kind of mechanism that could cause the kinds of systematic relocation of

convection suggested by these results. The remaining results, however, will show that the redistribution of convection and associated increases in cloud amount are consistent with changes in the phase of ENSO.

There are several pieces of information that indicate that the ISCCP cloud amount changes are connected with ENSO. First of all, Figures 5.15 and 5.16 respectively show the regression coefficient maps for the NCEP/NCAR and ERA-40 200 mb geopotential height reanalysis fields. According to Horel and Wallace (1981), these maps are consistent with the patterns of changes in the 200 mb heights associated with the redistribution of convective heating that occurs as ENSO changes phase. Secondly, Figures 5.17 and 5.18 show the results from the NCEP/NCAR 850 mb geopotential height and sea level pressure fields respectively. The patterns shown in these regression coefficient maps are consistent with the statistically derived definition of the Southern Oscillation as determined by Sir Gilbert Walker since the pressure is decreasing near the surface in the West Pacific and increasing in the East Pacific (Bjerknes 1969). The ERA-40 data for 850 mb geopotential height and sea level pressure, shown in Figures 5.19 and 5.20 respectively, show the same patterns and support the same conclusion. Another piece of evidence comes from the regression map for the NOAA OI v.2 SST data, which shows that increased cloud amount in the region of interest is connected with the presence of a tongue of cold water in the Equatorial East Pacific Ocean. The presence of a "cold tongue" is a convincing signature of a connection between the ISCCP D2 cloud amount and the phase of ENSO. Furthermore, the proxy cloud time series shown in each of the aforementioned figures show signatures of ENSO. Each of these figures show large negative excursions in El Niño years, including 1986-7, 1991-2, 1994-5, and 1997-

8, and large positive excursions in La Niña years, such as 1988-9 and 2000-2001. (Smith and Sardeshmukh 2000) It is no great surprise then that Figure 5.22 shows that the detrended ISCCP D2 all-cloud cloud amount anomaly time series exhibits a strong negative correlation with the Niño 3.4 Index (Trenberth and Stepaniak 2000). This index, which is based on the SST in a specific region of the tropical Pacific Ocean, accounts for 29.5% of the variance in the cloud amount time series. Therefore, one can conclude that most of the long-term variability demonstrated in the ISCCP D2 cloud amount data is directly related to variations in ENSO.

5.3 Diagnosis of the true cloud amount change in the region of interest using reanalysis data

The use of reanalysis data also provides several more ways of characterizing the cloud amount trend in the region of interest. First of all, because it has been shown that ENSO accounts for a large part of the long-term variability in cloud amount, the trend in the Niño 3.4 index should reflect how the true cloud amount has changed. Maps of the trends in the reanalysis fields can be compared with the patterns of the corresponding regression maps. Because the regression maps reflect how the reanalysis fields would change with a 1% increase in the ISCCP cloud amount, if the trends in the reanalysis fields appear to show the same patterns, then one can surmise the sign and magnitude of the real cloud amount trend in the region of interest. Finally, the proxy cloud time series, generated for each reanalysis field by taking the inner product of the regression map with the map of the corresponding reanalysis field for each month of the record, show how well the reanalysis fields reflect the regression map patterns. Again, because the regression map represents how the reanalysis field changes in response to an increase in

cloud amount, the proxy cloud time series are an analog for how the cloud amount in the region of interest would have to change if all of the changes in the reanalysis fields were due to the cloud amount. Using these means, the results presented in this section demonstrate that the cloud amount in the region of interest does not change in a statistically significant way.

Section 5.2 outlines the evidence provided by reanalysis data that indicates that ENSO is connected with the long-term variability in the ISCCP D2 cloud amount time series. Furthermore, because the location of the primary center of action for all of the reanalysis maps (east of 150°E and centered on the Equator) appears to be coincident with the centers of action visible in the OLR and PATMOS-A data, it is reasonable to expect that ENSO also accounts for much of the long-term variability in the true cloud amount in the region of interest. Therefore, we can expect that the trend in the Niño 3.4 index should be representative of the trend in the actual cloud amount in the region of interest, though with opposite sign. Returning to Figure 5.22, the blue line represents the linear fit to the Niño 3.4 index. The slope of this line is -4.3×10^{-4} yr^{-1} and has a t-score of -0.30. Because this t-score does not exceed ±2.00, this trend is not significantly different from zero, and is consistent with the conclusions reached in Chapter 4 that the true cloud amount trend is not different from zero.

Comparing the regression maps for each reanalysis field to maps of the trend of the corresponding reanalysis fields also provides a sense of the sign and magnitude of the true cloud amount changes in the region of interest. Figures 5.23, 5.24, and 5.25 show the trend maps for each of the NCEP/NCAR reanalysis fields plus the NOAA OI v.2 SST reanalysis and the GPCP and CMAP precipitation reanalyses. For reasons mentioned in

Chapter 2, the ERA-40 reanalysis data are not used for this portion of the study. By examination, all of the reanalysis trend maps shown in these figures show patterns of opposite sign than their corresponding regression maps except for the 850 mb meridional wind in Figure 5.23 (bottom). Because the regression maps represent how the reanalysis fields would change with an increase in cloud amount, the overwhelming majority of the reanalysis fields are changing in a manner consistent with a decrease in cloud amount. However, the magnitudes shown in the reanalysis trend maps appear to be smaller than the magnitude reflected by any of the regression maps. This indicates that the true magnitude of the cloud amount trend is likely to be less than 1% per year. While it is impossible to tell from a visual inspection if the trends in cloud amount indicated by these reanalysis trends are significantly different from zero, this result is consistent with previous observations that the true cloud amount change is small in magnitude.

Finally, the trends in the proxy cloud time series that are calculated for each reanalysis field can give a sense of how the true cloud amount in the region of interest is changing with time. Table 5.1 gives a summary of how the proxy cloud time series correlate with the ISCCP D2 anomaly cloud amount time series and also shows the t-score for the slope of each time series. From this table, and also by visual inspection of each of these time series, two observations become immediately apparent. First of all, each of these time series are highly correlated with the anomaly cloud amount time series shown in Figure 5.22. This is not a great surprise since the anomaly cloud amount time series is one of the inputs for the procedure that generated them. However, while some are negative and some are positive, it is immediately apparent that regardless of sign the true cloud amount trend is likely not different from zero.

5.4 Conclusions

The use of reanalysis data provides several opportunities to evaluate the cloud amount trends evident in the ISCCP D2 cloud dataset. By examining the patterns of how the ISCCP D2 all-cloud cloud amount anomaly time series regresses onto each of the reanalysis fields, it is evident that most of the long-term variability in the ISCCP data is due to variations in ENSO. Since the trend in the Niño 3.4 index is not significantly different from zero, this is consistent with a true cloud amount trend that is also not different from zero. This result is verified by comparing the regression coefficient maps with the corresponding maps for trends in the reanalysis data. These comparisons indicate that the trend in the true cloud amount may be negative, but also that it is less than 1% yr^{-1}. Finally, by observing the trends in the proxy cloud time series for each of these reanalysis fields, it is apparent that the expression of the regression map patterns in the reanalysis data does not change significantly in time. These results all support the conclusion that the true cloud amount trend is not significantly different from zero.

The results presented in this portion of the study are consistent with many of the conclusions drawn from the previous chapters. First of all, because ENSO is shown to be responsible for much of the long-term variability in the ISCCP D2 total cloud amount time series, it is then reasonable to expect that the characteristics of the ISCCP cloud amount data should reflect changes in the location and/or intensity of convection in the region of interest, such as those changes evident in Chapter 3. Furthermore, because the OLR and PATMOS-A data also show patterns that appear to be consistent with changes in the intensity or location of convection, this gives additional support to the conclusion that ENSO variability is a significant part of the variability of the true cloud amount in

the region of interest. The result that the reanalysis data indicate that there is no significant long-term trend in the true cloud amount in the region of interest is consistent with the polar-orbiting satellite datasets, which also did not show significant trends. While the OLR and PATMOS-A data seemed to indicate a small positive trend in the cloud amount, the reanalysis data do not support a consistent conclusion about the sign of the true cloud amount trends. Therefore, the only conclusion that can be reached is simply that the trend in the true cloud amount over the period of record is not significantly different from zero. This means that the ISCCP D2 regionally averaged all-cloud cloud amount trend evident in Figure 3.1 must be rejected as a realistic representation of the cloud amount trends in the region of interest.

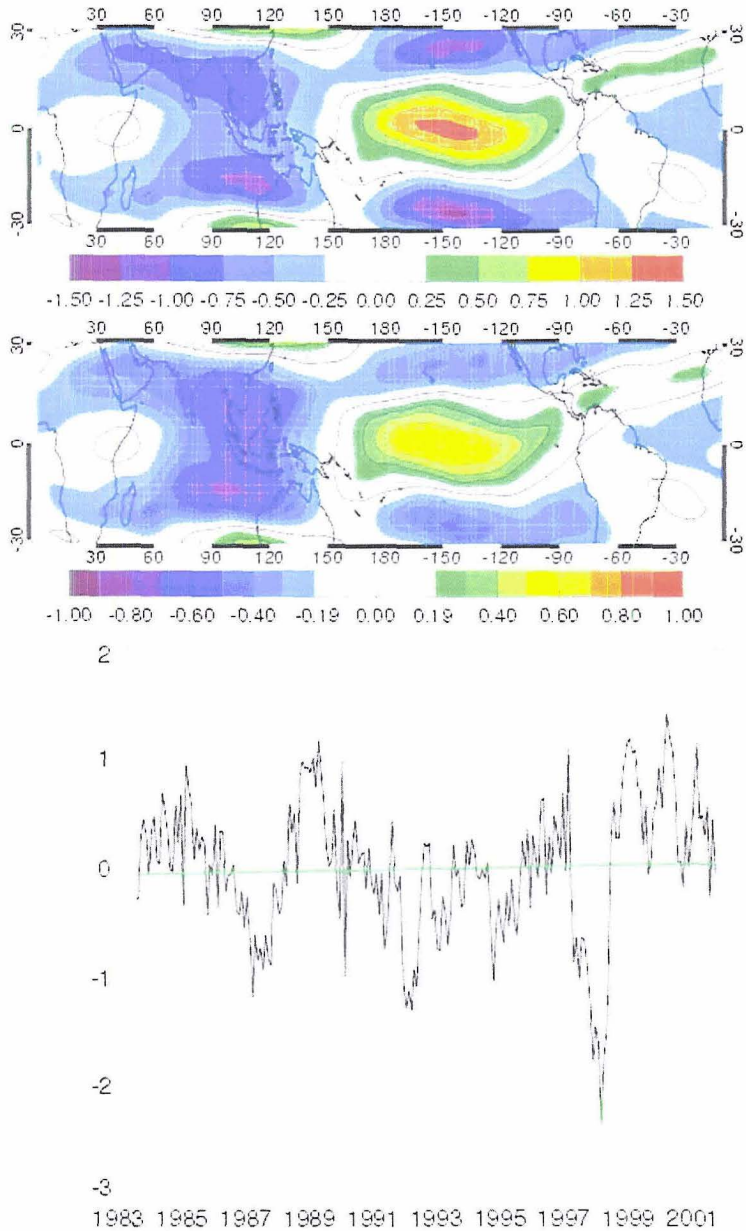

Figure 5.1: (top) The map showing the distribution of regression coefficients obtained from regressing the ISCCP D2 all-cloud cloud amount anomaly time series of the region of interest onto the time series of NCEP/NCAR 200 mb zonal wind at each grid point. (middle) The map showing the distribution of correlation coefficients obtained from correlating those time series. Colored contours indicate regions where the regression coefficients are statistically significant. (bottom) The proxy cloud time series obtained from projecting the regression coefficient map onto the map of 200 mb zonal wind at each time step plotted with the linear trend in green.

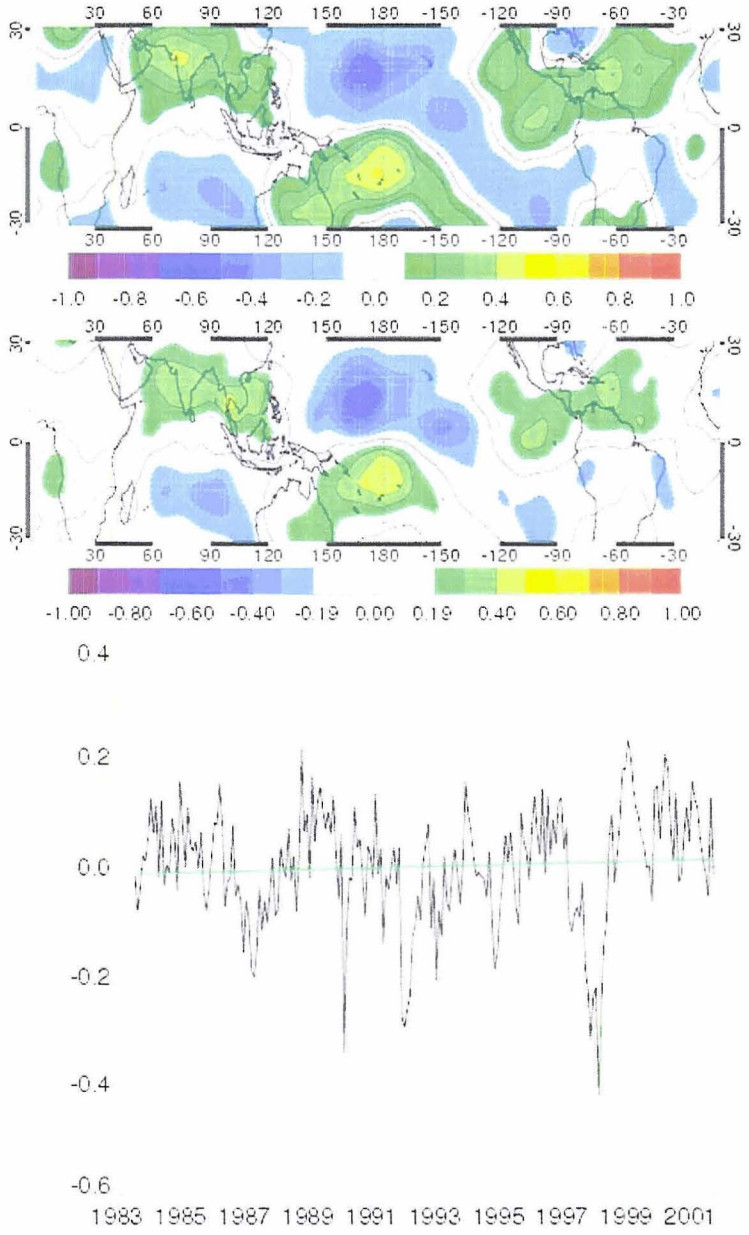

Figure 5.2: (top) The map showing the distribution of regression coefficients obtained from regressing the ISCCP D2 all-cloud cloud amount anomaly time series of the region of interest onto the time series of NCEP/NCAR 200 mb meridional wind at each grid point. (middle) The map showing the distribution of correlation coefficients obtained from correlating those time series. Colored contours indicate regions where the regression coefficients are statistically significant. (bottom) The proxy cloud time series obtained from projecting the regression coefficient map onto the map of 200 mb meridional wind at each time step plotted with the linear trend in green.

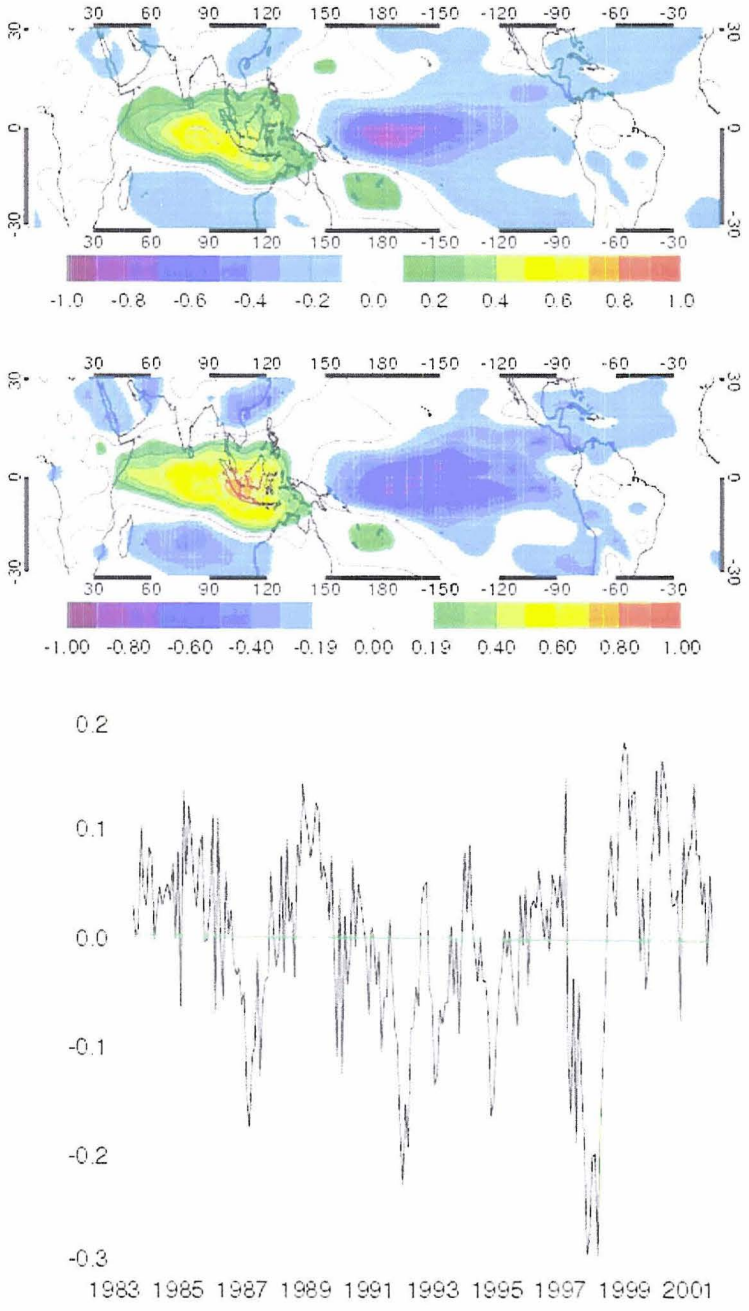

Figure 5.3: (top) The map showing the distribution of regression coefficients obtained from regressing the ISCCP D2 all-cloud cloud amount anomaly time series of the region of interest onto the time series of NCEP/NCAR 850 mb zonal wind at each grid point. (middle) The map showing the distribution of correlation coefficients obtained from correlating those time series. Colored contours indicate regions where the regression coefficients are statistically significant. (bottom) The proxy cloud time series obtained from projecting the regression coefficient map onto the map of 850 mb zonal wind at each time step plotted with the linear trend in green.

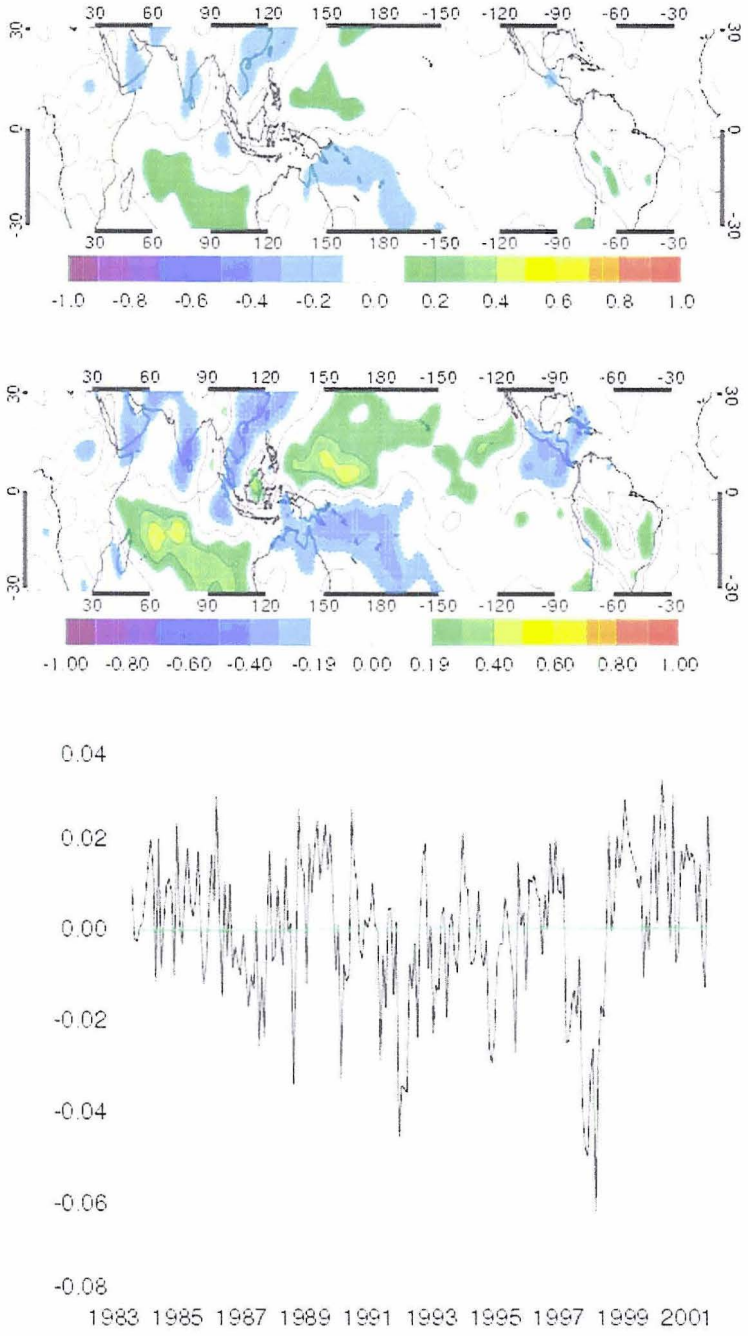

Figure 5.4: (top) The map showing the distribution of regression coefficients obtained from regressing the ISCCP D2 all-cloud cloud amount anomaly time series of the region of interest onto the time series of NCEP/NCAR 850 mb meridional wind at each grid point. (middle) The map showing the distribution of correlation coefficients obtained from correlating those time series. Colored contours indicate regions where the regression coefficients are statistically significant. (bottom) The proxy cloud time series obtained from projecting the regression coefficient map onto the map of 850 mb meridional wind at each time step plotted with the linear trend in green.

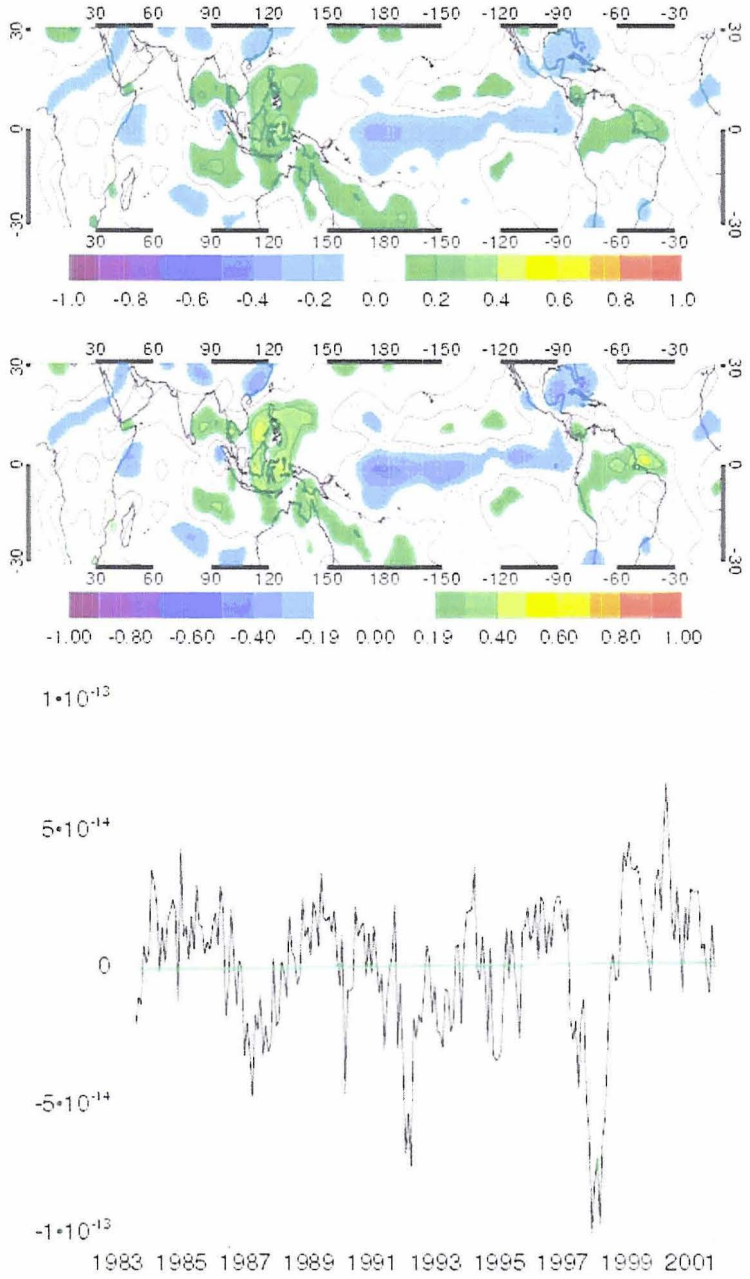

Figure 5.5: (top) The map showing the distribution of regression coefficients obtained from regressing the ISCCP D2 all-cloud cloud amount anomaly time series of the region of interest onto the time series of NCEP/NCAR 200 mb divergence at each grid point. (middle) The map showing the distribution of correlation coefficients obtained from correlating those time series. Colored contours indicate regions where the regression coefficients are statistically significant. (bottom) The proxy cloud time series obtained from projecting the regression coefficient map onto the map of 850 mb divergence at each time step plotted with the linear trend in green.

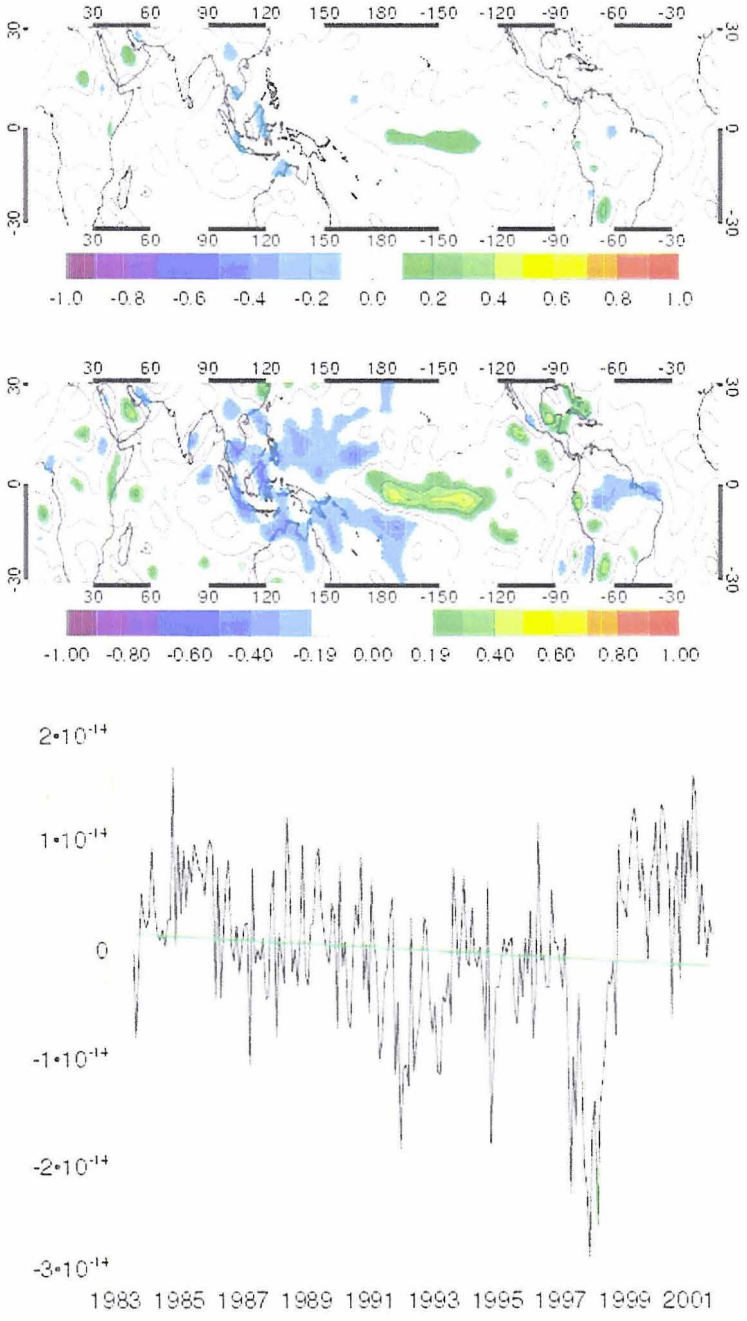

Figure 5.6: (top) The map showing the distribution of regression coefficients obtained from regressing the ISCCP D2 all-cloud cloud amount anomaly time series of the region of interest onto the time series of NCEP/NCAR 850 mb divergence at each grid point. (middle) The map showing the distribution of correlation coefficients obtained from correlating those time series. Colored contours indicate regions where the regression coefficients are statistically significant. (bottom) The proxy cloud time series obtained from projecting the regression coefficient map onto the map of 850 mb divergence at each time step plotted with the linear trend in green.

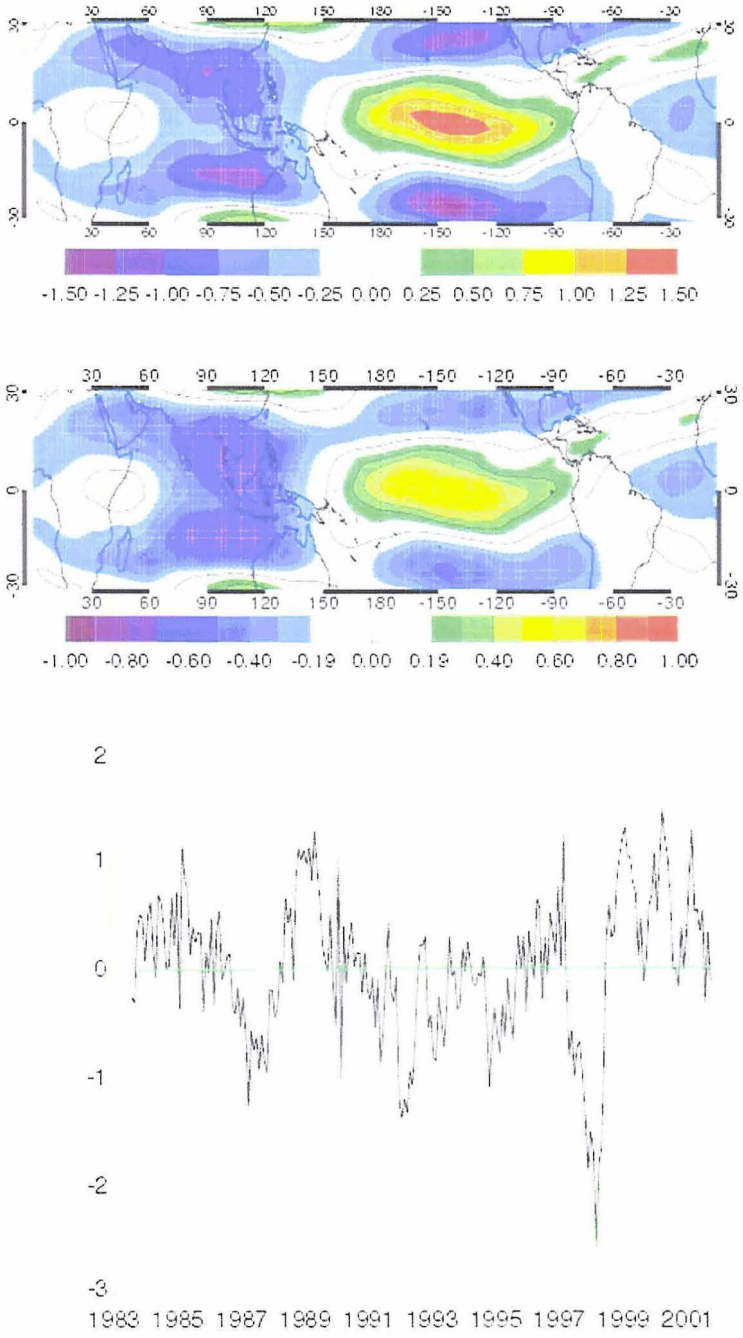

Figure 5.7: (top) The map showing the distribution of regression coefficients obtained from regressing the ISCCP D2 all-cloud cloud amount anomaly time series of the region of interest onto the time series of ERA-40 200 mb zonal wind at each grid point. (middle) The map showing the distribution of correlation coefficients obtained from correlating those time series. Colored contours indicate regions where the regression coefficients are statistically significant. (bottom) The proxy cloud time series obtained from projecting the regression coefficient map onto the map of 200 mb zonal wind at each time step plotted with the linear trend in green.

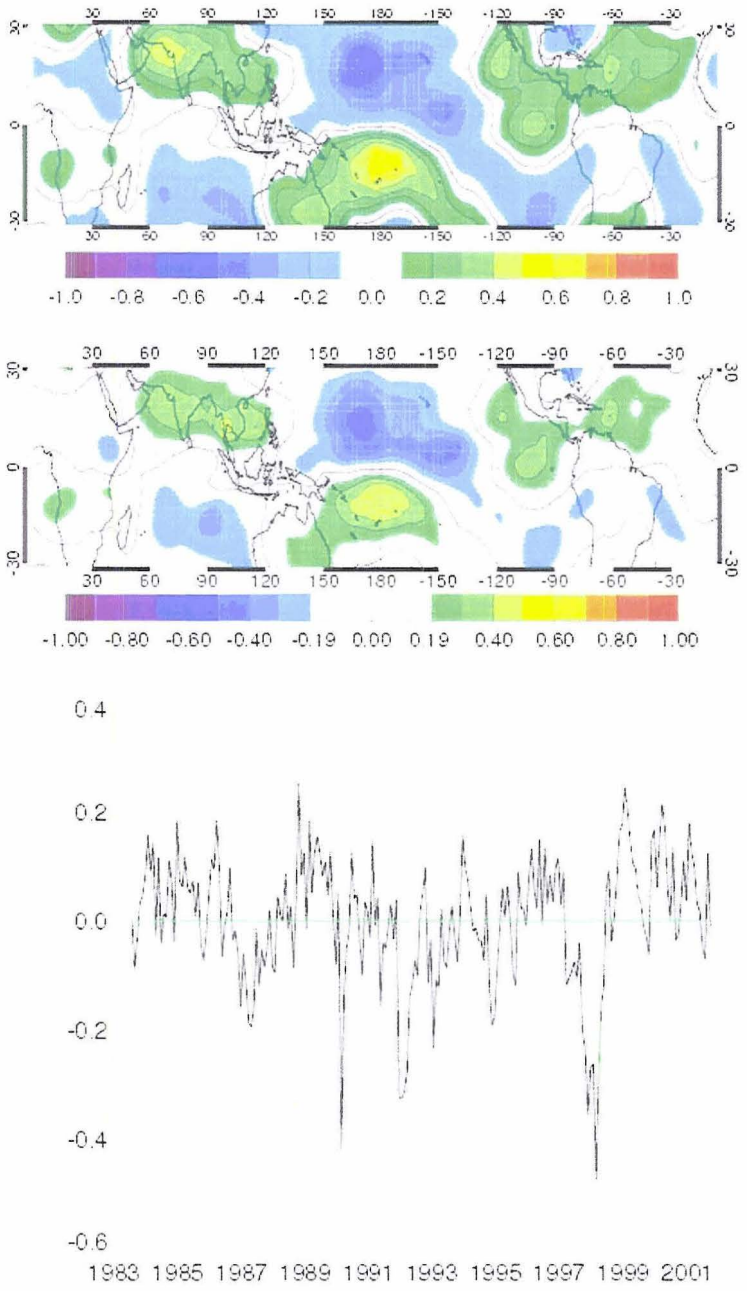

Figure 5.8: (top) The map showing the distribution of regression coefficients obtained from regressing the ISCCP D2 all-cloud cloud amount anomaly time series of the region of interest onto the time series of ERA-40 200 mb meridional wind at each grid point. (middle) The map showing the distribution of correlation coefficients obtained from correlating those time series. Colored contours indicate regions where the regression coefficients are statistically significant. (bottom) The proxy cloud time series obtained from projecting the regression coefficient map onto the map of 200 mb meridional wind at each time step plotted with the linear trend in green.

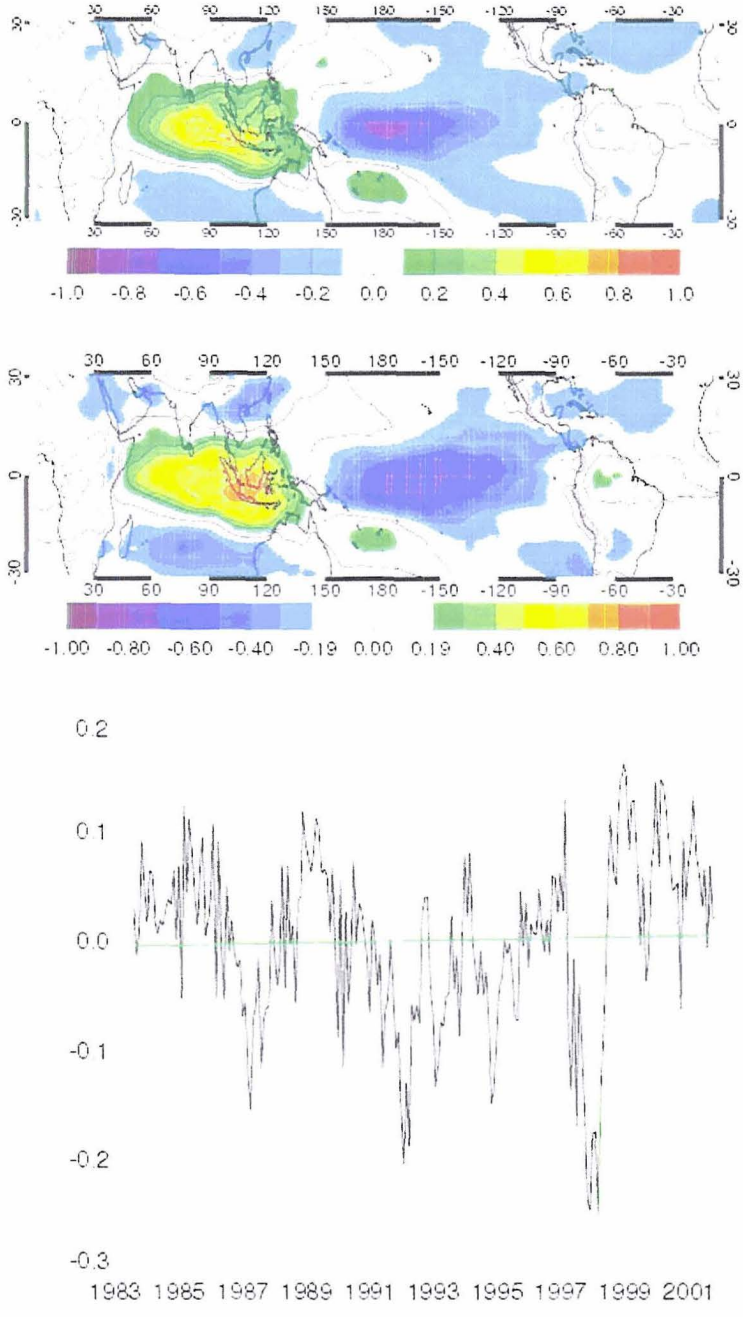

Figure 5.9: (top) The map showing the distribution of regression coefficients obtained from regressing the ISCCP D2 all-cloud cloud amount anomaly time series of the region of interest onto the time series of ERA-40 850 mb zonal wind at each grid point. (middle) The map showing the distribution of correlation coefficients obtained from correlating those time series. Colored contours indicate regions where the regression coefficients are statistically significant. (bottom) The proxy cloud time series obtained from projecting the regression coefficient map onto the map of 850 mb zonal wind at each time step plotted with the linear trend in green.

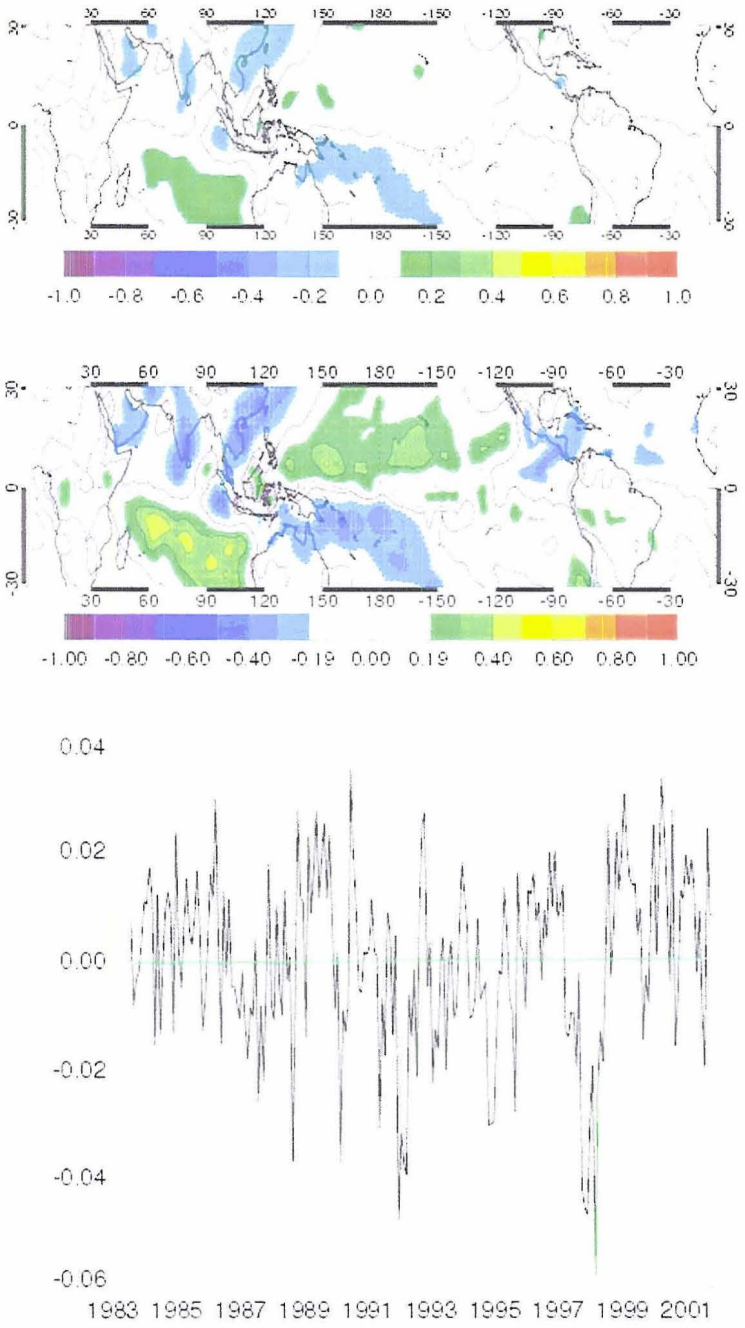

Figure 5.10: (top) The map showing the distribution of regression coefficients obtained from regressing the ISCCP D2 all-cloud cloud amount anomaly time series of the region of interest onto the time series of ERA-40 850 mb meridional wind at each grid point. (middle) The map showing the distribution of correlation coefficients obtained from correlating those time series. Colored contours indicate regions where the regression coefficients are statistically significant. (bottom) The proxy cloud time series obtained from projecting the regression coefficient map onto the map of 850 mb meridional wind at each time step plotted with the linear trend in green.

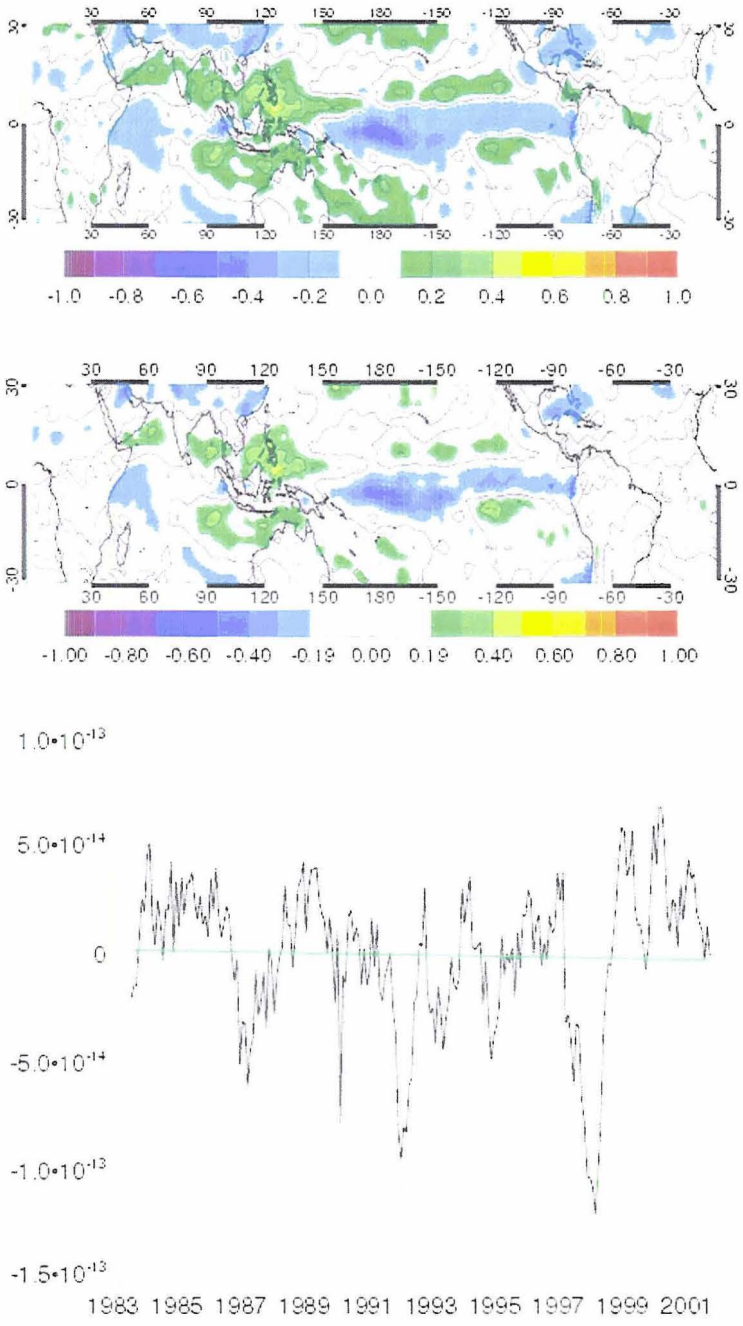

Figure 5.11: (top) The map showing the distribution of regression coefficients obtained from regressing the ISCCP D2 all-cloud cloud amount anomaly time series of the region of interest onto the time series of ERA-40 200 mb divergence at each grid point. (middle) The map showing the distribution of correlation coefficients obtained from correlating those time series. Colored contours indicate regions where the regression coefficients are statistically significant. (bottom) The proxy cloud time series obtained from projecting the regression coefficient map onto the map of 200 mb divergence at each time step plotted with the linear trend in green.

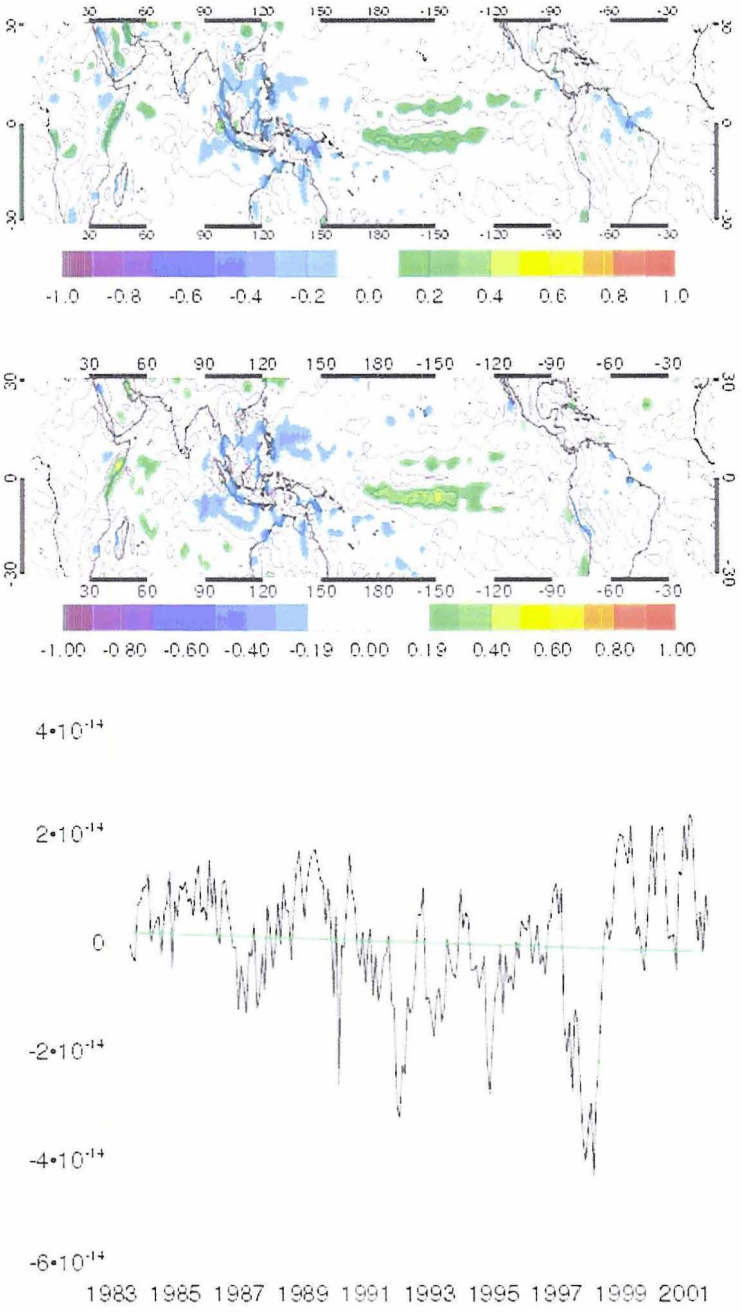

Figure 5.12: (top) The map showing the distribution of regression coefficients obtained from regressing the ISCCP D2 all-cloud cloud amount anomaly time series of the region of interest onto the time series of ERA-40 850 mb divergence at each grid point. (middle) The map showing the distribution of correlation coefficients obtained from correlating those time series. Colored contours indicate regions where the regression coefficients are statistically significant. (bottom) The proxy cloud time series obtained from projecting the regression coefficient map onto the map of 850 mb divergence at each time step plotted with the linear trend in green.

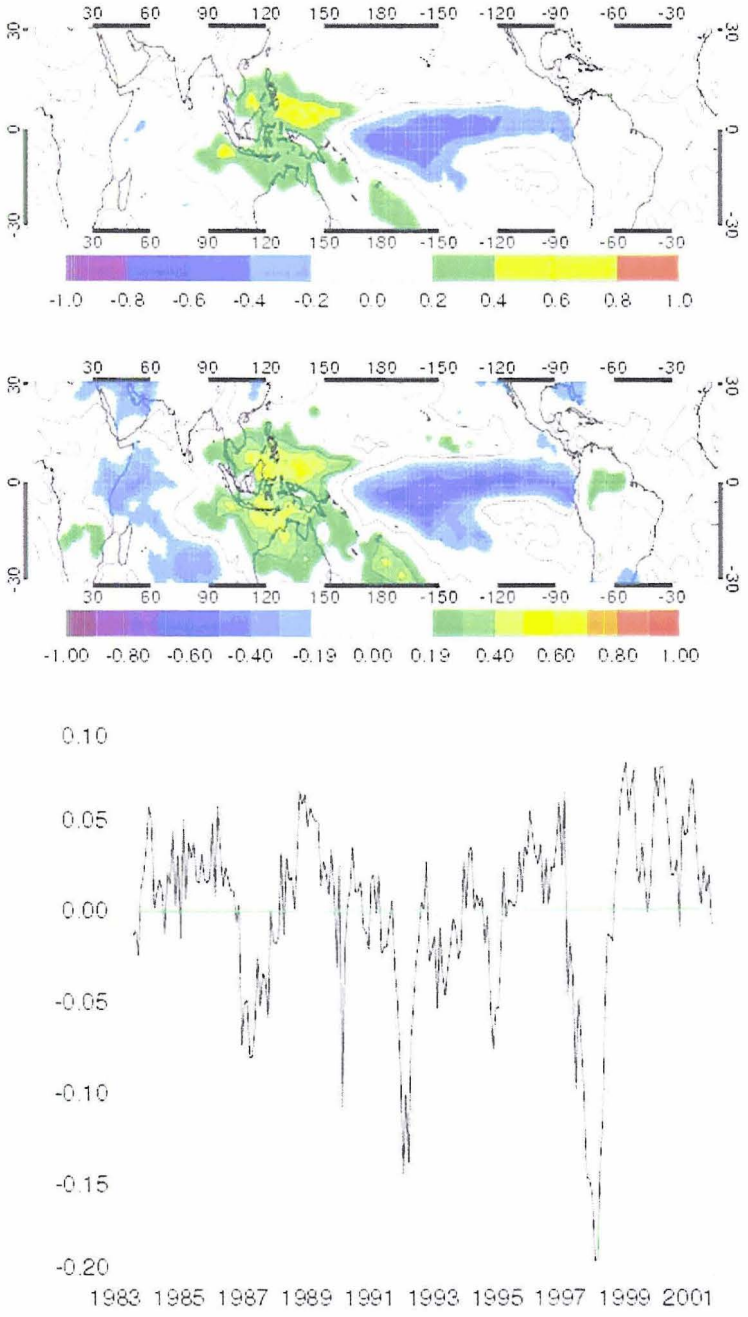

Figure 5.13: (top) The map showing the distribution of regression coefficients obtained from regressing the ISCCP D2 all-cloud cloud amount anomaly time series of the region of interest onto the time series of GPCP precipitation at each grid point. (middle) The map showing the distribution of correlation coefficients obtained from correlating those time series. Colored contours indicate regions where the regression coefficients are statistically significant. (bottom) The proxy cloud time series obtained from projecting the regression coefficient map onto the map of precipitation at each time step plotted with the linear trend in green.

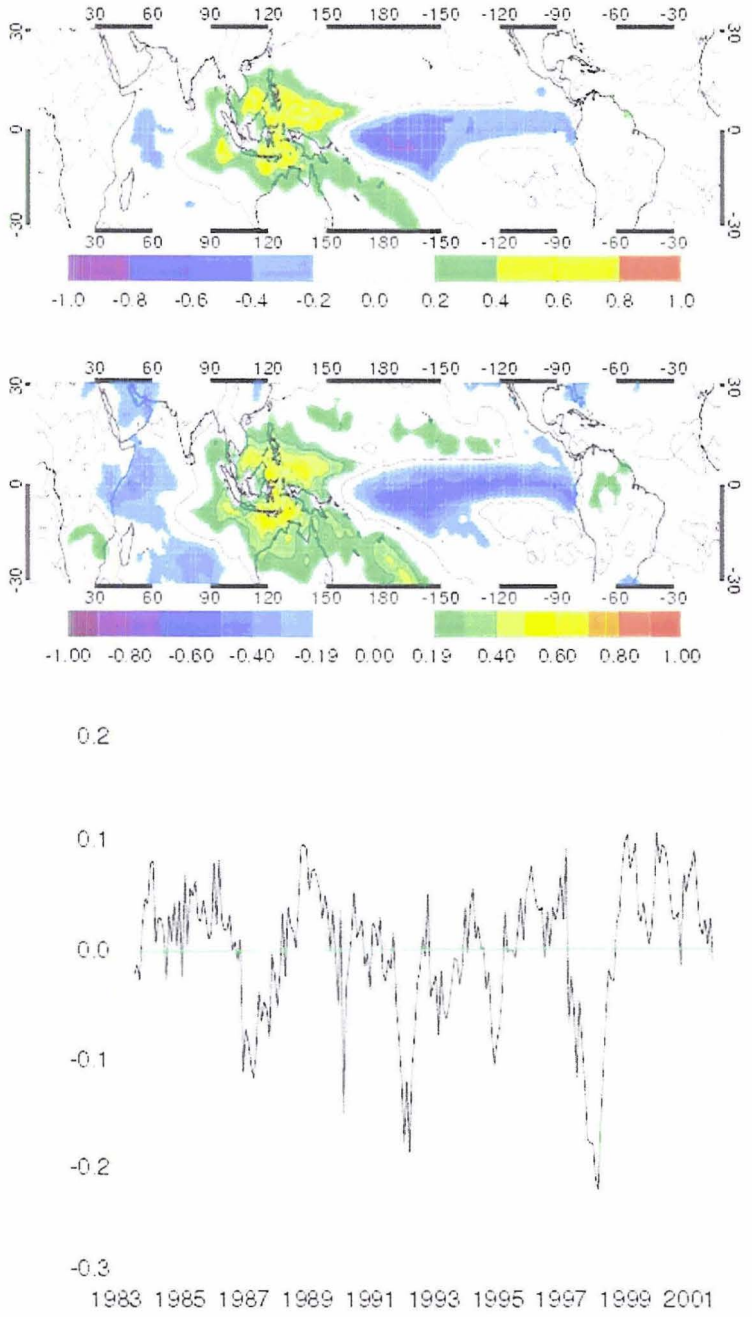

Figure 5.14: (top) The map showing the distribution of regression coefficients obtained from regressing the ISCCP D2 all-cloud cloud amount anomaly time series of the region of interest onto the time series of CMAP precipitation at each grid point. (middle) The map showing the distribution of correlation coefficients obtained from correlating those time series. Colored contours indicate regions where the regression coefficients are statistically significant. (bottom) The proxy cloud time series obtained from projecting the regression coefficient map onto the map of precipitation at each time step plotted with the linear trend in green.

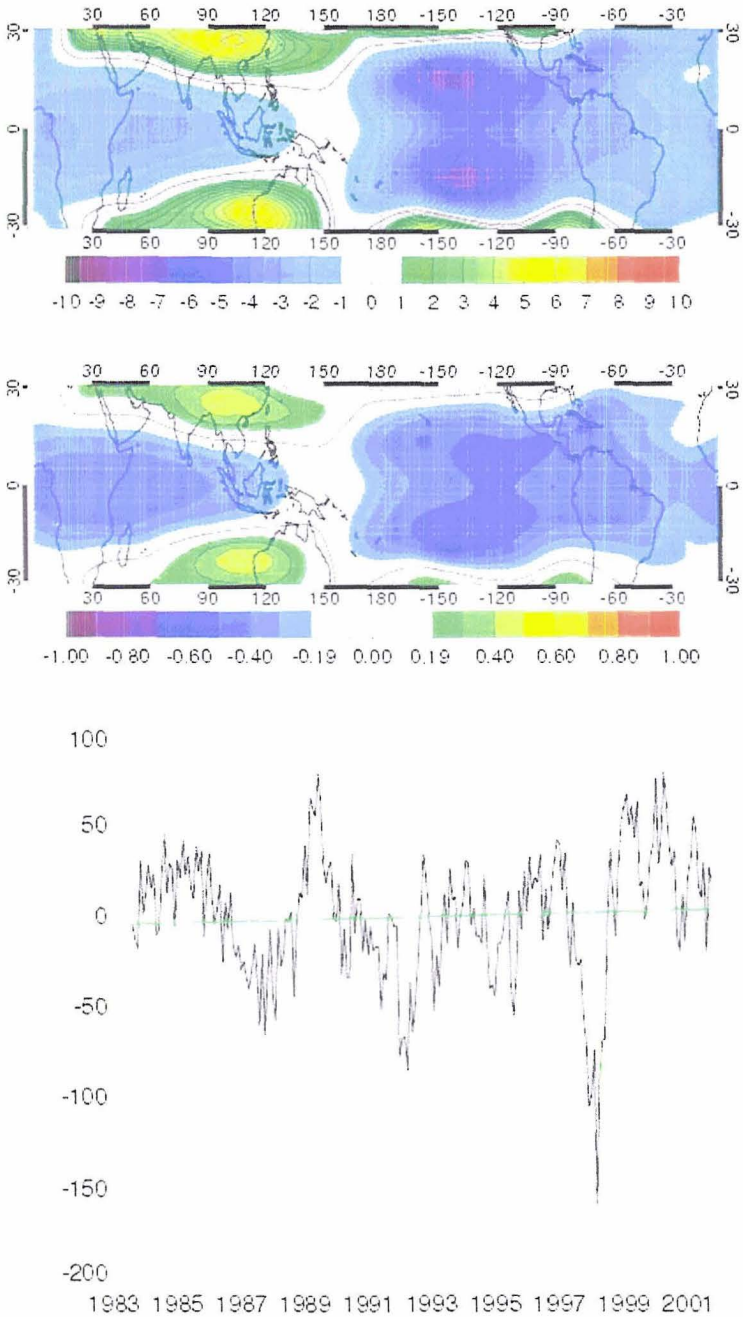

Figure 5.15: (top) The map showing the distribution of regression coefficients obtained from regressing the ISCCP D2 all-cloud cloud amount anomaly time series of the region of interest onto the time series of NCEP/NCAR 200 mb geopotential height at each grid point. (middle) The map showing the distribution of correlation coefficients obtained from correlating those time series. Colored contours indicate regions where the regression coefficients are statistically significant. (bottom) The proxy cloud time series obtained from projecting the regression coefficient map onto the map of 200 mb geopotential height at each time step plotted with the linear trend in green.

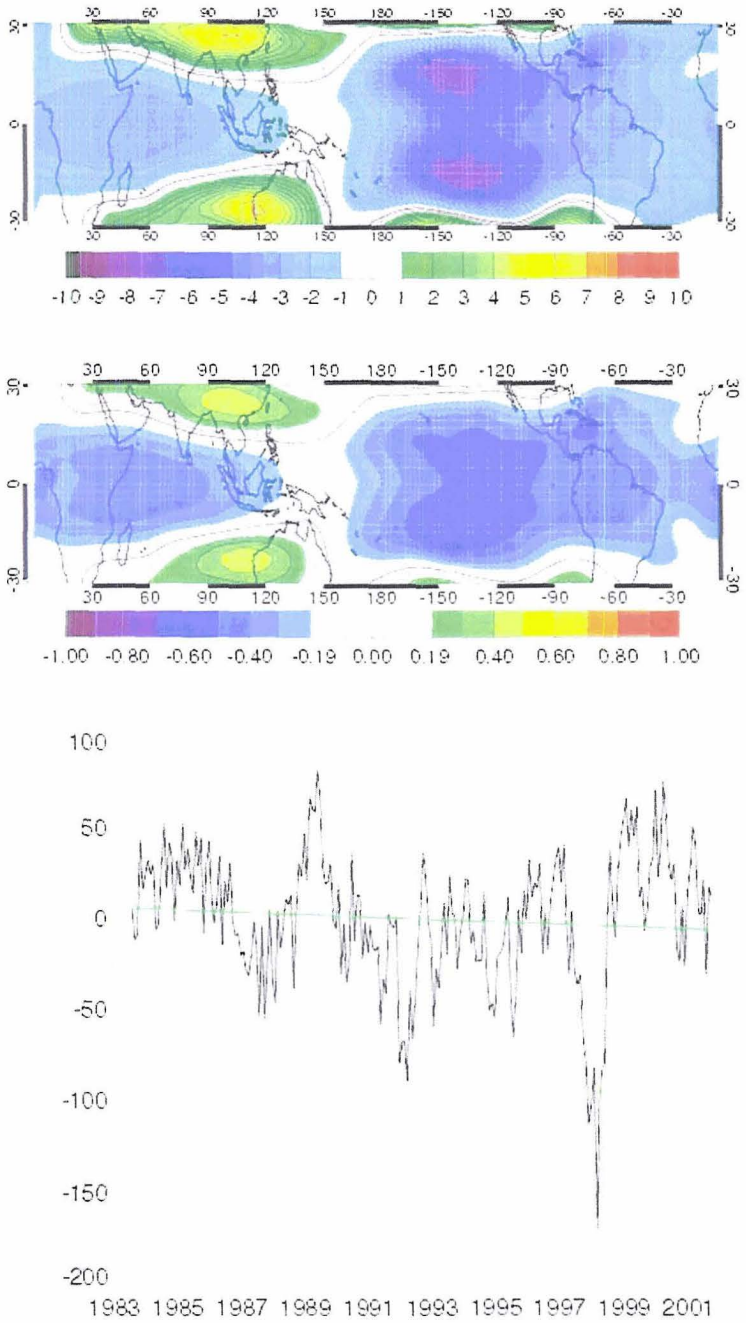

Figure 5.16: (top) The map showing the distribution of regression coefficients obtained from regressing the ISCCP D2 all-cloud cloud amount anomaly time series of the region of interest onto the time series of ERA-40 200 mb geopotential height at each grid point. (middle) The map showing the distribution of correlation coefficients obtained from correlating those time series. Colored contours indicate regions where the regression coefficients are statistically significant. (bottom) The proxy cloud time series obtained from projecting the regression coefficient map onto the map of 200 mb geopotential height at each time step plotted with the linear trend in green.

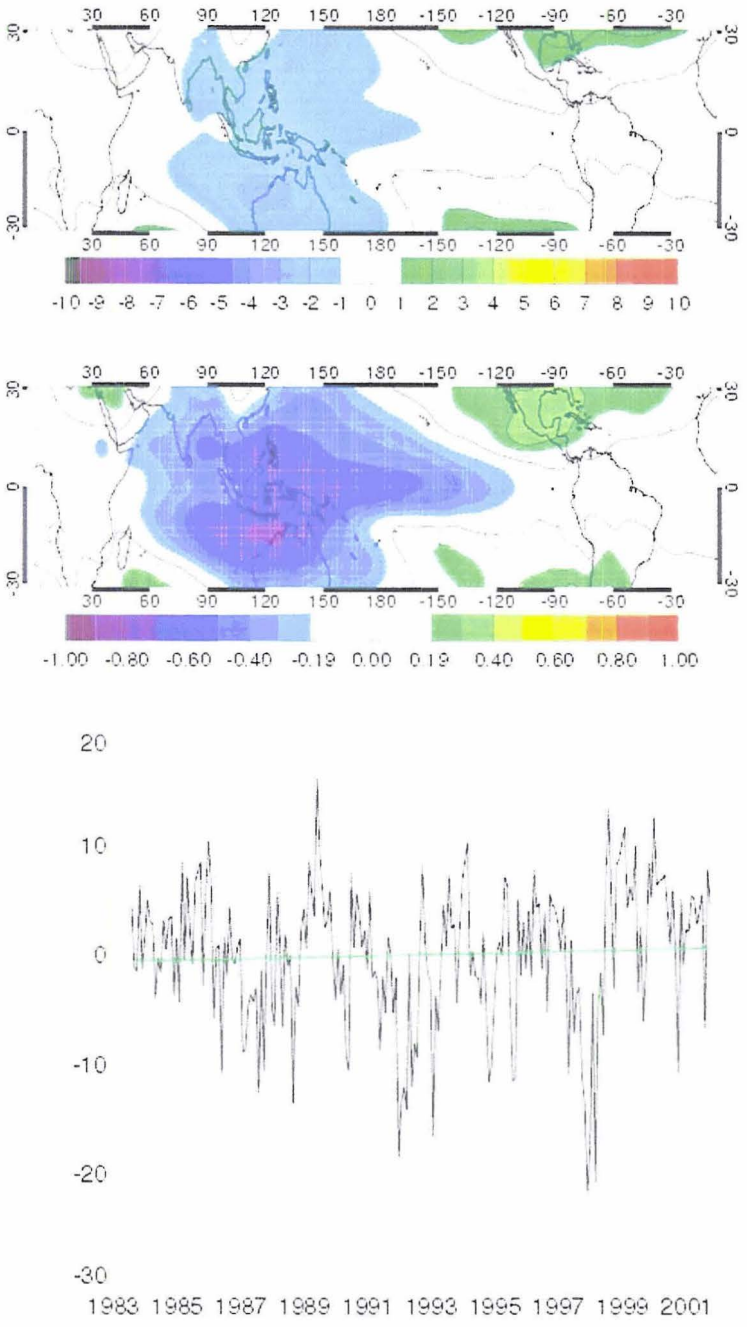

Figure 5.17: (top) The map showing the distribution of regression coefficients obtained from regressing the ISCCP D2 all-cloud cloud amount anomaly time series of the region of interest onto the time series of NCEP/NCAR 850 mb geopotential height at each grid point. (middle) The map showing the distribution of correlation coefficients obtained from correlating those time series. Colored contours indicate regions where the regression coefficients are statistically significant. (bottom) The proxy cloud time series obtained from projecting the regression coefficient map onto the map of 850 mb geopotential height at each time step plotted with the linear trend in green.

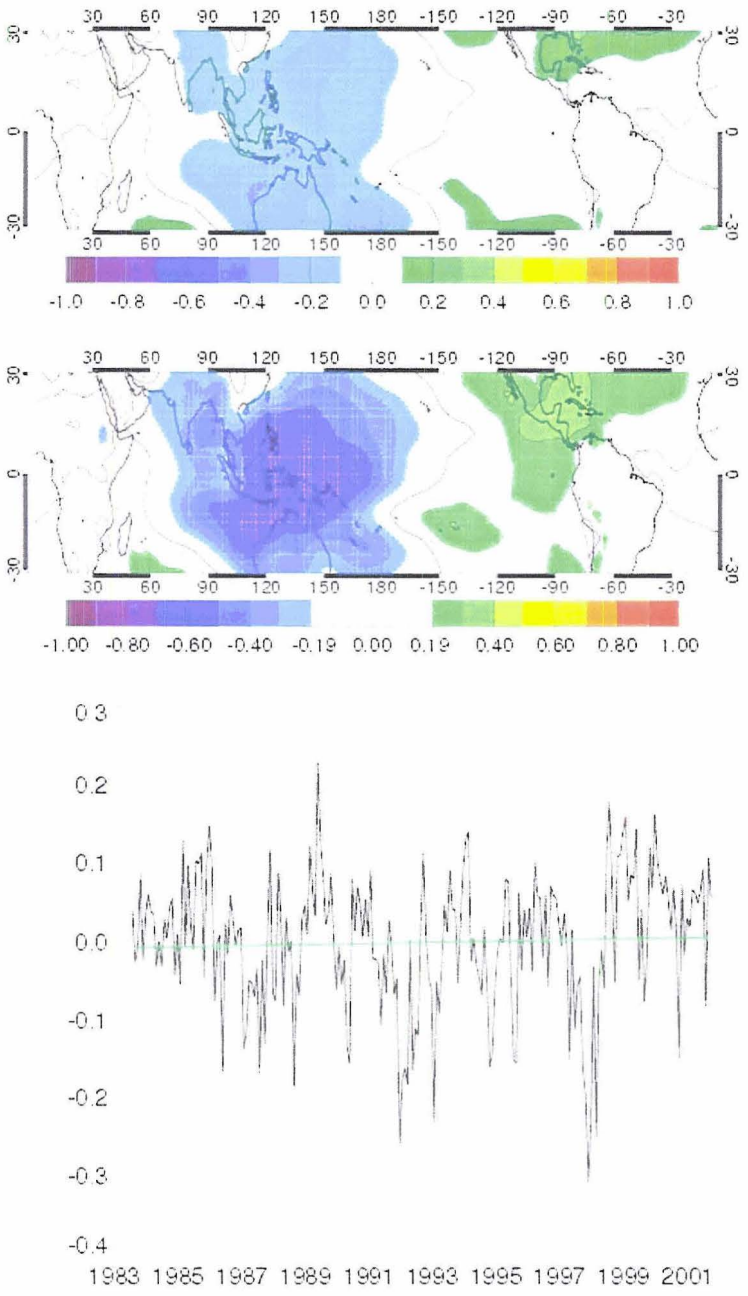

Figure 5.18: (top) The map showing the distribution of regression coefficients obtained from regressing the ISCCP D2 all-cloud cloud amount anomaly time series of the region of interest onto the time series of NCEP/NCAR sea level pressure at each grid point. (middle) The map showing the distribution of correlation coefficients obtained from correlating those time series. Colored contours indicate regions where the regression coefficients are statistically significant. (bottom) The proxy cloud time series obtained from projecting the regression coefficient map onto the map of sea level pressure at each time step plotted with the linear trend in green.

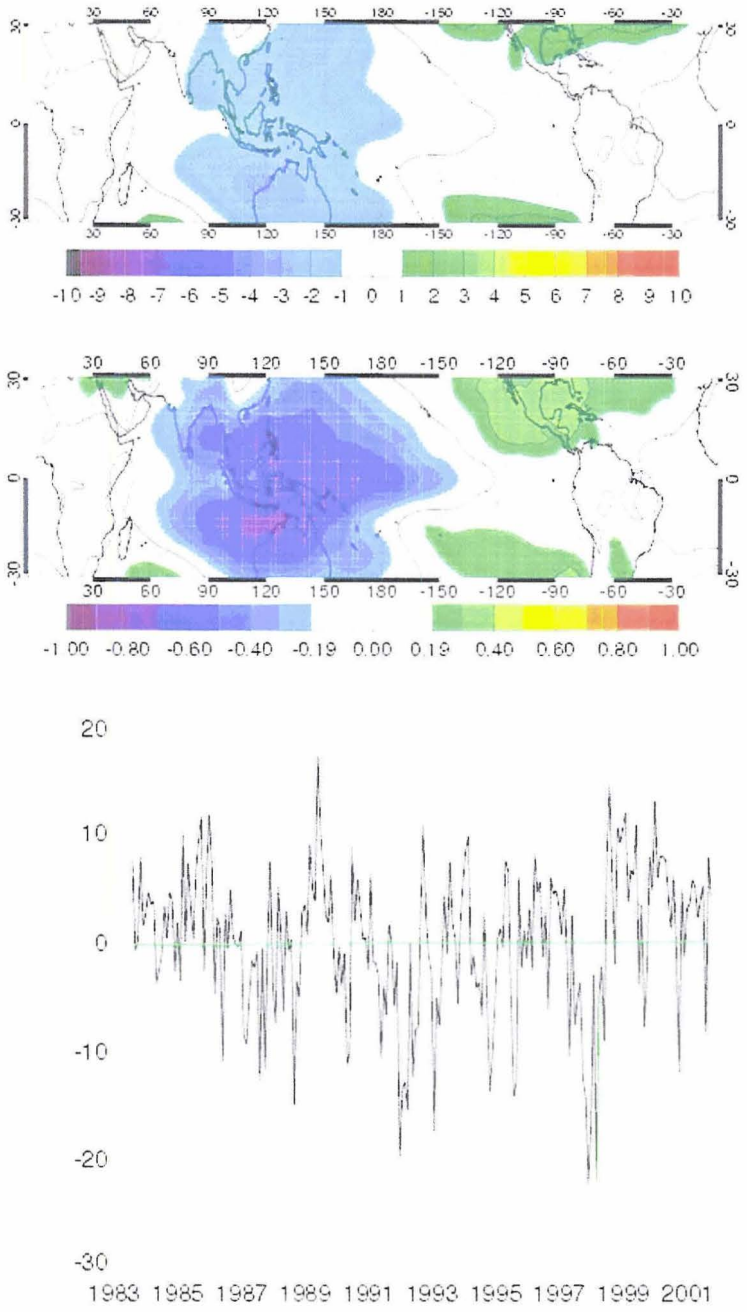

Figure 5.19: (top) The map showing the distribution of regression coefficients obtained from regressing the ISCCP D2 all-cloud cloud amount anomaly time series of the region of interest onto the time series of ERA-40 850 mb geopotential height at each grid point. (middle) The map showing the distribution of correlation coefficients obtained from correlating those time series. Colored contours indicate regions where the regression coefficients are statistically significant. (bottom) The proxy cloud time series obtained from projecting the regression coefficient map onto the map of 850 mb geopotential height at each time step plotted with the linear trend in green.

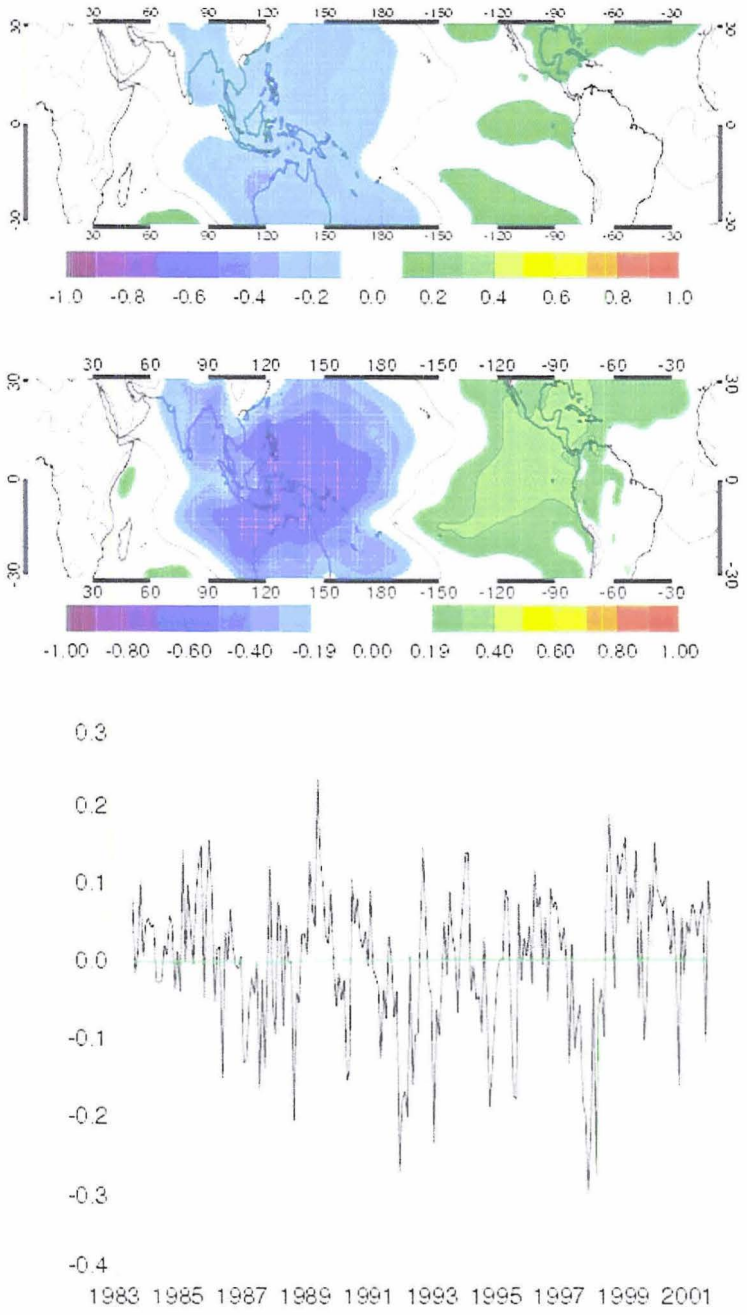

Figure 5.20: (top) The map showing the distribution of regression coefficients obtained from regressing the ISCCP D2 all-cloud cloud amount anomaly time series of the region of interest onto the time series of ERA-40 sea level pressure at each grid point. (middle) The map showing the distribution of correlation coefficients obtained from correlating those time series. Colored contours indicate regions where the regression coefficients are statistically significant. (bottom) The proxy cloud time series obtained from projecting the regression coefficient map onto the map of sea level pressure at each time step plotted with the linear trend in green.

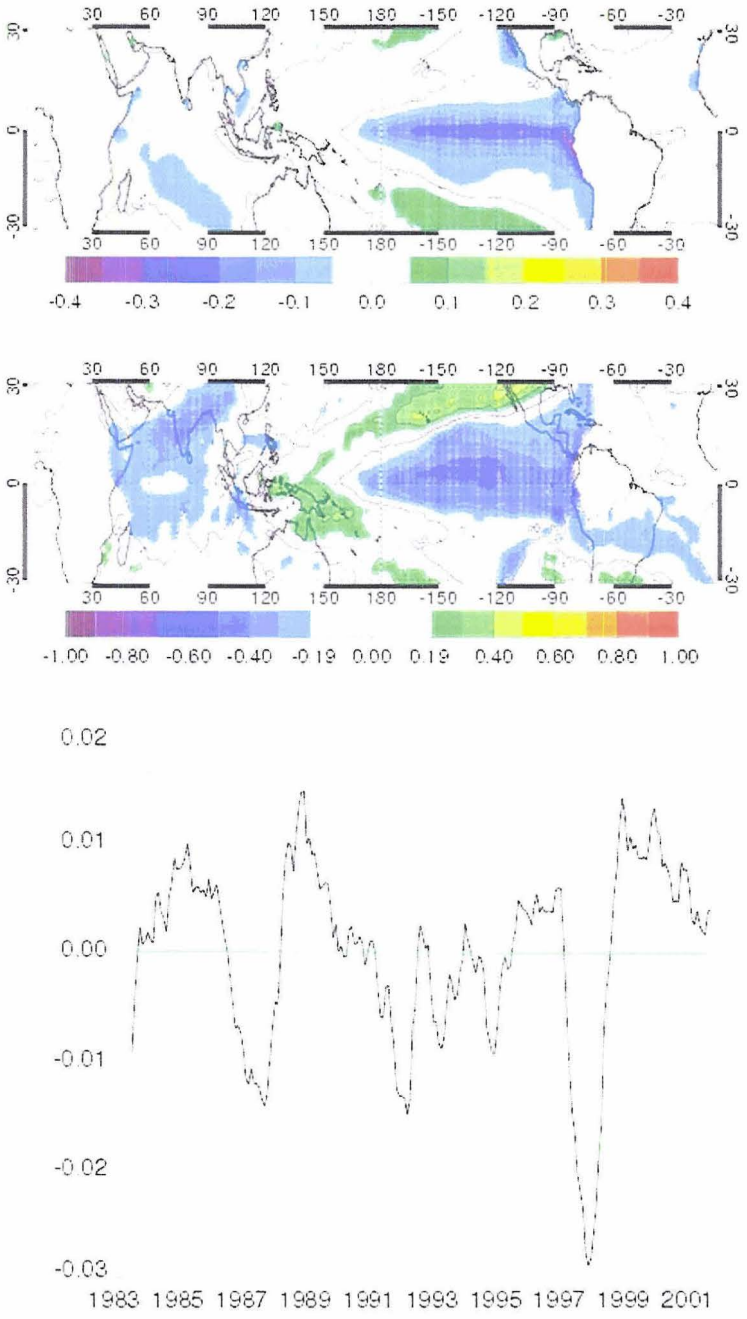

Figure 5.21: (top) The map showing the distribution of regression coefficients obtained from regressing the ISCCP D2 all-cloud cloud amount anomaly time series of the region of interest onto the time series of NOAA OI v.2 SST at each grid point. (middle) The map showing the distribution of correlation coefficients obtained from correlating those time series. Colored contours indicate regions where the regression coefficients are statistically significant. (bottom) The proxy cloud time series obtained from projecting the regression coefficient map onto the map of sea surface temperature at each time step plotted with the linear trend in green.

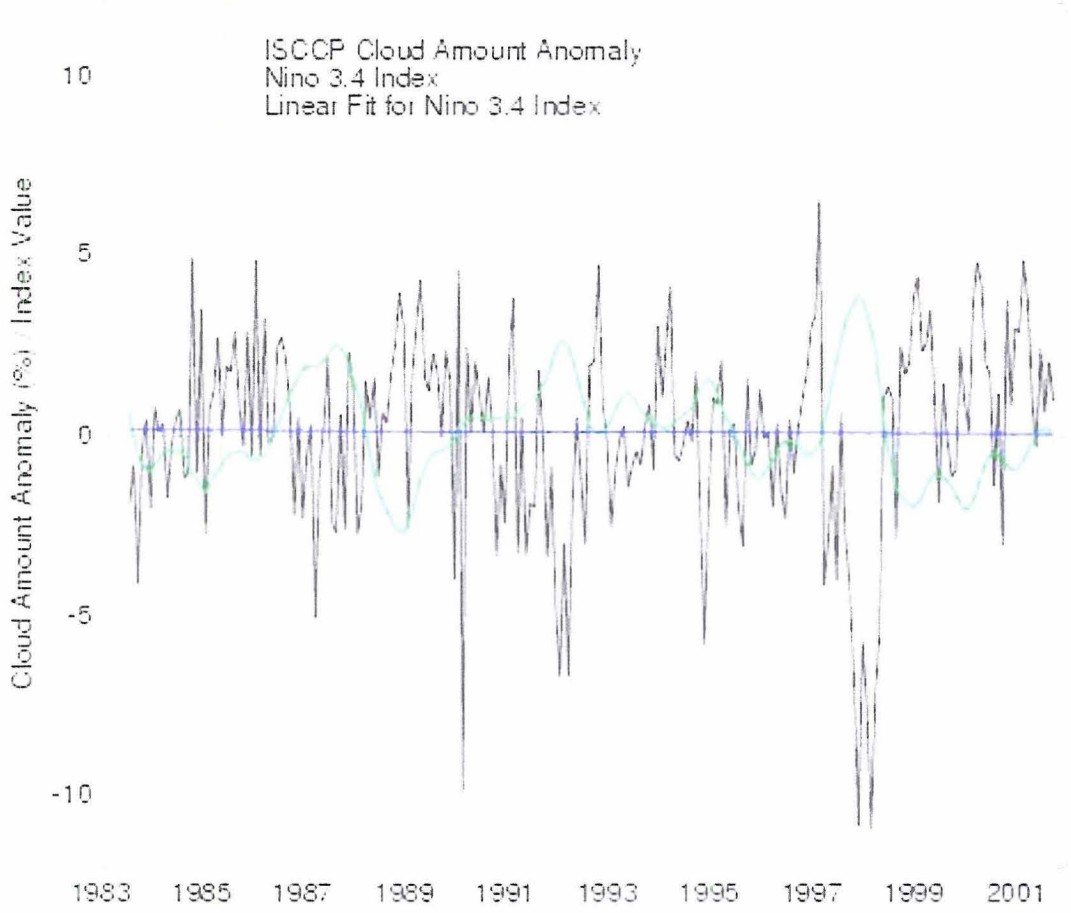

Figure 5.22: The detrended ISCCP D2 all-cloud cloud amount anomaly time series (black) plotted with the time series of the Niño 3.4 index (green). The Niño 3.4 index accounts for 29.5% of the variance of the ISCCP cloud amount time series. The linear regression fit to the Niño 3.4 index is plotted in blue, the slope of which, -4.3×10^{-4} yr^{-1}, is not significantly different from zero.

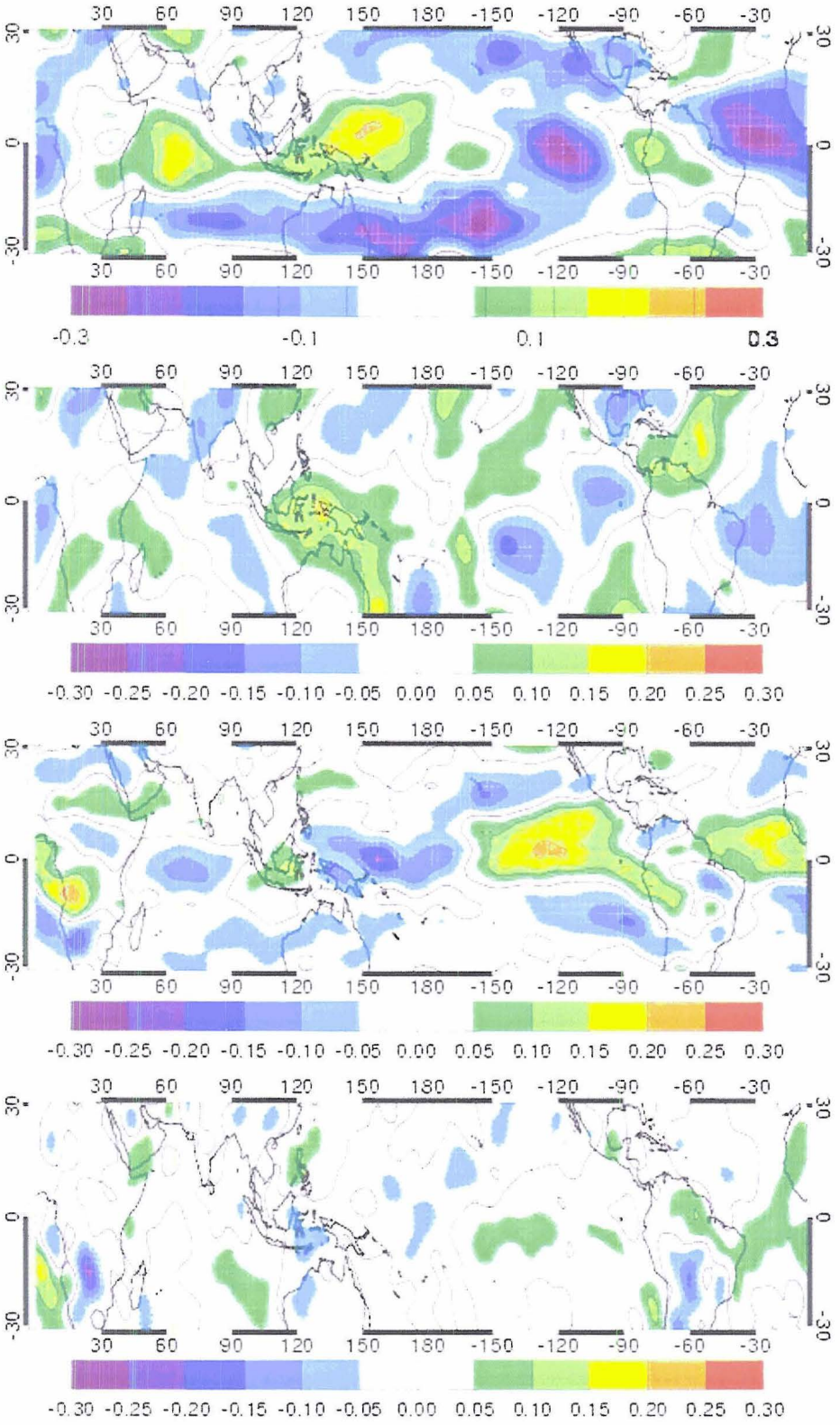

Figure 5.23: Maps of trends in NCEP/NCAR reanalysis data from July 1983 to September 2001 for (from top to bottom): 200 mb zonal wind (in m s^{-1} yr^{-1}); 200 mb meridional wind (in m s^{-1} yr^{-1}); 850 mb zonal wind (in m s^{-1} yr^{-1}); 850 mb meridional wind (in m s^{-1} yr^{-1}).

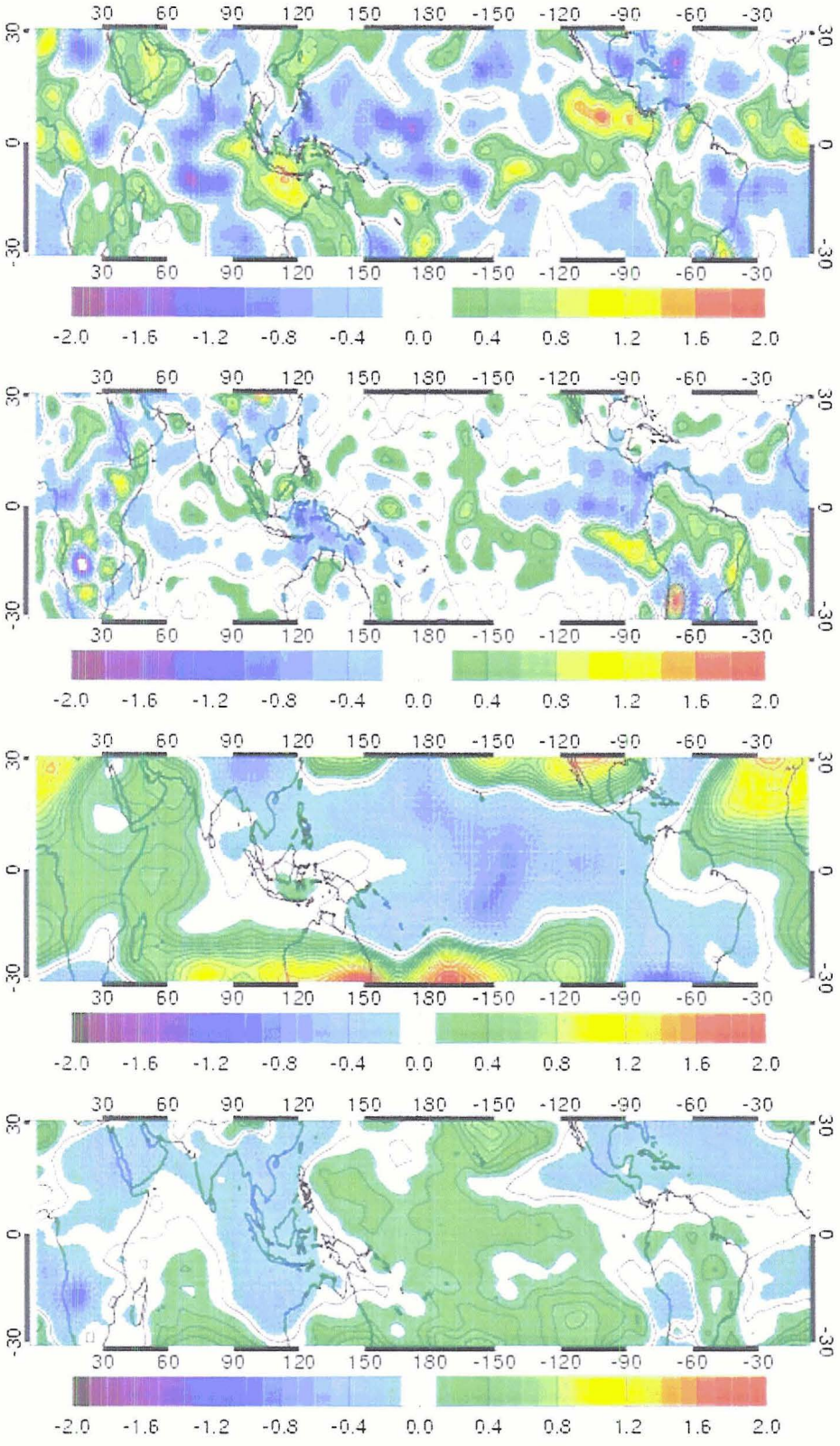

Figure 5.24: Maps of trends in NCEP/NCAR reanalysis data from July 1983 to September 2001 for (from top to bottom): 200 mb divergence (in s^{-1} yr^{-1}); 850 mb divergence (in s^{-1} yr^{-1}); 200 mb geopotential height (in m yr^{-1}); and 850 mb geopotential height (in m yr^{-1}).

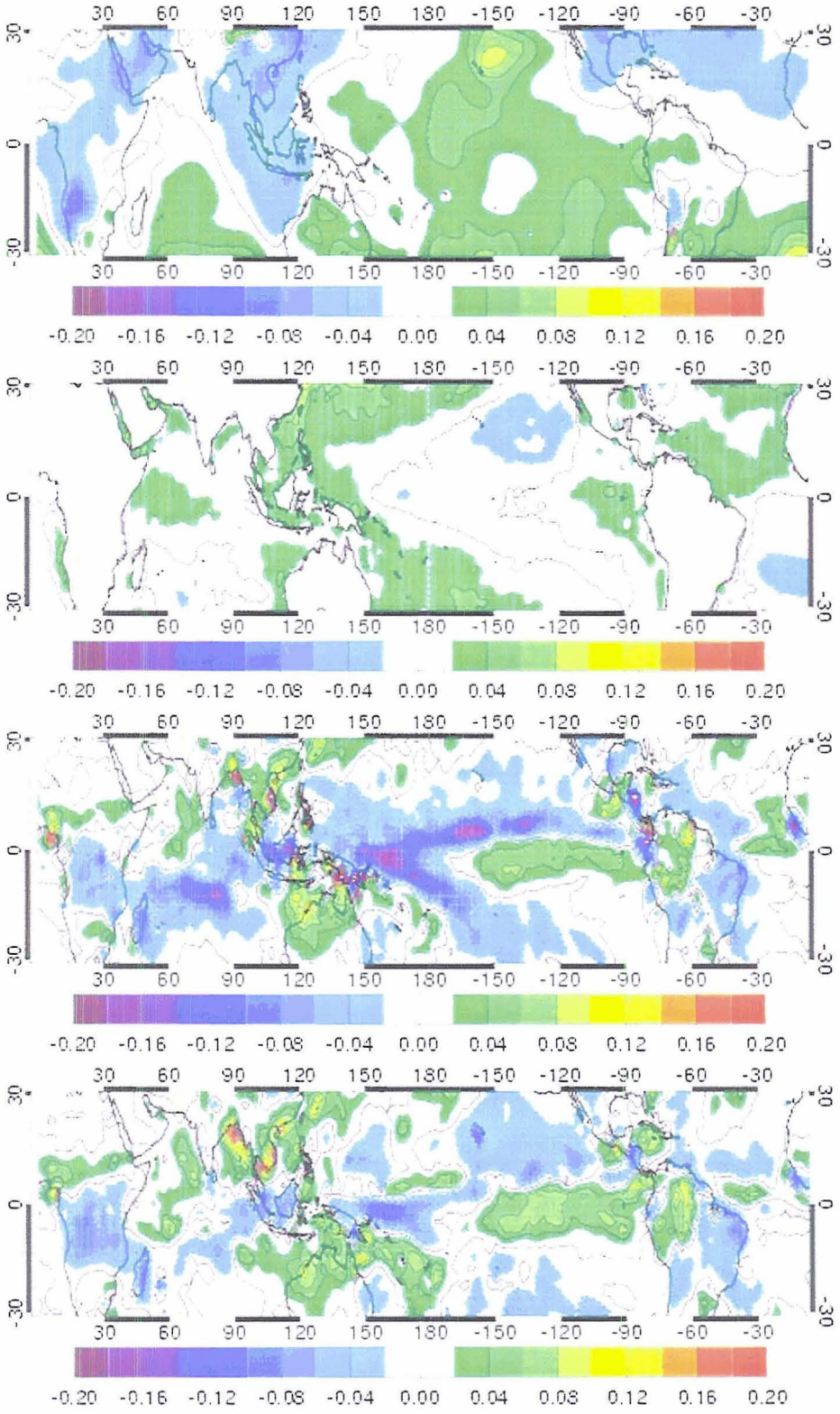

Figure 5.25: Maps of trends in reanalysis data from July 1983 to September 2001 for (from top to bottom): NCEP/NCAR sea level pressure (in mb yr^{-1}); NOAA OI v.2 SST (in K^{-1} yr^{-1}); CMAP precipitation rate (in mm day^{-1} yr^{-1}); and GPCP precipitation rate (in mm day^{-1} yr^{-1}).

Table 5.1: The slopes of the proxy cloud time series for each reanalysis field and their correlations to the regionally averaged ISCCP D2 all-cloud cloud amount anomaly time series

Dataset	Correlation to Cloud Amount Variance Time Series	T-score for Correlation	Slope of Proxy Cloud Time Series	T-score for Slope
		NCEP/NCAR Reanalysis		
200 mb Zonal Wind	**0.75**	**11.14**	5.2×10^{-3} ms^{-1} yr^{-1}	0.64
850 mb Zonal Wind	**0.79**	**12.81**	-3.2×10^{-4} ms^{-1} yr^{-1}	-0.28
200 mb Meridional Wind	**0.74**	**11.02**	1.5×10^{-3} ms^{-1} yr^{-1}	1.05
850 mb Meridional Wind	**0.72**	**10.22**	2.3×10^{-5} ms^{-1} yr^{-1}	0.11
200 mb Divergence	**0.76**	**11.70**	1.4×10^{-16} s^{-1} yr^{-1}	0.41
850 mb Divergence	**0.69**	**9.38**	-1.6×10^{-16} s^{-1} yr^{-1}	-1.63
200 mb Geopotential Height	**0.68**	**9.20**	4.5×10^{-1} m yr^{-1}	0.96
850 mb Geopotential Height	**0.58**	**7.10**	6.7×10^{-2} m yr^{-1}	0.79
Sea Level Pressure	**0.56**	**6.80**	7.5×10^{-4} mb yr^{-1}	0.65
		ERA-40 Reanalysis		
200 mb Zonal Wind	**0.75**	**11.27**	1.7×10^{-3} ms^{-1} yr^{-1}	0.21
850 mb Zonal Wind	**0.79**	**12.89**	5.3×10^{-4} ms^{-1} yr^{-1}	0.51
200 mb Meridional Wind	**0.75**	**11.31**	4.4×10^{-5} ms^{-1} yr^{-1}	0.03
850 mb Meridional Wind	**0.65**	**9.52**	4.8×10^{-5} ms^{-1} yr^{-1}	0.23
200 mb Divergence	**0.80**	**13.27**	-2.4×10^{-16} s^{-1} yr^{-1}	-0.56
850 mb Divergence	**0.83**	**14.67**	-2.0×10^{-16} s^{-1} yr^{-1}	-1.27
200 mb Geopotential Height	**0.69**	**9.39**	-6.5×10^{-1} m yr^{-1}	-1.35
850 mb Geopotential Height	**0.58**	**7.07**	1.6×10^{-2} m yr^{-1}	0.18
Sea Level Pressure	**0.57**	**6.83**	1.6×10^{-4} mb yr^{-1}	0.13
		Other Reanalysis Data		
CMAP Precipitation Reanalysis	**0.78**	**12.39**	1.7×10^{-4} mm day^{-1} yr^{-1}	0.22
GPCP Precipitation Reanalysis	**0.80**	**13.05**	5.4×10^{-5} mm day^{-1} yr^{-1}	0.08
NOAA OI v.2 SST	**0.61**	**7.74**	-1.0×10^{-5} °C yr^{-1}	-0.09

For statistical significance at the 95% confidence level, the t-scores must exceed ±2.00. Values in **bold** pass this test allowing us to reject the null hypothesis that either there is no correlation or that the slope is not different than zero.

CHAPTER 6: SUMMARY OF CONCLUSIONS AND CONCLUDING REMARKS

6.1 Summary of results and conclusions

The purpose of this study is to characterize and verify the trends in the ISCCP D2 dataset. In order to avoid the influence of the high correlation between the cloud amount and the changing viewing angle of the geosynchronous satellites, the region defined as 90°E to 180° and 30°N to 30°S is selected for study because the satellite coverage is relatively constant. The presented analysis shows:

- The average cloud amount from July 1983 through September 2001 has been decreasing by 2.6% per decade according to ISCCP;
- The patterns of the ISCCP changes suggest a relationship to changes in the distribution and/or intensity of convection, though not all ISCCP data consistently support this conclusion;
- The NOAA Interpolated OLR and PATMOS-A data also support a relationship between cloud amount changes in the region of interest and the redistribution of convection, but unlike ISCCP, trends in these two polar-orbiter based datasets are not significantly different from zero;
- Reanalysis data demonstrate that the nature of how cloud amount changes in the region of interest are related to changes in the general circulation in a manner are indeed consistent with a redistribution of convection;

- The correlation analysis with reanalysis data shows that most of the long-term variations in cloud amount are correlated with variations in ENSO. This explains why the results from all three satellite datasets consistently indicate changes in the distribution of convection;
- The reanalysis data confirm that the change in the true regionally averaged cloud amount is not significantly different from zero, in agreement with the polar-orbiter based satellite data;

Therefore, while the ISCCP D2 dataset has apparently captured the climate variability associated with ENSO also evident in other independent data sources, there is no corroborating evidence that the long-term trend in the all-cloud cloud amount in the region of interest is real.

6.2 Concluding remarks

These results call the climate trend analyses of Chen et al. (2002) and Pallé et al. (2004) into question, since both studies used ISCCP data as an input to their algorithms for finding long-term trends. In doing so, these analyses were likely predetermined to produce trends. The Wielicki et al. (2002) results are not as easily dismissed, though in a letter of response to their findings, Trenberth (2002) points out possible contamination due to calibration issues among platforms and that the data processing used in their data may introduce errors through the aliasing of semiannual and diurnal cycles. These results serve to highlight the dangers of using satellite data to diagnose climate changes without first testing to see if the satellite data is not introducing anomalous signals into the analyses.

It is important to note, however, that the ISCCP dataset was not developed for the purpose of long-term climate trends. Rather, it was established to deduce the physical properties of clouds for use in improving the parameterization of clouds in climate models (Rossow et al. 1996). Based on the fact that a strong ENSO signal was found in the ISCCP data, there is however demonstrated potential for being able to use ISCCP data to study climate variability in clouds. This suggests that in the future it may be possible to use ISCCP data in studying other modes of climate variability. However, it is apparent that further work must be done before ISCCP cloud amount data can be used for any trend analysis. Despite efforts to select a region that minimized the viewing angle problem, the magnitude of the slope of the ISCCP data was shown to be unreasonably large and negative while the slopes observed in the rest of the datasets do not differ significantly from zero. Therefore, there must be other contamination in the ISCCP data. This contamination may take the form of calibration errors when new satellite platforms are introduced, but it may also involve data processing errors that have not yet been identified. It is the author's hope that efforts in the near future will be able to identify and correct the problems highlighted by this study. Until this work is completed, ISCCP D2 data should probably not be used for any studies that require the detection of long-term trends in cloud data.

REFERENCES

Barkstrom, B.R., 1984: The Earth Radiation Budget Experiment (ERBE). *Bull. Amer. Meteor. Soc.*, **65**, 1170-1185.

Bengtsson, L., S. Hagemann, and K.I. Hodges, 2004: Can climate trends be calculated from reanalysis data? *J. Geophys. Res.*, **109**, D11111, doi:10.1029/2004JD004536.

Bjerknes, J., 1969: Atmospheric teleconnections from the equatorial Pacific. *Mon. Wea. Rev.*, **97**, 163-172.

Campbell, G.G., 2004: View angle dependence of cloudiness and the trend in ISCCP cloudiness. *Extended Abstracts, Thirteenth Conf. on Satellite Meteorology and Oceanography,* Norfolk, VA, Amer. Meteor. Soc., Online, P6.6.

—. Personal Communication. August 2004.

Chen, J., B.E. Carlson, and A.D. Del Genio, 2002: Evidence for strengthening of the tropical general circulation in the 1990s. *Science*, **295**, 838-841.

Gibson, R., P. Kallberg, and S. Uppala, 1996: The ECMWF Re-Analysis (ERA) project. ECMWF Newsletter 73, 7–17. [Available on PDF from ECMWF, http://www.ecmwf.int/publications/newsletters/list.html].

Gruber, A. and A.F. Krueger, 1984: The Status of the NOAA outgoing longwave radiation dataset. *Bull. Amer. Meteor. Soc.*, **65**, 958-959.

Horel, J.D. and J.M. Wallace, 1981: Planetary-scale phenomena associated with the southern oscillation. *Mon. Wea. Rev.*, **109**, 813-829.

Huffman, G.J., and Coauthors, 1996: The Global Precipitation Climatology Project (GPCP) combined precipitation dataset. *Bull. Amer. Meteor. Soc.*, **77**, 5-20.

Kalnay, E.M., and Coauthors, 1996: The NCEP/NCAR reanalysis project. *Bull. Amer. Meteor. Soc.*, **77**, 437-471.

Kistler, R., and Coauthors, 2001: The NCEP-NCAR 50-Year Reanalysis: Monthly Means CD-ROM and Documentation. *Bull. Amer. Meteor. Soc.*, **82**, 247-268.

Liebmann, B. and C.A. Smith, 1996: Description of a complete (interpolated) outgoing longwave radiation dataset. *Bull. Amer. Met. Soc*, **77**, 1275-1277.

Lin, B., B.A. Wielicki, L.H. Chambers, Y. Hu, and K-M Xu, 2002: The iris hypothesis: a negative or positive feedback?, *J. Climate*, **15**, 3-7.

Lindzen, R., M.D. Chou, and A. Hou, 2001: Does the Earth have an adaptive iris?, *Bull. Amer. Meteor. Soc.*, **82**, 417-432.

Miller, R.L., 1997: Tropical thermostats and low cloud cover. *J. Climate*, **10**, 409-440.

Pallé, E., P.R. Goode, P. Montañes-Rodriguez, S.E. Koonin, 2004: Changes in the Earth's reflectance over the past two decades. *Science*, **304**, 1299-1301.

Pierrehumbert, R., 1995: Thermostats, radiator fins, and the local runaway greenhouse. *J. Atmos. Sci.*, **52**, 1784-1806.

Reynolds, R.W., N.A. Rayner, T.M. Smith, D.C. Stokes, and W. Wang, 2002: An improved in situ and satellite SST analysis for climate. *J. Climate*, **15**, 1609-1625.

Riehl, H. and J.S. Malkus, 1958: On the heat balance in the equatorial trough zone. *Geophysica*, **6**, 503-537.

Rossow, W.B. and R.A. Schiffer, 1999: Advances in understanding clouds from ISCCP. *Bull. Amer. Meteor. Soc.*, **80**, 2261-2287.

—, A.W. Walker, D.E. Beuschel, and M.D. Roiter, 1996: International Satellite Cloud Climatology Project (ISCCP) documentation of new cloud datasets. WMO/TD-No. 737, World Meteorological Organization, 115 pp.

Schiffer, R.A. and W.B. Rossow, 1983: The International Satellite Cloud Climatology Project (ISCCP) – the first project of the World Climate Research Project, *Bull. Amer. Meteor. Soc.*, **64**, 779-784.

Simmons, A.J. and J.K. Gibson, eds, 2000: The ERA-40 project plan, ERA-40 Project Report Series, No. 1, 63 pp. [Available on PDF from ECMWF, http://www.ecmwf.int/publications/library/do/references/list/192].

Smith, C.A. and P. Sardeshmukh, 2000: The effect of ENSO on the intraseasonal variance of surface temperature in winter. *Int. J. Climatol.*, **20**, 1543-1557.

Stowe, L.L., P.A. Davis, and E.P. McClain, 1999: Scientific basis and initial evaluation of the CLAVR-1 global clear/cloud classification algorithm for the Advanced Very High Resolution Radiometer. *J. Atmos. Oceanic Technol*, **16**, 656-681.

—, H. Jacobowitz, G. Ohring, K.R. Knapp, and N.R. Nalli, 2002: The Advanced Very High Resolution Radiometer (AVHRR) Pathfinder Atmosphere (PATMOS) climate dataset: initial analyses and evaluations. *J. Climate*, **15**, 1243-1260.

Trenberth, K.E., 2002: Changes in tropical clouds and radiation. *Science*, **296**, 2095.

—, and D.P. Stepaniak, 2000: Indices of El Niño evolution. *J. Climate*, **14**, 1697-1701.

Waliser, D.E. and C. Gautier, 1993: A satellite-derived climatology of the ITCZ. *J. Climate*, **6**, 2162-2174.

Wielicki, B.A., and Coauthors, 2002: Evidence for large decadal variability in the tropical mean radiative energy budget. *Science*, **295**, 841-844.

Wilks, D.S., 1995: *Statistical Methods in the Atmospheric Sciences.* International Geophysical Series, Vol. 59, Academic Press, 467 pp.

Xie, P. and P.A. Arkin, 1997: Global precipitation: a 17-year monthly analysis based on gauge observations, satellite estimates, and numerical model outputs. *Bull. Amer. Meteor. Soc.*, **78**, 2539-2558.